Universidade Federal de Minas Gerais
Programa de Pós-Graduação em Engenharia Metalúrgica, Materiais e de Minas

Daniela Fátima Gomes

# Mathematical models of the continuous casting of blooms and beam blanks: Analysis of secondary cooling to cast both geometries with the same roll configuration

# Modelo matemático para o lingotamento de blocos e beam blanks: Análise de uma mesma configuração de rolos de suporte no resfriamento secundário para produzir ambas as geometrias

Belo Horizonte
2022

Daniela Fatima Gomes

# Mathematical models of the continuous casting of blooms and beam blanks: Analysis of secondary cooling to cast both geometries with the same roll configuration

Tese apresentada ao Programa de Pós-Graduação em Engenharia Metalúrgica, Materiais e de Minas da Universidade Federal de Minas Gerais, como requisito parcial à obtenção do título de Doutora em Engenharia Metalúrgica, Materiais e de Minas.

Área de concentração: Metalurgia Extrativa

Orientador: Prof. Maurício Covcevich Bagatini

Coorientador: Prof. Roberto Parreiras Tavares

Belo Horizonte

2022

Gomes, Daniela Fátima.
G633m Mathematical models of the continuous casting of blooms and beam blanks [recurso eletrônico]: analysis of secondary cooling to cast both geometries with same roll configuration / Daniela Fátima Gomes. – 2022.
1 recurso online (119 f.: il., color.): pdf.

Orientador: Maurício Covcevich Bagatini.
Coorientador: Roberto Parreiras Tavares.

Tese (doutorado) - Universidade Federal de Minas Gerais, Escola de Engenharia.

Bibliografia: f. 114-119.
Exigências do sistema: Adobe Acrobat Reader.

1. Engenharia Metalúrgica - Teses. 2. Fundação contínua – Teses. 3. Calor – Transmissão – Teses. I. Bagatini, Maurício Covcevich. II. Tavares, Roberto Parreiras. III. Universidade Federal de Minas Gerais. Escola de Engenharia. IV. Título.

CDU: 669(043)

Ficha catalográfica elaborada pela Bibliotecária Letícia Alves Vieira - CRB-6/2337
Biblioteca Prof. Mário Werneck - Escola de Engenharia da UFMG

**UNIVERSIDADE FEDERAL DE MINAS GERAIS**
**ESCOLA DE ENGENHARIA**
**Programa de Pós-Graduação em Engenharia Metalúrgica, Materiais e de Minas**

A tese intitulada **"Mathematical Models oftheContinuous Casting ofBloomsand Beam Blanks: AnalysisofSecondaryCoolingtoCast Both GeometrieswiththeSameRollConfiguration"**, área de concentração: Metalurgia Extrativa, apresentada pela candidata **Daniela Fatima Gomes**, para obtenção do grau de Doutora em Engenharia Metalúrgica, Materiais e de Minas, foi aprovada pela comissão examinadora constituída pelos seguintes membros:

Dr. Maurício CovcevichBagatini
Orientador (UFMG)

Dr. Roberto Parreiras Tavares
Coorientador (UFMG)

Dr. Bernardo Martins Braga
(UFMG)

Dr. Breno Totti Maia
(LumarMetals)

Dr. Leandro Rocha Lemos
(UFMG)

Dra. Claudia Regina Serantoni
(Gerdau Açominas)

Dr. StephanoPapadopoli Tonelli Piva
(Vallourec)

Dr. Leonardo Neves
(CEFET-MG)

Coordenador do Programa de Pós-Graduação em Engenharia Metalúrgica, Materiais e de Minas/UFMG

Belo Horizonte, 31 de outubro de 2022

# Agradecimentos

A Deus, pela saúde, sabedoria e habilidades a mim concedida. À minha família, pelo apoio aos meus estudos, em especial a minha mãe, Rosalina Fátima Souza, minha tia Angelina Auxiliadora Souza e minha avó Djanira Gonçalves Dias por terem me inspirado e apoiado todas as minhas conquistas. Ao meu esposo, Renato Pereira Nominato por fazer dos meus sonhos, nossos sonhos, pelo amor incondicional e dedicação a nossa família. Ao Professor Mauricio Covcevich Bagatini e ao PPGEM, por tornarem possível o desenvolvimento desse trabalho. Ao Professor Roberto Parreiras Tavares, pela dedicação em orientar, ensinar, por sempre acreditar na minha capacidade. É uma imensa honra ser sua orientanda no trabalho final da graduação, mestrado e agora no doutorado. Ao meu amigo Bernardo Martins Braga, pela orientação, ajuda imprescindível e críticas que me desafiaram a estudar e ir além do que eu pensava ser capaz. Aos amigos do trabalho, em especial ao Carlos Berlini Filho, Gabriela Pereira Maciel e Claudia Regina Serantoni pelas conversas importantíssimas e pelo apoio a esse trabalho.

# Abstract

Mathematical models were developed for heat transfer, mechanical stresses due to thermal gradients, and contact forces for the continuous casting process of blooms and beam blanks. The thermal models were validated by temperature measurements with a thermal imaging camera, traveling thermocouple tests, and measurements of the solid shell thickness in the breakout events that occurred during production. The mechanical properties necessary for the mechanical model were obtained by a hot tensile test with partial melting of the sample.

The motivation of this work is to evaluate the possibility of using a single configuration of support and containment rolls and cooling spray to produce both blooms and beam blanks. Thus, two proposals were made for a common setup (1) Cast the bloom with beam blank rolls (2) Cast the beam blank with blooms rolls. These two proposals were simulated, and the results were compared with the current configuration of each of the blooms and beam blanks continuous casting. Thermal and Mechanical analysis suggests that it is possible to have a common Setup for blooms and beam blanks in Zone 2.

However, in ”Proposition II”, the temperature profile of the flange tip starts to have temperature gradients 50°C/m. This can affect the surface quality of the beam blank in this region. So ”Proposition I” is preferred to support both geometries

Until the time of writing, no studies were found where two geometries were analyzed aiming at the production with part of the common secondary cooling, nor mechanical models for blooms and beam blanks whose region of interest is the secondary cooling zone. Mechanical properties data for the studied steel, ASTM A572, were not found, nor were the results of tests with walking thermocouple in ”beam blank”. So, it is concluded that this work has all those exposed original contributions to the scientific community.

Keywords: continuous casting, common setup, heat transfer, stress, distortion beam blanks, and blooms.

# Resumo

Modelos matemáticos foram desenvolvidos para transferência de calor, tensões mecânicas devido a gradientes térmicos e forças de contato para o processo de lingotamento contínuo de blocos e beam blanks. Os modelos térmicos foram validados por medições de temperatura com uma câmera termografica, testes com termopar em movimento e medições de eventos de rompimento de pele que ocorreram durante a produção. As propriedades mecânicas necessárias para o modelo mecânico foram obtidas por um teste de tração a quente com fusão parcial da amostra num simulador tipo GLEBLE.

A motivação deste trabalho é avaliar a possibilidade de usar uma única configuração de rolos de suporte para parte da zona de resfriamento por sprays para produzir blocos e beam blanks.

Portanto, duas propostas foram feitas para uma configuração comum (1) Lingotar o bloco com rolos de beam blank; (2) Lingotar o beam blank com rolos de bloco.

Essas duas propostas foram simuladas, e os resultados foram comparados com a configuração atual do lingotamento de cada uma das geometrias. A análise térmica e mecânica sugere que é possível ter uma configuração comum para os blocos e beam blanks na Zona 2.

No entanto, na proposta (2), o perfil de temperatura da ponta do flange começa a ter gradientes de temperatura de 50°C/m. Isso pode afetar a qualidade da superfície do beam blank nesta região. Portanto, ”Proposição I” é a mais indicada para suportar as duas geometrias.

Até o momento da escrita desse trabalho, não foram encontrados estudos onde duas geometrias foram analisadas visando a produção com parte do resfriamento secundário comum, nem modelos termomecânicos para blocos e beam blanks cuja região de interesse é a zona de resfriamento secundário.

Dados de propriedades mecânicas para o aço estudado, ASTM A572, não foram encontrados, nem os resultados de testes com termopar em movimento no ”beam blank”. Portanto, conclui-se que este trabalho tem todas essas contribuições originais para a comunidade científica.

Palavras chave: lingotamento contínuo, setup comum, transferência de calor, tensão, distorção beam blanks, e blocos.

# List of Figures

# List of Tables

# Summary

# 1. Introduction

The modern steel-making process can be divided into six main steps: 1) Ironmaking, 2) Primary steelmaking, 3) Secondary steelmaking, 4) Continuous casting, 5) Primary forming, and 6) Manufacturing. Of these, continuous casting is the most critical, as defects that originated during this step can propagate downstream and are difficult to be detected and fixed.

In the continuous casting process, liquid steel is transferred from the ladle to the tundish, which is connected to one or more copper molds. In the molds, liquid steel is cooled and partially solidifies. At the exit of the mold, the cross-section of the product is composed of three regions: 1) The solid shell near the surface, 2) The mushy zone (temperatures between the liquidus and the solidus), and 3) The liquid at the center. The mold defines the geometry of the product (e.g. slabs, billets, blooms, beam blanks). After the primary cooling zone, the steel goes to the secondary cooling zone where it is further cooled by water sprays. At the end of the process, the solidified material is cut and further processed according to the application.

On the machine where this study was performed, two distinct configurations of the support and containment foot rollers and cooling sprays, are used to produce blooms and beam blanks. Every time a new production campaign starts (i.e. a change from one product to another) the operation team needs to change the setup. This is a complicated task that requires eight technicians working for fourteen hours and it is usually executed twice a month. It also raises the risk of accidents and can increase maintenance costs.

Changes in the production process are common in the steel-making industry. Companies are always trying to find faster, cheaper, and safer ways to operate. This process optimization can be performed by, for example, replacing old machinery, updating automation software, re-calculating operational parameters, or redefining operational procedures. However, companies can sometimes struggle to analyze if a process can be changed or not. A feasibility study might require experiments to be performed, and such can be expensive and potentially dangerous. Usually, it is also necessary to stop the production line for a few hours (or a few days), which is likewise, not desirable. In this context, simulation can be a very useful tool. If a process is correctly modeled, simulations can be run to analyze what would be the impact of making modifications on it. Only after this assessment, and possible adjustments in the initial proposed solution based on the feedback from the simulation, would the company then perform the experiments.

In this work, thermo-mechanical models will be developed for the continuous casting of two different geometries, blooms and beam blanks, with a focus on the secondary cooling zone. The motivation of this study is to analyze the feasibility of a change in the continuous casting

equipment to simplify and standardize the process to produce different geometries, using heat transfer and thermo-mechanical simulation.

To perform the desired analysis, the following steps were implemented in this work:

1. Heat transfer, solidification and thermo-mechanical models were developed for the continuous casting of steel blooms and beam blanks.

2. Industrial tests were performed for both blooms and beam blanks to validate the model. To measure the temperature values, thermal images were taken in the dry zone of the machine and traveling thermocouple experiments were executed, where the thermocouple was embedded in the as-cast from the secondary cooling to the dry area. In addition, solidified skin measurements were taken in breakout shells.

3. As the bloom has a smaller section, two setups were proposed: (1) Cast the bloom with the original beam blank setup. For this, the side and web rolls need to fit the bloom. Thus, the web rolls must move 90mm away from the initial position to adjust to the bloom and the beam blank lateral rolls must approach 10mm. (2) Adjust the bloom rolls set up to fit the beam blank. In this case, the side rolls need to approach 10mm each other, and the inner and outer radius rolls need to move 50mm to fit the beam blank.

4. The changes proposed in the setup of the machine were analyzed using mechanical and thermo-mechanical models. A comparison of the temperature, stress and distortion profiles for the original setups and the modified options were simulated, to assess which option would be most suitable.

In this document, the methodology and results are presented in a scientific article format, in this order:

- Paper I - Mathematical modeling of the continuous casting of blooms and beam blanks.

  This work presents the simplified model that was initially developed and the first validation tests with a thermal imaging camera and skin measurements on rupture events. Published at ”Computer Methods in Materials Science” and attached at the end of this document.

- Paper II - Thermal behavior of blooms and beam-blanks during continuous casting: Development and validation of a mathematical model for heat transfer.

  It presents the results of an enhanced model, adding the radiation between the beam blank flanges, heat transfer conditions by contact with rollers, and validation results with the traveling thermocouple test.

- Paper III - Mechanical behavior on blooms and beam blanks’ continuous casting: Development of a mathematical model for stress and distortion

This work presents the entire theoretical basis for the development of thermomechanical models, the result of the hot ductility test and the stress and distortion simulations in the as-cast solidified skin on the secondary cooling zone.

- Paper IV - Thermal and Mechanical Behavior of blooms and beam blanks continuous casting: Analysis of secondary cooling to cast both geometries with the same roll configuration.

  This work presents the comparison of heat transfer, temperature profile, stress and distortion of the two common roll setups proposed.

# 2. Introdução

O processo moderno de fabricação de aço pode ser dividido em seis etapas principais: 1) produção de ferro-gusa; 2) refino primário; 3) refino secundário; 4) lingotamento contínuo; 5) laminação; e 6) manufatura. Destes, o lingotamento contínuo é o mais crítico, pois defeitos gerados nessa etapa podem propagar para as etapas seguintes e são difíceis de serem detectados e corrigidos.

No lingotamento contínuo, aço líquido é transferido da panela para o distribuidor, que é conectado a um ou mais moldes de cobre. No molde, o aço líquido é resfriado e solidifica parcialmente. Na saída do molde, a seção transversal do produto é composta de três regiões: 1) A casca solidificada próxima a superfície, 2) A zona mista (temperaturas entre liquidus e solidus), e 3) A zona líquida no centro. O molde define a geometria do produto (barras, blocos,placas ou beam blanks). Após a zona de resfriamento primária, o aço vai para a zona de resfriamento secundário onde é resfriado por sprays de água ou água/ar (tipo ”airmist”). No final do processo, o material solidificado é cortado e processado de acordo com a aplicação.

Na máquina de lingotamento, na qual esse estudo foi realizado,duas configurações distintas de rolos na zona de resfriamento por sprays são utilizadas para produzir blocos e beam blanks. Sempre que uma nova campanha de produção é iniciadas (troca de um produto para o outro) o time de operação precisa realizar a troca do setup. Essa é uma tarefa complexa e demanda quatorze horas de trabalho de oito técnicos e normalmente é realizada duas vezes por mês. Essa tarefa também aumenta o risco de acidentes e pode aumentar o curso de manutenção.

Mudanças no processo produtivo são comuns na siderurgia. Empresas estão sempre buscando maneitas mais rápidas, baratas e mais seguras de operação. Essa otimização de processos pode ser realizada, por exemplo, através da substituição de equipamento antigo, atualização de software de automação, alteração nos parâmetros operacionais ou redefinição de processos.

Porém, empresas podem ter dificuldade em analisar se um processo pode ser alterado ou não. Um estudo de viabilidade pode exigir a execução de experimentos, e estes podem ser caros e potencialmente perigosos. Normalmente, também é necessário interromper a linha de produção por algumas horas (ou alguns dias), o que também não é desejado. Nesse contenxto, a simulação pode ser uma ferramenta muito útil.

Se um processo for corretamento modelado, simulações podem ser realizadas para analisar quais seriam os impactos causados por modificações.

Nesse trabalho, modelos térmicos e mecânicos foram desenvolvidos para o lingotamento

contínuo de dois produtos com geometrias diferentes, blocos e beam blanks, com foco na zona de resfriamento secundário. A motivação do trabalho é analisar a viabilidade de uma alteração na máquina de lingotamento contínup para simplificar e padronizar o processo de produzir duas geometrias, usando simulações de transferência de calor e termomecânica.

Para realizar a análise desejada, os seguintes passos foram implementados nesse trabalho:

1. Modelos de transferência de calor, solidificação e termomecânicos foram desenvolvidos para o lingotamento contínuo de blocos e beam blanks.

2. Testes industriais foram realizados para blocos e beam blanks para validar os modelos. Para medir a temperatura, imagens de câmera termográgica foram registradas na zona seca da máquina e ensaios com termopar realizados, onde o termopar foi inserido no produto lingotado na zona de resfriamento secundário e klevado pela velocidade de lingotamento até a área seca. Além disso, medidas da pele solidificada com realizadas em cascas de breakout.

3. Como o bloco é menor, duas configurações foram propostas: (1) O lingotamento de blocos com a configuração de rolos original do beam blank. Para isso, os rolos laterais e de alma precisam ser aproximados para se ajustar as dimensões do bloco. (2) O lingotamento de beam blanks com a configuração de rolos original do bloco. Nesse caso, os rolos das faces larga e estreita precisam ser afastados para se ajustar as dimensões do beam blank.

4. As alterações propostas para a configuração dos rolos foram analisadas utilizando modelos mecânicos e termo mecânicos. A comparação do perfil de temperatura, tensão e deformação entre a configuração incial e a nova configuração proposta foi realizada para definir qual das propostas é a mais indicada.

Nesse documento, a metodologia e os resultados são apresentados no formato de artigos científicos, nesse ordem:

- Artigo I - Modelagem matemática do lingotamento contínuo de blocos e beam blanks. Esse trabalho apresenta a versão inicial do modelo e a primeira validação com imagens de câmera termográfica e medidas de pele solidificada de breakouts. Publicado em ”Computer Methods in Materials Science” e em anexo ao final desse documento.

- Artigo II - Comportamento térmico de blocos e beam blanks durante o lingotamento contínuo: Desenvolvimento e validação de um modelo matemático para transferência de calor. Esse trabalho apresenta os resultados de um modelo melhorado, com a adição da radiação entre flanges do beam blank, transferência de calor para os rolos de suporte e validação dos resultados com o ensaio com termopar.

- Artigo III - Comportamento mecânico de blocos e beam blanks durante o lingotamento

contínuo: Desenvolvimento de um modelo para tensão e deformação. Esse trabalho apresenta a base teórica para o desenvolvimento do modelo termomecânico, o resultado do teste de tensão a quente e as simulações de tensão e deformação no produto lingotado na zona de resfriamento secundário.

- Artigo IV - Comportamento térmico e mecânico de blocos e beam blanks durante o lingotamento contínuo: Análise do resfriamento secundário para o lingotamento de ambas geometrias com a mesma configuração de rolos Esse trabalho apresenta a comparação de transferência de calor, perfil de temperatura, tensão e deformação das duas configurações propostas. .

# 3. Objectives

The main objective of the present work is to investigate the feasibility of using a single configuration of support rolls to manufacture two types of geometry (blooms and beam blanks) in part of the secondary cooling zone of the continuous casting machine. This analysis requires an understanding of heat exchange and mechanical deformation. Therefore, the specific objectives of the present research are:

- Develop heat-transfer, solidification, stress and strain thermo-mechanical models for the continuous casting of blooms and beam blanks.
- Validation of the models developed with experimental data.
- Propose common setup options for the secondary cooling zone.
- Simulate and analyze the changes in the configuration of the support foot rollers and a comparison of the temperature profiles, solidification, and mechanical deformation between the original and the modified process for blooms and beam blanks.

# 4. Literature Review

This chapter contains:

1. A brief description of the continuous casting process including heat transfer, solidification, and mechanical deformation phenomena that occur during steel cooling;
2. A discussion about the most common quality problems that might happen and how the operating parameters can influence the final quality of the product;
3. An analysis of a selected set of techniques to model the continuous casting process described in the literature and their limitations.

## 4.1 Continuous casting process

The continuous casting process is the most frequently used method to obtain as-cast products in the steel industry. The high productivity and potential to obtain different shapes are some of the advantages of this technique [Bobadilla et al., 1993], [Thomas, 2002], [Vynnycky, 2018]. A ladle containing liquid steel is positioned in an arm of a rotational tower and a long nozzle is attached to the ladle gate valve. When the ladle is opened, steel is poured into the tundish, which has one or more outlets that are connected to a mold where the steel starts the solidification process. A schematic view of this process can be seen in figure 4.1.

The tundish is made of refractory material to reduce thermal losses and the molds are usually made of copper due to the high thermal conductivity of this material. Flux powders or oils are used to lubricate the mold walls and to prevent the sticking of the steel. The cooling in the mold is called primary cooling because it is where the solidified skin begins to form. The solid layer is responsible for containing the liquid region of the material being cast.

After exiting the mold, the geometry is maintained by support rolls, which have a curvature according to the machine radius. Between the rolls, there are sprays to continue the cooling process and guarantee total solidification. The region of the machine where there are water sprays is called the secondary cooling zone. This process is illustrated in figure 4.2.

Many factors can affect the as-cast heat flux, solidification, and mechanical deformation. Some examples are the steel chemical composition, the steel superheat, the strand geometry, the mold characteristics, and mold powders, the sprays' water flux, and casting speed

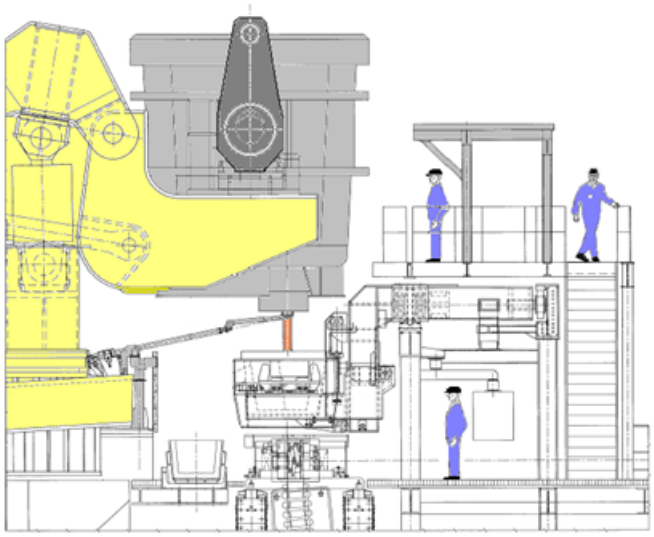

Figure 4.1: Schematic of the tower arm with the ladle in casting position

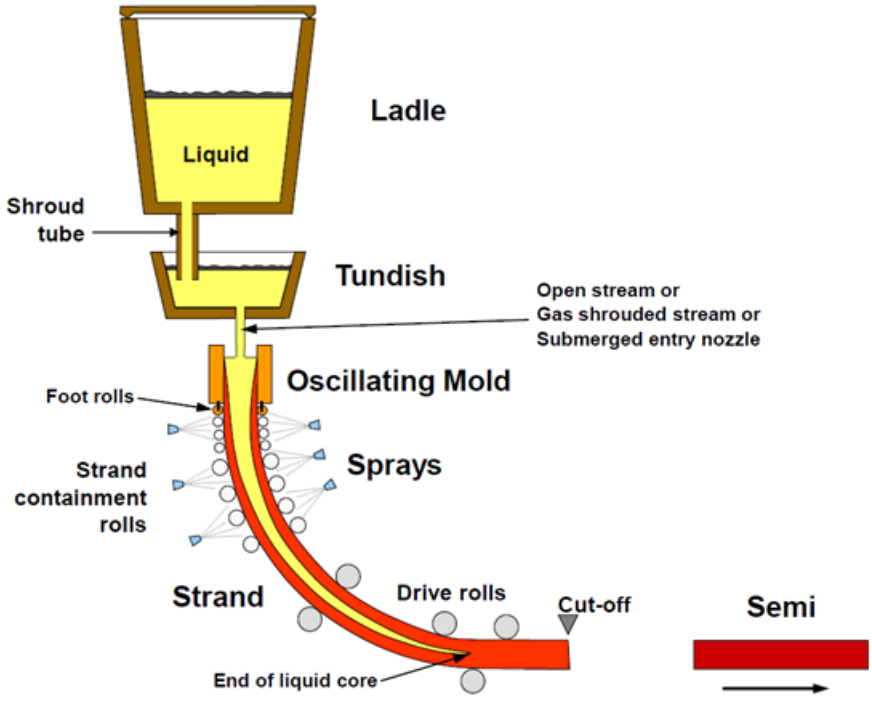


Figure 4.2: Continuous casting overview scheme [Brimacombe and Sorimachi, 1977b]

[Assunção et al., 2014].

### 4.1.1 Primary cooling phase

During the primary cooling phase, as liquid steel enters the mold, heat is transferred from the steel to the water that is used to cool the mold and flux powder is added to lubricate the mold walls.

Due to the high temperature of the environment (approximately 1500°C), the powder melts forming a layer of liquid mold slag between the mold and the steel. Subsequently, the mold slag infiltrates between the steel shell and the oscillating mold, creating a thin slag film that solidifies into glassy and crystalline phases. The properties of the slag film affect the strand lubrication and mold heat transfer. As the metal begins to solidify, the volume occupied by the material decreases leaving gap regions, which are filled with air. The cross-section of the product can be divided into three regions, the solid shell near the surface, the mushy zone (temperatures between the liquidus and the solidus temperatures), and the liquid in the center.

Figures 4.3 and 4.4 show schematic views of the primary cooling phase.

Mold powders are usually mixtures of several mineralogical components. The chemical composition of the mold powders has a strong effect on the stability of the continuous casting process at all casting speeds. The main functions of mold powders are to provide strand lubrication and to control the mold heat transfer in the horizontal direction between the steel shell and the copper mold [Kromhout, 2013]. Figure 4.5 shows a schematic representation of the different layers of the mold powder in the mold.

The heat transfer between the liquid steel and the water in the mold can be modeled using a common analogy with electric resistors. Each layer described before can be interpreted as thermal resistance and the heat flowing from the liquid steel needs to pass through all of these resistances as described in figure 4.6.

Improper cooling during this stage can lead to different types of issues. The most severe one is the rupture of the solidified skin which will cause a leak of liquid metal that can damage the mold and even cause explosions if it gets in contact with water. Other types of defects that might be generated during this stage are depressions, longitudinal mid-face cracks, longitudinal corner cracks, transverse mid-face, and corner cracks. 1

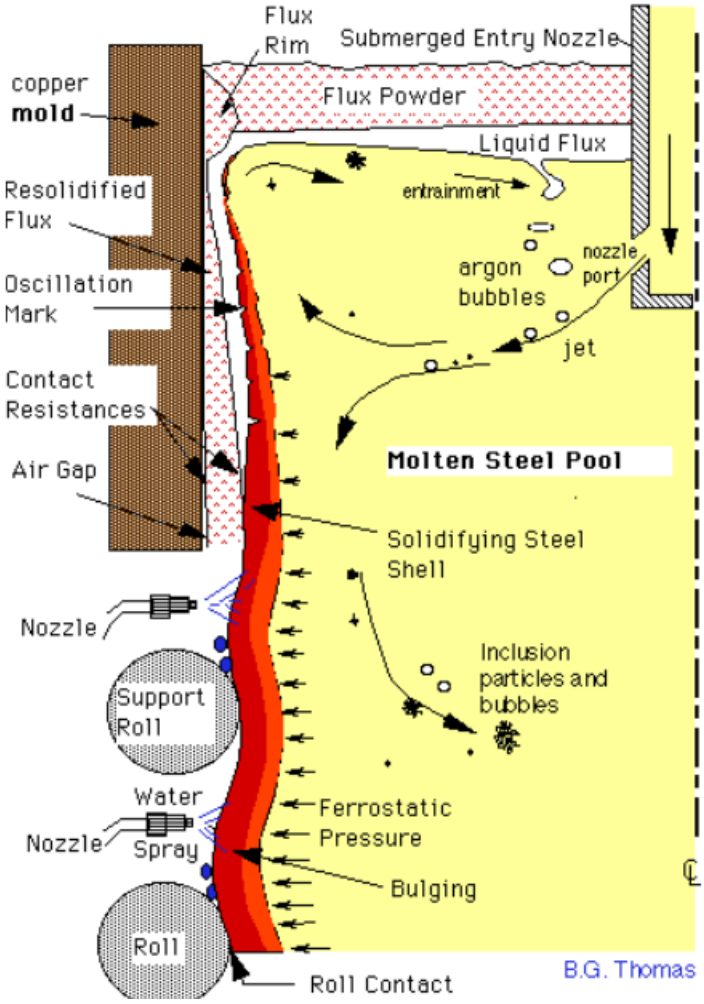


Figure 4.3: Continuous casting primary cooling phase [Thomas, 2003]

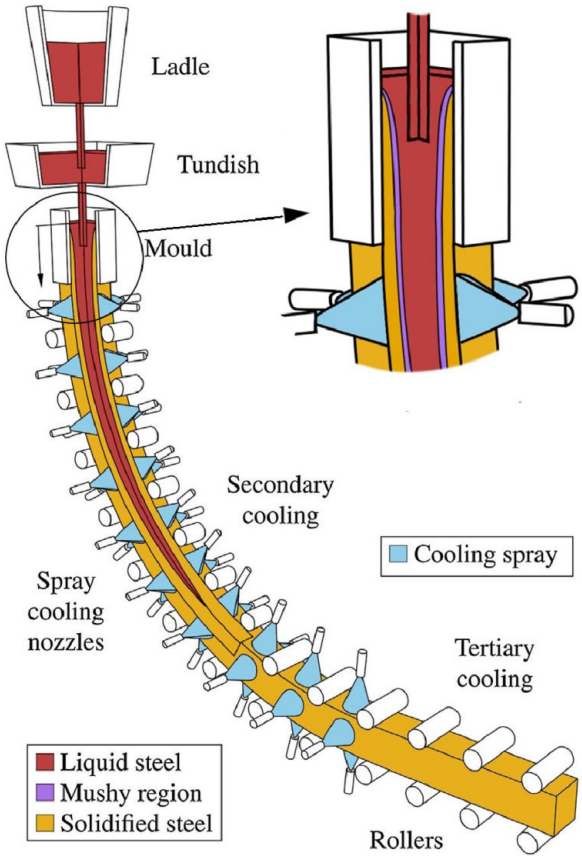


Figure 4.4: Schematic of a continuous caster [Brezina et al., 2021]

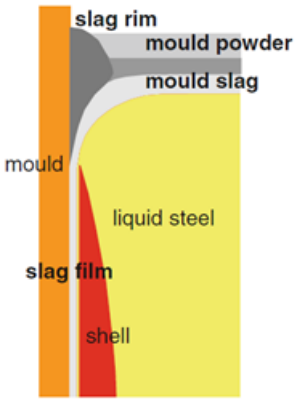


Figure 4.5: Schematic representation of mold powder [Kromhout, 2013]

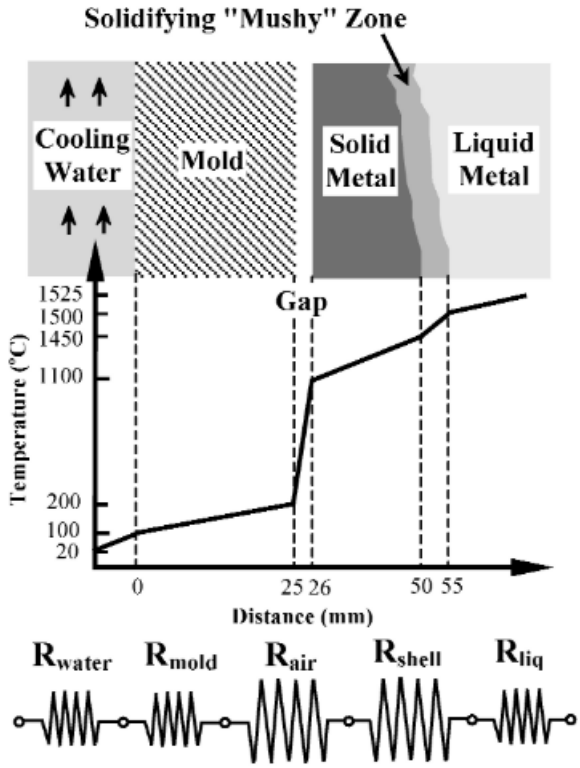


Figure 4.6: Heat transfer at the mold represented with the thermal resistances analogy [Sengupta et al., 2004]

### 4.1.2 Secondary cooling phase

After cooling in the mold, the steel is cooled by water or air/water sprays. There are cooling zones along the strand, this set is called secondary cooling. In this region, heat transfer phenomenon is composed of convection due to the water sprays, and conduction due to the roll contact, and radiation.

Inadequate cooling in the spray zone can also lead to defect formation. Figure 4.7 shows a scheme of cooling modes in the spray region. Undercooling, overcooling, and uneven heat transfer conditions, caused by the different heat transfer mechanisms, can aggravate previously generated defects in the mold or cause cracks and shape defects in the casting product.

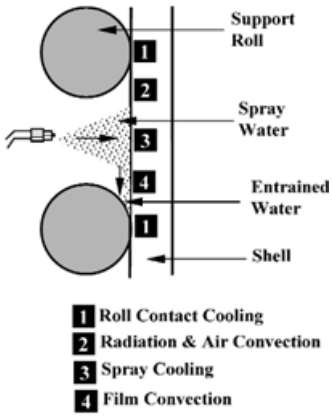


Figure 4.7: Schematic of the different cooling zones between the support foot rolls and spray nozzles [Meng and Thomas, 2003]

The cooling promoted by sprays is related to the type of spray used, the area wetted by the spray and can be affected by the water boiling regime. Water droplets from the spray nozzles strike the surface of the strand at high temperatures, vaporizing instantly and creating a boundary that blocks water contact with the strand surface, as shown in figure 4.8. Heat transfer tends to be higher in the central spray region, where water droplet has higher speed values and penetrates the vapor boundary, and the cooling rate increases with increasing water flow in the sprays.

The extraction of heat by the cooling water is very complex because it is governed by the water boiling phenomena, which depends highly on the temperatures, as shown in figure 4.9.

According to [Sengupta et al., 2005b], four mechanisms of heat transfer can be distinguished when the cooling water comes in contact with a hot surface:

- For temperature values lower than 100°C (convective cooling), heat transfer occurs by natural convection currents and the heat-transfer coefficient is very low.

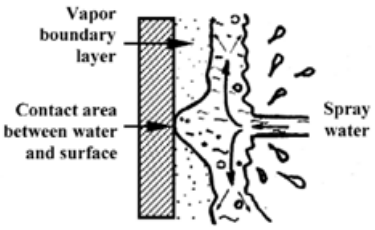


Figure 4.8: Detail of water spray-cooling process [Sengupta et al., 2005b]

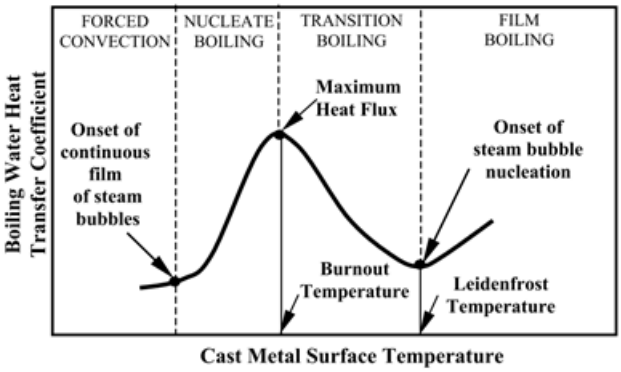


Figure 4.9: Water boiling curve [Sengupta et al., 2005b]

- For temperature values between 100°C and the burnout temperature (nucleate boiling), as the surface temperature increases, bubbles of water vapor form on the metal surface, break off and flow in the water film, eventually escaping from the free surface. The intensity of bubble formation and breakaway continues to increase as the surface temperature rises. This effect enhances the circulation in the water film causing the heat transfer coefficient to increase rapidly until it reaches a maximum (referred to as the burnout point). The burnout temperature is about 500°C to 700°C for steel and increases with increasing water flow rate.

- For temperature values between the burnout temperature and the Leidenfrost temperature (transition boiling), the bubbles start sticking to the metal surface and a layer of vapor begins to form, which reduces the heat transfer rate. The heat-transfer coefficient decreases sharply with increasing temperature, as the vapor film continues to cover more of the metal surface, with ever-decreasing amounts of metal surface exposed directly to water. When the metal surface is fully covered by a stable vapor film, the heat-transfer coefficient associated with the boiling curve reaches a minimum, which is referred to as the Leidenfrost point. The Leidenfrost temperature varies between 700°C and 1000°C for steel.

- For temperature values higher than the Leidenfrost point (film boiling), heat is transferred by conduction through the stable vapor film. The heat transfer coefficient does not change much with temperature and is very low compared to that at the burnout point.

Due to the strong relationship between the heat transfer coefficient and the surface temperature, heat extraction rates by secondary cooling can change rapidly with time and location near the Leidenfrost temperature.

High heat transfer rates associated with nucleate boiling can cause surface temperature to decrease rapidly. In contrast, the low heat transfer rates associated with film boiling can allow surface temperature to increase.

In addition to the strand surface temperature, other parameters affect the heat transfer in secondary cooling, such as water flow rate, type of spray nozzle and speed, size and angle of incidence of water droplets.

## 4.2 Quality issues and operational parameters

The internal and superficial qualities of the as-cast are fundamental for the performance of the product. [Szekeres, 2015] summarized the most relevant internal defects and grouped the probable causes for them. According to [Szekeres, 2015], the main defects are oxide-type nonmetallic inclusions, highly-localized segregation, cracks, and porosity. The factors responsible for these imperfections can be grouped into three areas:

- Causes associated with the preparation of the liquid steel and the fluid flow in the tundish.
- Factors related to the chemical composition of the steel. Higher levels of certain elements such as carbon, sulfur, phosphorus, aluminum, nitrogen, and niobium make steel more prone to quality problems.
- Problems arise from the interaction of the caster and the strand because the strand is solidifying while it moves through the caster. The solid steel layer is subjected to various stresses, mechanical and thermal. These stresses can generate quality problems such as cracks, surface bulging and skin breakout [Assunção et al., 2014].

  Mechanical stresses are generated by the following factors or a combination of them:

  1. Friction between the surface of the mold and the solid layer of the strand.
  2. Ferrostatic pressure.
  3. Misalignment of the rolls in the secondary cooling region.
  4. Bending and straightening [Prabhakar, 1980].

Thermal stresses appear due to intense temperature variations in the solidified layer. When there is a change in the rate of heat extraction on the surface, temperature gradients change rapidly, leading to thermal expansion and generating stresses in the solidified layer that can cause defects [Assunção et al., 2014]. Cracks are common defects and have been observed in different regions of the as-cast section, as described in figure 4.10, a schematic drawing showing different types of cracks in a bloom section, and figure 4.11, a cross-section schematic of cracks in a beam blank.

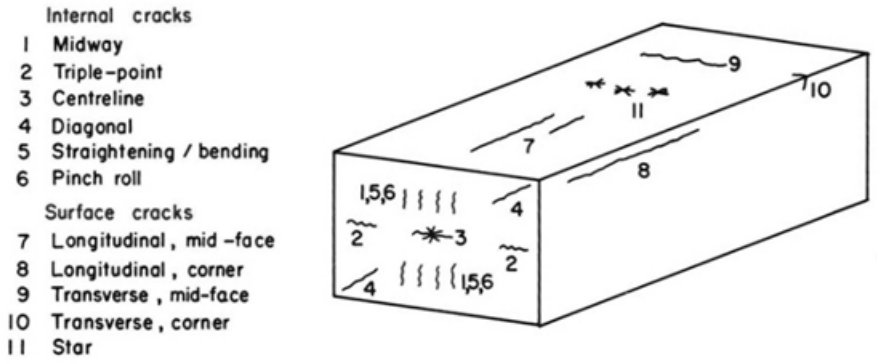


Figure 4.10: Different types of cracks in a bloom section [Brimacombe and Sorimachi, 1977a]

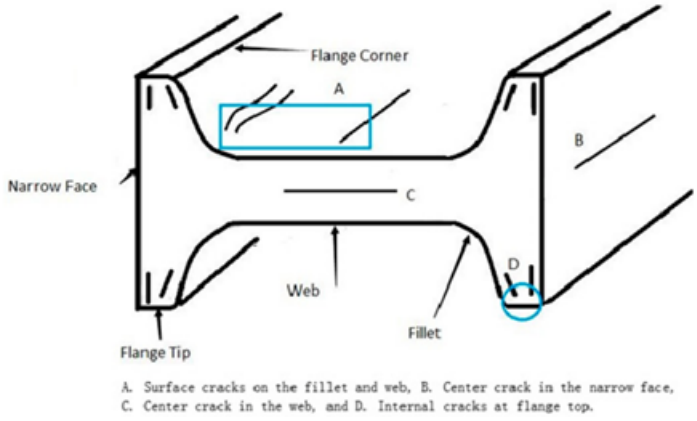


Figure 4.11: Different types of cracks in a beam blank section [Yang et al., 2018a]

As the raw material of H-beam production, the beam blank has the advantages of fewer rolling passes, high production capacity, low maintenance cost, and high product quality of the rolling material [Xu and Zhu, 2015], [Xu et al., 2010]. However, because of the complexity of its section, there are often more quality problems in the casting strand than with other blank types [Lee et al., 2000]. For any geometry, crack formation is associated with steel ductility, which is influenced by the temperature. There are three important zones of low ductility in steel. (1) The first zone is above 1200°C and is related to all internal cracks and surface longitudinal cracks. (2) The second zone is between 900°C and 1200°C and probably accounts for transverse surface cracks. (3) The third zone is between 600°C and 900°C and can contribute to the edge

crack formation at the straighter of the strand. Besides the influence of temperature, other characteristic parameters of casting influence the formation of internal and external cracks. Internal cracks have their formation influenced by chemical composition, as shown in the figure 4.12 and described by [Brimacombe and Sorimachi, 1977a].

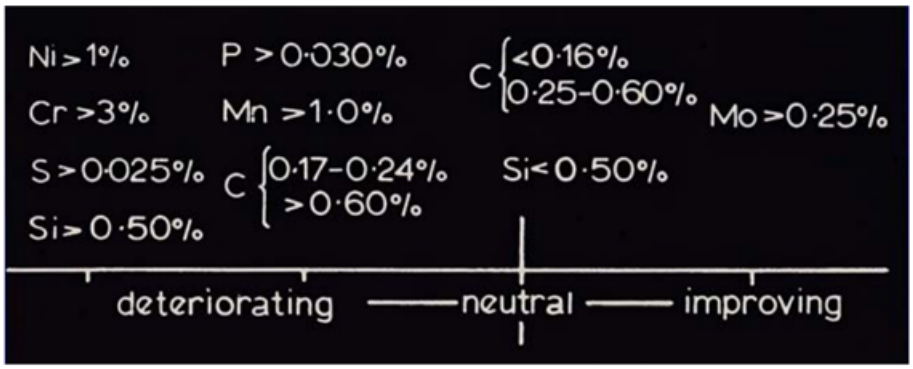


Figure 4.12: Alloy element effect on internal cracks
[Brimacombe and Sorimachi, 1977a]

As explained in the previous chapters, continuous casting involves several phenomena, so the mathematical modeling of this process is challenging as well as obtaining experimental data since it involves high temperatures and exposure to safety risks. In the next chapter, a review of the mathematical modeling works found in the open literature is presented.

## 4.3 Mathematical models for continuous casting

Mathematical models of the continuous casting process have been developed since the appearance of digital computers and have become more sophisticated over the years [Thomas, 2002]. The usage of these models enables engineers to analyze specific phenomena with fewer interventions in the production, as experiments can be replaced and supplemented by computer simulations. Some of the most common objectives when developing models for the continuous casting of steel are:

- Prediction of the temperature at the strand surface and its temporal and spatial gradients;
- Calculation of the thickness of the solidified shell and the stress levels in it;
- Evaluation of the strand deformation based on thermal contraction/expansion;
- Optimization of the operational parameters, such as water flow rate, casting speed, superheating, and mold powders properties. In these models that aim to optimize the process parameters, the outputs (total heat transfer, heat transfer rate, heat transfer uniformity,

von misses stress) calculated by the models are analyzed to achieve the best combination between the quality of the product and production rate.

- Process control using information from mathematical models running in real-time.

A mathematical model is a representation of a real-life system. The complexity of a model is defined not only by the complexity of the system being modeled but also by the purpose of such a model. A model should be as simple as possible, simplifications can and should be made if they do not introduce a loss of accuracy and do not lead to false conclusions. The determination of the mathematical equations to be used, and the boundary conditions to be considered will depend on the phenomena being studied, the casting equipment, the strand geometry, the model objectives, and the available computing power.

In the present work, thermo-mechanical models for blooms and beam blanks were developed to carry out a detailed analysis of the thermal profile and the stresses imposed on both geometries to verify the possibility of using the same support rollers configuration to cast both products.

In the next sections, mathematical models developed for continuous casting will be presented. The capabilities and limitations of existing models will be discussed. The approach chosen for the study of this work will be explained.

### 4.3.1 Heat transfer models

Mathematical modeling is usually divided into steps such as problem definition, determination of the equations that govern the phenomena to be studied, the definition of the domain, selection of the physical properties, and specification of the boundary conditions.

As described by [Patankar, 1980] and [Versteeg and Malalasekera, 2007] the heat transfer is governed by a general energy equation. The energy conservation equation can be written as a function of temperature in equation 4.1 or enthalpy in equation 4.2.

In the late 1960s and early 1970s, [Mizikar, 1970] and [Lait et al., 1974] pioneered the first finite-difference models of shell solidification. The models solve the following transient heat-conduction equation, subject to carefully chosen boundary conditions, by following a transverse slice through the shell as it travels downward at the casting speed [Thomas, 2002].

An important aspect of heat transfer modeling in continuous casting is the definition of the heat transfer directions that will be considered. This definition must be performed considering

the available computational capacity and the geometry of the shaft. The one-dimensional heat transfer approximation is reasonable when the temperature gradient in one direction is much greater than the temperature gradients in the other directions, as in thin slab casting. However, the consideration of two-dimensional heat transfer is more suitable in cases of casting billets or very thick slabs [Assunção et al., 2014].

$$\rho \frac{c_p^{eq} \partial T}{\partial t} = \frac{\partial}{\partial x}\left(k_{ef} \frac{\partial T}{\partial x}\right) + \frac{\partial}{\partial y}\left(k_{ef} \frac{\partial T}{\partial y}\right) + \frac{\partial}{\partial z}\left(k_{ef} \frac{\partial T}{\partial z}\right) + S \tag{4.1}$$

where: t – the time of simulation [s]; T – the temperature [$°C$]; $k_{ef}$ – the thermal conductivity [$W.m^{-1}.°C^{-1}$]; $c_p^{eq}$ – the equivalent heat capacity of steel [$J.kg^{-1}.K^{-1}$]; $\rho$ – the density of steel [$kg.m^{-3}$]; x, y, z – the direction of the coordinate system, along the transversal section [m]. S is the source term

The enthalpy formulation can be written as:

$$\rho \cdot \frac{dH}{dt} = \nabla k \cdot \nabla T \tag{4.2}$$

H is the enthalpy ($J.Kg^{-1}$)

During the continuous casting, there is the liquid-solid phase transformation that needs to be considered. The enthalpy formulation already includes latent heat associated with the phase transformation. This latent heat needs to be included in temperature formulation using either the source term or the equivalent specific heat methods [Assunção et al., 2014]. The source term method accounts for the effect of latent heat of fusion in the source term of the heat transfer equation.

The equivalent specific heat method considers the effect of latent heat of fusion by replacing the specific heat with an equivalent specific heat as shown in equation 4.3

$$c_p^{eq} = c_p + L_f \cdot \frac{df_l}{dT} \tag{4.3}$$

Many authors do not consider the heat conduction along the casting direction. This simplification is supported by the analysis of the Peclet Number that can be written as Equation 4.4:

$$Pe = \frac{\rho \cdot Cp \cdot v \cdot L}{k} \tag{4.4}$$

As explained by [Patankar, 1980] and [Versteeg and Malalasekera, 2007] the Peclet num-

ber is the ratio between convection and conduction heat flows. If the number of Peclet is very high, the effect of conduction is small compared to the effects of convection.

Equations 4.1 and 4.2 do not include the contribution of heat transfer associated with the movement of the liquid steel. To incorporate this contribution without modeling the liquid flow, one strategy commonly used is to artificially increase the value of the heat conductivity of the steel in the liquid and mushy regions, defining an effective heat conductivity according to equation 4.5 as described in [Wang et al., 2005].

$$k_{ef} = k[1 + (1 - C)f_l^2] \tag{4.5}$$

Where: - k is the thermal conductivity $[W.m^{-1}.K^{-1}]$; - C is a constant ranging between 5 and 10; - $f_l$ is the liquid fraction of the steel.

The liquid fraction can be calculated according to models of microsegregation based on the chemical composition of the steel using equilibrium or non-equilibrium approaches [Won et al., 2000]. The equilibrium approach is reasonable in the case of diffusion of interstitial elements, such as carbon. The liquid fraction is then calculated according to the lever rule, Equation 4.6.

$$f_l = \frac{(T_0 - T_L) - k(T_0 - T)}{(1 - k)(T_0 - T)} \tag{4.6}$$

$$k = \frac{C_{liq}}{C_{sol}} = \frac{T_0 - T_L}{T_0 - T_S} \tag{4.7}$$

Where: - $T_0$ is the melting temperature of pure iron [K], - $T_L$ is the liquidus temperature of the steel [K], - $T_S$ is the solidus temperature of the steel [K], - T is the temperature of the steel in the control volume [K], - $C_{liq}$ is the weight percentage of solute in the liquid phase [%], - $C_{sol}$ is the weight percentage of solute in the solid phase [%].

Other methods that could be used to evaluate the liquid fraction are Scheil, Clyne-Kurz Ohanaka and Brody Flemings. Scheil's model equation, shown in Equation 4.8 assumes no diffusion in the solid phase, complete diffusion in the liquid phase and a local equilibrium in the solid-liquid interface.

$$f_l = \frac{T_0 - T}{T_0 - T_L}^{\frac{1}{k-1}} \tag{4.8}$$

Brody and Fleming's model assumes complete diffusion in the liquid phase and incomplete back fusion in the solid phase.

$$f_l = 1 + \gamma k \cdot \frac{T_0 - T}{T_0 - T_L}^{\frac{1}{k-1}} \tag{4.9}$$

$$\gamma = \frac{D_{sol}}{V_{sol} L_p} \tag{4.10}$$

Where: $\gamma$ is the Brody-Fleming constant, $D_{sol}$ is the diffusion coefficient $[m^2 s^{-1}]$, $V_{sol}$ is the solidification speed $[ms^{-1}]$, $L_p$ is the mushy zone length.

To improve the Brody-Flemings method, Clyne-Kurz proposed replacing the Brody-Flemings solidification parameter ($\gamma$), by the Clyne-Kurz solidification parameter ($\Omega$) as shown in equation 4.11.

$$f_l = 1 + \Omega k \cdot \frac{T_0 - T}{T_0 - T_L}^{\frac{1}{k-1}} \tag{4.11}$$

Figure 4.13 shows the results obtained by [Won and Thomas, 2001] in the comparison among the lever rule, Scheil's rule, the Brody-Flemings method and the method of Clyne-Kurz in calculating the concentration of carbon in the liquid phase and at the interface between the liquid and solid phases of a steel with 0.13% of C. The lever rule and the Clyne-Kurz method showed very close microsegregation results. On the other hand, the Brody-Flemings method predicted a very low concentration of carbon, which is not physically reasonable. Scheil's rule overestimated carbon segregation since this rule neglects diffusion in the solid phase.

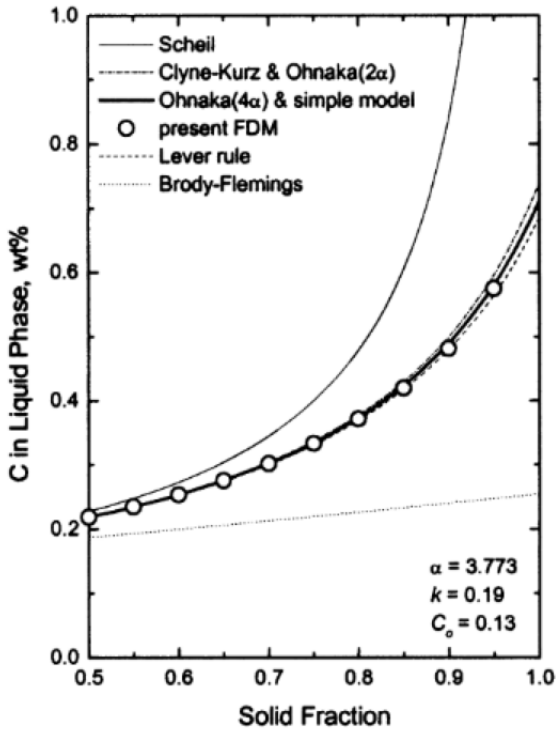


Figure 4.13: Comparison of carbon concentration in the liquid calculated by different approaches

### 4.3.2 Mechanical deformation models

All along the metal cooling tensions occurs due to the metal thermal contractions, ferrostatic pressure, steel phase transformations and contact with the support rollers. These stresses can contribute to defects in shape, cracks and the breaking of solidified skin. Thermal models have been developed for the solidification but then alone are not able to provide a complete understanding of the product quality [Thomas and Bellet, 2018]. To understand the deformations suffered by the solidified skin and the mechanisms of crack formation, an analysis of stresses and distortions is crucial. As explained by [Thomas and Bellet, 2018] the thermo-mechanical analysis is an enormous challenge due to a series of factors, among them:

- Many interacting physical phenomena are involved in stress-strain formation. Stress arises primarily from the mismatch of strains caused by large temperature gradients, and depends on the time and microstructure-dependent inelastic flow of the material.
- Predicting distortions and residual stresses in cast products requires calculations of the history of the cast product and its environment over huge temperature intervals. This makes the mechanical problem highly non-linear, involving liquid-solid interaction and complex constitutive equations. Even identifying the numerous metallurgical parameters involved in those relations is a daunting task.

- The coupling between the thermal and the mechanical problems is an additional difficulty. This coupling comes from the mechanical interaction between the casting and the mold components, through gap formation or the build-up of contact pressure, modifying locally the heat exchange. This adds some complexity to the non-linear heat transfer resolution.
- Accounting for the mold and its interaction with the casting makes the problem multidomain, usually involving numerous deformable components with coupled interactions
- Cast parts usually have very complex three-dimensional shapes, which puts great demands on the interface between CAD design and the mechanical solvers, and computational resources.
- The important length scales range from microns (dendrite arm shapes) to tens of meters (metallurgical length of a continuous caster), with a similar huge order-of-magnitude range in time scales.

One of the major difficulties in the thermomechanical analysis of casting processes is the concurrent presence of liquid, mushy and solid regions which move with time as solidification progresses. Several different strategies have been developed, according to the process and model objectives.[Thomas and Bellet, 2018]. One strategy consists in extracting the solidified regions of the casting domain based on the thermal analysis results. Then, a small-strain thermo-mechanical analysis is carried out on just this solid subdomain, using a standard solid-state constitutive model. Besides difficulties with the extraction process, especially when the solidified regions have complex unconnected shapes, this method may have numerical problems with the application of the liquid hydrostatic pressure onto the new internal boundary of the solidified region. However, this simple strategy is very convenient for many practical problems[Thomas and Bellet, 2018]. Other strategies are detailed by [Thomas and Bellet, 2018]. In this work, this was the strategy chosen due to a more simple implementation in the tool used to simulate the problem, ANSYS 17.1. The same strategy were used by [Sengupta et al., 2005a] and [Huespe et al., 2000]

Some publications study the mechanical interactions in continuous casting can (1) Mold Shrinkage phenomena (2) the Straightening process, where the formation of cracks may occur depending on the temperature, applied force value, additional stresses due to roller misalignment [Suzuki et al., 1982], [Fernandes Reis, 2012], [Fernandes, 2005] (3) soft reduction, which is used to improve the internal quality of the ingot material by the application of compressive force, (4) Bulging phenomenon, which is defined as the maximum deformation of the slab between the two casting rolls [Qin et al., 2019].

As explained by [Thomas and Bellet, 2018], the modeling of mechanical behavior requires the solution of 1) the equilibrium or momentum equations, relating force and stress; 2) the constitutive equations, which correlate stress and strain; and 3) compatibility equations,

connecting strain and displacement. This is because the boundary conditions specify either force or displacement at different boundary regions of the domain, Ω.

$$\nabla \cdot \sigma + \rho g - \rho \frac{dv}{dt} = 0 \tag{4.12}$$

where $\sigma$ is the stress tensor, $\rho$ is the density, g denotes gravity, v is the velocity field and $\frac{dv}{dt}$ denotes the total (particular) time-derivation.

In the solid state, metallic alloys can be modeled either as elastic-plastic or elastic-viscoplastic materials. In the latter class of models, one of the simplest is expressed as follows, but it should be mentioned that a lot of models of different complexity can be found in the literature

$$\{\epsilon\} = \{\epsilon^{el}\} + \{\epsilon^{pl}\} + \{\epsilon^{th}\} \tag{4.13}$$

where: $\{\epsilon\}$ - total deformation [%]; $\{\epsilon^{el}\}$ - incremental elastic strain component [%]; $\{\epsilon^{pl}\}$ - incremental plastic strain component [%]; $\{\epsilon^{th}\}$ - incremental thermal strain component [%].

The stress is related to the elastic strain by:

$$\{\sigma\} = [D]\{\epsilon^{el}\} \tag{4.14}$$

where: $\{\sigma\}$ - the stress vector; [D] - the elasticity or elastic stiffness matrix or stress-strain matrix.

$$\{\epsilon\} = \{\epsilon^{pl}\} + \{\epsilon^{th}\} + [D^{-1}]\{\sigma\} \tag{4.15}$$

where: $\{\epsilon\}$ - the total strain vector; $\{\epsilon^{pl}\}$ - plastic strain vector; $\{\epsilon^{th}\}$ - the thermal strain vector; $\{\epsilon^{th}\} = \Delta T[\alpha_x^{se}\alpha_y^{se}\alpha_z^{se}\ 0\ 0\ 0]^T$

$$[D]^{-1} = \begin{bmatrix} 1/E_x & -\nu_{xy}/E_x & -\nu_{xz}/E_x & 0 & 0 & 0 \\ -\nu_{yx}/E_y & 1/E_y & -\nu_{yz}/E_y & 0 & 0 & 0 \\ -\nu_{zx}/E_z & -\nu_{zy}/E_z & 1/E_z & 0 & 0 & 0 \\ 0 & 0 & 0 & 1/G_{xy} & 0 & 0 \\ 0 & 0 & 0 & 0 & 1/G_{yz} & 0 \\ 0 & 0 & 0 & 0 & 0 & 1/G_{xz} \end{bmatrix} \tag{4.16}$$

$\alpha_x^{se}$ is the secant coefficient of thermal expansion in the x direction.

The modeling may be including the mushy zone, but in the present work, the mushy zone will not be taken into consideration. Among the scientific publications related to mathematical modeling of steel continuous casting, there is the one developed by [Meng and Thomas, 2003], which consists of a model that includes a one-dimensional (1-D) transient finite-difference calculation of heat conduction within the solidifying steel shell coupled with a two-dimensional (2-D) steady-state heat conduction within the mold wall for steel slabs. The model was developed in FORTRAN and has a running time shorter than one minute on a personal computer. The model was verified by comparing to the analytical solutions to similar problems and simulation data presented in the literature. The validation was performed by the comparison of surface temperature measurements and the solidified skin thickness. In this case, the simplification for 1-D geometry contributes to a smaller run time without decreasing the model accuracy. This simplification is reasonable for the slab geometry because the heat is transferred preferentially in one direction [Assunção et al., 2014]. However, for thicker geometries such as blooms or not uniform geometries such as beam blanks this simplification cannot be applied.

The 2D approximation was adopted by [Hardin et al., 2003] to model the heat transfer and solidification of steel slabs. In addition, a microsegregation solidification model that approximates the effects of steel chemistry and cooling rate is incorporated into the model. Measured slab surface temperatures recorded from an operating caster were compared with predictions from the transient model. Another 2-D mathematical model of heat transfer and solidification for the continuous casting of cylindrical bars was developed by [Assunção et al., 2014] applying the non-uniform water distribution approach. The model was validated with surface temperature measurements of the steel in the industrial facility and with the experimental investigation of the heat transfer coefficients of the secondary cooling zone. The results of the uniform and non-uniform water distribution approaches were compared and showed that the non-uniform distribution approach is more representative to analyze the localized thermal phenomena and

that specific water flow distribution plays a more important role in the thermal behavior of steel than the total water flow. These works did not include the deformation suffered by strand casting. Those deformations were studied by [Chen et al., 2009], which developed a 2-D computational thermo-mechanical model for beam blank continuous casting using the software ANSYS to optimize beam blank operational parameters. The work had experimental validation and allowed control of the number of cracks in the cast material. When it comes to beam blanks, in the last decades the research has been concentrated on the thermal and mechanical behavior of the strand in the mold [Lee et al., 2000], [Yang et al., 2018b], [Kim et al., 1991], and few works had been done to analyze the solidification during the period of secondary cooling and the existing ones are focused on slab casting [Luo et al., 2012].

### 4.3.3 Boundary conditions

In this chapter, the boundary conditions used for modeling heat transfer and mechanical deformations in continuous casting will be exposed. In the thermal part, we will talk about boundary equations in all regions of the cooling. In the mechanical part, only the regions after the primary cooling, which was the focus of the present work, will be exposed.

**Heat Withdrawal in the Mold**

The heat transfer in the mold involves several thermal resistances from the shaft to the mold wall. Figure 4.14 shows a schematic view of the mold, the gap formed, the casting powder layer and the strand and each of them has a specific thermal conductivity The thermal conductivity of the air that fills the gap is the lowest of all and offers the highest thermal resistance.

The boundary condition in the mold can be heat flux from the strand to the mold wall. One way to obtain the heat flow in the mold is through the average heat flow. This technique is more suitable when you want to study the phenomenon in a global way because it does not represent the local flow of the mold regions [Assunção et al., 2014]. One way to model the heat exchange in the mold is using empirical equations related to the residence time of the as cast in the primary cooling regions. Figure 4.15 shows industrial data of the average heat flux data as a function of residence time. This technique was used by [Assunção et al., 2014] to model the cooling of round billets, [Liu et al., 2008] calculated the heat flux in a bloom mold and [Chen et al., 2009] who developed a 2-dimensional model for a beam blank also uses the residence time in the mold to calculate the heat flux.

Figure 4.17 was proposed by [Lait et al., 1974] for calculating heat flux as a function of

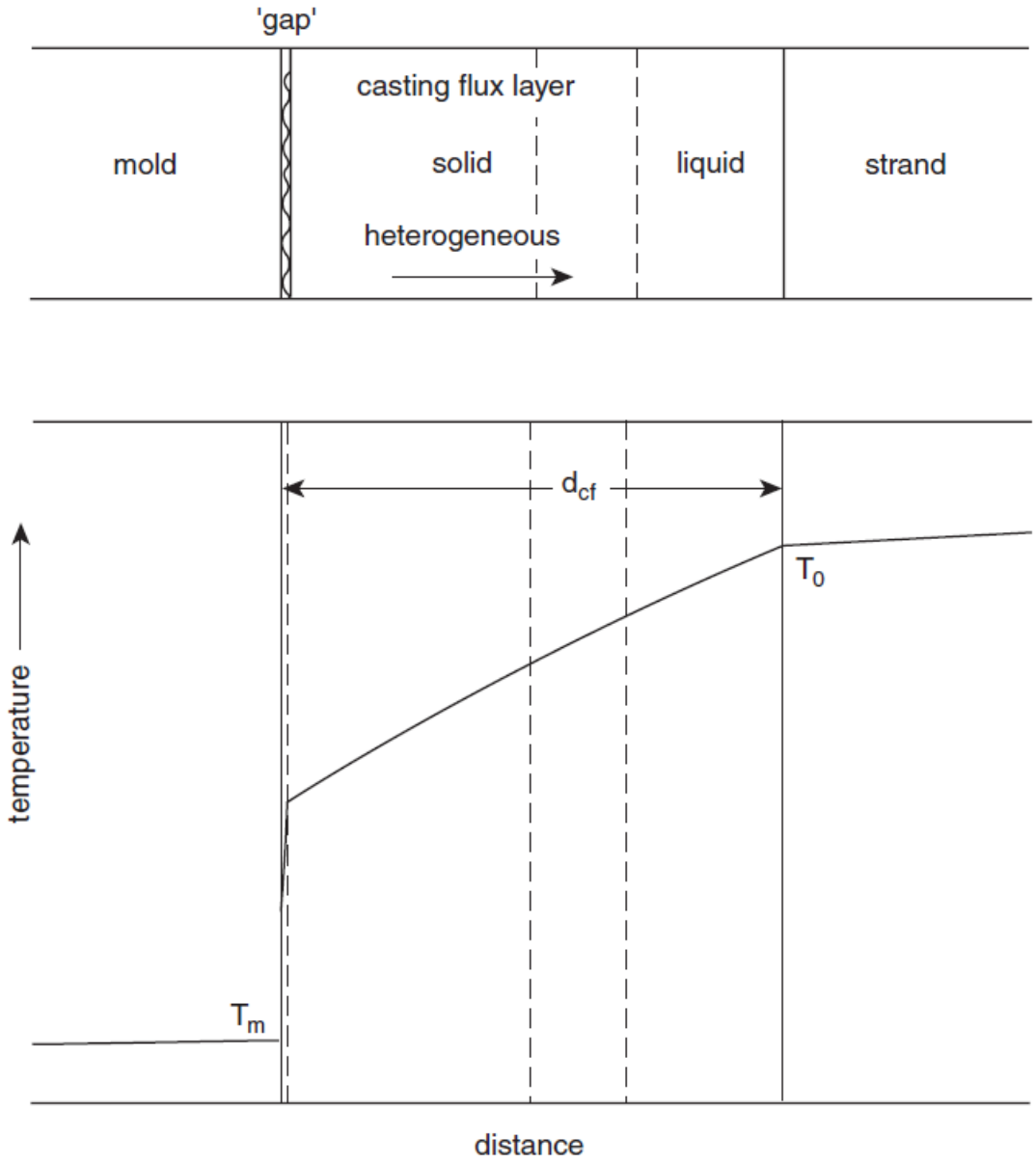


Figure 4.14: Schematic representation of casting flux layer between the surface of the strand and the wall of the mold, and temperature profile [Brimacombe and Sorimachi, 1977a]

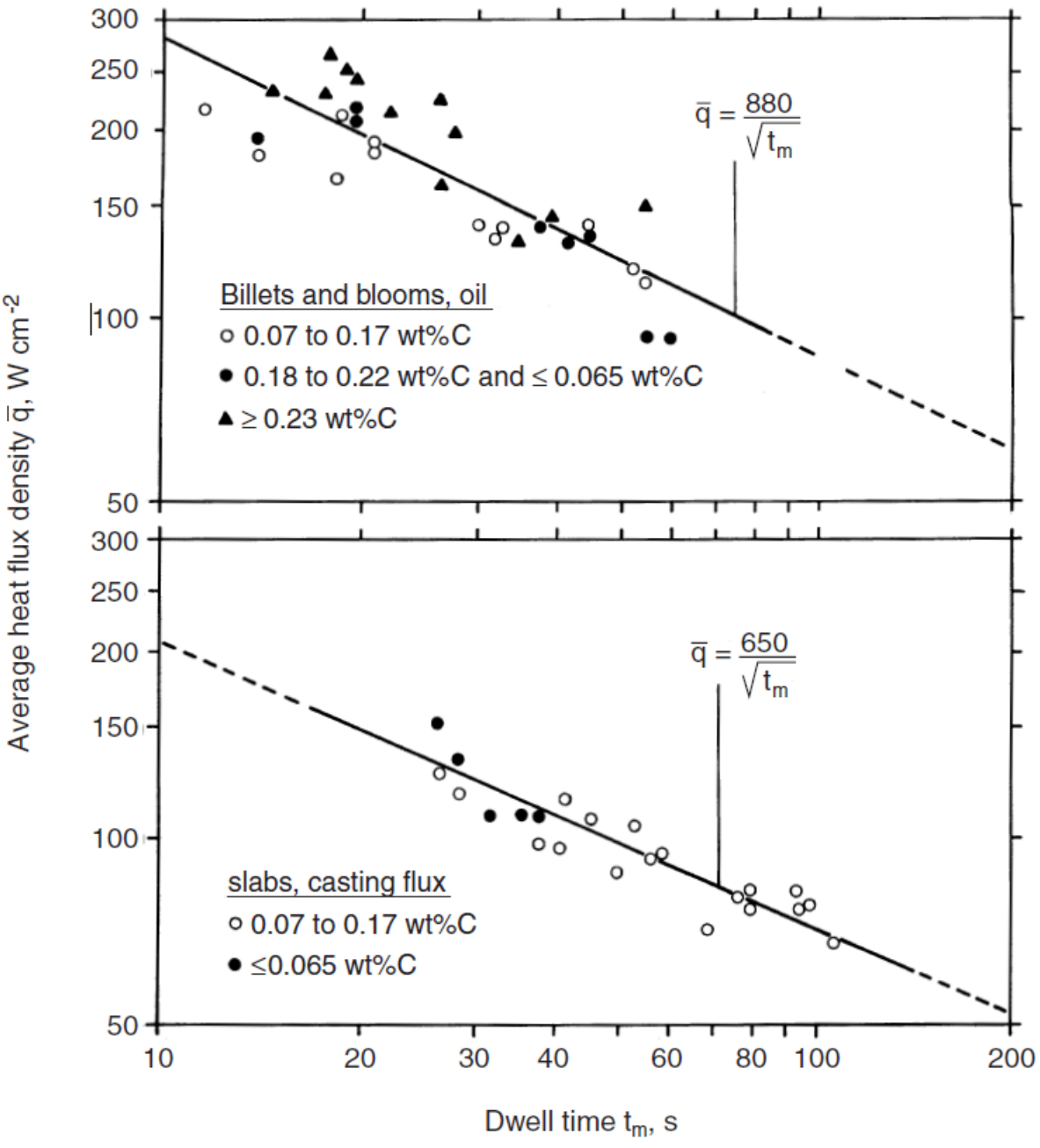


Figure 4.15: Plant data of average heat flux density in a mold as a function of dwell time [Brimacombe and Sorimachi, 1977a]

residence time

$$q_{mold} = 2.679 - 0.221\sqrt{t_m} \tag{4.17}$$

$q_{mold}$ is the average heat flux in the mold $t_m$ is the residence time in the mold

The residence time can be calculated as a ratio of the length of the mold and the casting speed, as shown in equation 4.18

$$t_m = \frac{L_m}{v} \tag{4.18}$$

Equations 4.19 and 4.20 show how [Liu et al., 2008] calculated the mold heat tranfer in a mathematical model developed for a bloom.

$$q_{mold} = 2680 - b\sqrt{\frac{L_m}{v}} \tag{4.19}$$

$$b = \frac{1.5(2680000 - q_*)}{\sqrt{\frac{L_m}{v}}} \tag{4.20}$$

[Chen et al., 2009] to calculate the heat flux in beam blank mold, equation 4.21

$$q_{mold} = 2688 - 227\sqrt{t_m} \tag{4.21}$$

When using the equations as a function of residence time, it is necessary to pay attention to the fact that they are empirical equations that may not apply in some processes, which makes it necessary to use correction factors. It is important to note that there are equations listed in the literature that can be used to calculate the heat flux in the mold, as can be seen in the book, [AISE Steel Foundation, 2003].

The choice of the appropriate equation to calculate the heat flux depends both on the focus of the study and on the instrumentation present in the plant that provides the data for the calculation. As in any stage of the development of mathematical models, it is important to verify and validate the results obtained.

**Heat and Mechanical Withdrawal in the Secondary Cooling**

The heat transfer in the secondary zone occurs due to radiation, spray cooling and contact with the support rolls as shown in figure 4.16.

The boundary condition is the heat transfer that can be described by equation 4.22:

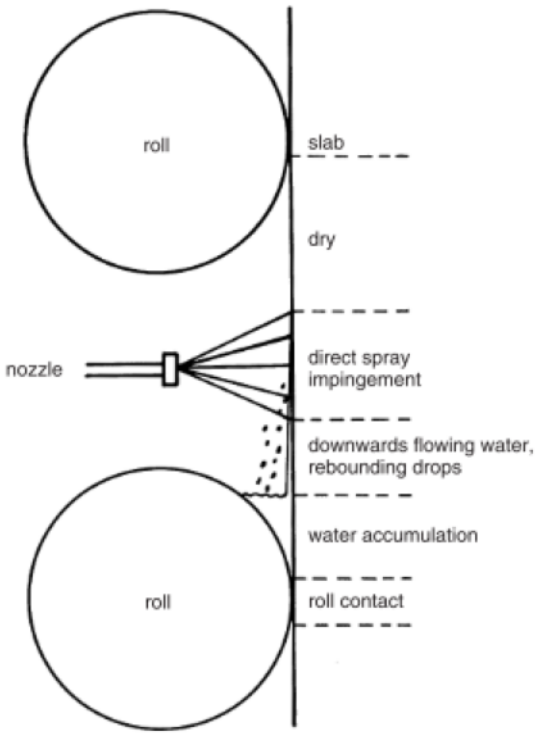


Figure 4.16: Regions with different heat transfer mechanisms between a roll pair in the spray zone of a slab caster [Brimacombe and Sorimachi, 1977a]

$$q = h_{roll}(T - T_{roll}) \tag{4.22}$$

Where: q - the heat flux due de contact with the roll $[W.m^{-2}]$, $h_{roll}$ - the heat transfer coefficient $[W.m^{-2}.°C^{-1}]$, and $T_{roll}$ - the roll temperature $[°C]$.

The heat flow in the spray region can be calculated using equations 4.23 and 4.24:

$$q = h_{spray}(T_s - T_w) \tag{4.23}$$

It is common to find in the literature equations that relate $h_{Spray}$– heat transfer coefficient in the spray cooling to $W$ – water flow rate density as shown in equation 4.24.

$$h_{spray} = aW^b \tag{4.24}$$

where: $h_{spray}$ – heat transfer coefficient in the spray cooling $[W.m^{-2}.K^{-1}]$; $T_s$ – the temperature in the strand surface $[°C]$; $T_w$ – the temperature of the water $[°C]$; $W$ – water flow rate density $[L.min^{-1}.m^{-2}]$; a, b – empirical constants dependent on the type of spray nozzle.

Figure 4.17 shows data of $h_{spray}$ as a function of water flux density

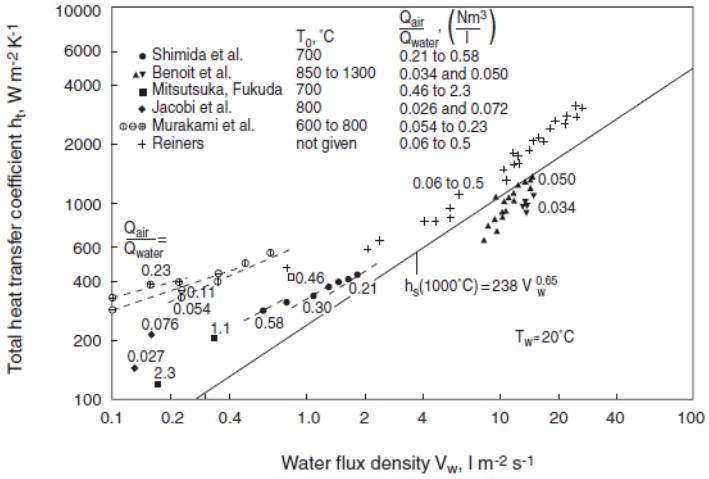


Figure 4.17: Data on heat transfer coefficient under air-water nozzles as a function of water flux density [AISE Steel Foundation, 2003].

$h_{Spray}$ is a variable that depends on the type of spray, the spray wet area and the distance from the spray nozzle to the surface to be cooled. Figure4.18 shows a variation of heat transfer coefficient with the position on sprayed targe

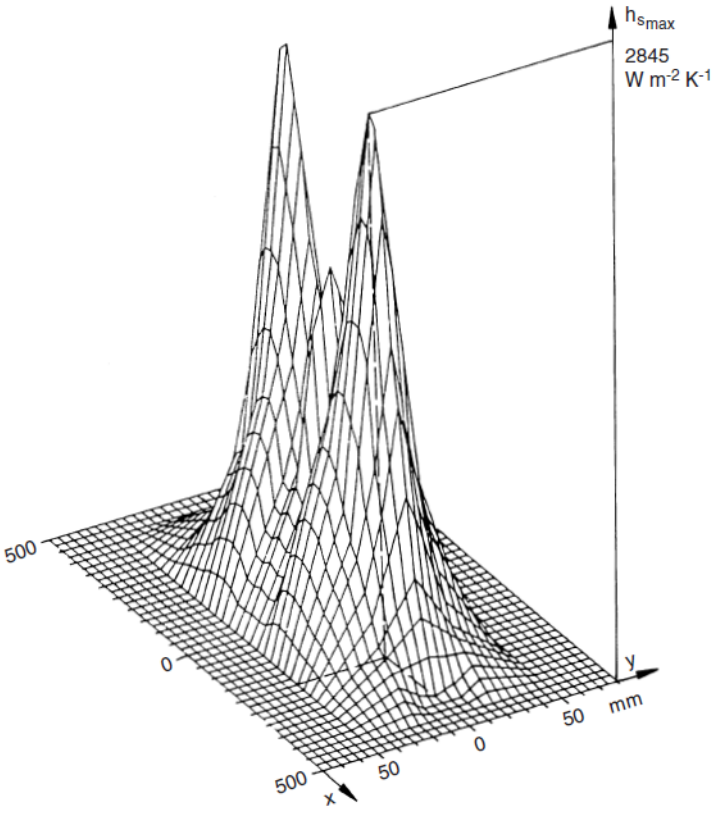


Figure 4.18: Variation of heat transfer coefficient with the position on a sprayed target. [AISE Steel Foundation, 2003]

The heat transfer coefficient varies within the region where the spray sprays water. The water distribution is not uniform and is an important factor to consider in secondary

cooling.[Assunção et al., 2014]

The $h_{Spray}$ can be estimated by spray nozzle tests,[Assunção et al., 2014], or calculated by direct or inverse methods using a series of measured temperature data.

The radiation heat flow zone can be calculated using equation 4.25:

$$q = \sigma\epsilon(T_s^4 - T_e^4) \tag{4.25}$$

where: $sigma$ – Stefan–Boltzmann constant; $\epsilon$ – emissivity; $T_e$ – temperature of the environment [°C]

As for the mechanical stress model for secondary cooling, it is important to understand that in this region the as-cast did not solidify completely and can be modeled as a shell whose thickness corresponds to the solidified skin in this region. The ferrostatic pressure exerted by the liquid portion inside the geometry is one of the forces that generate tension in the walls and can cause deformations. This pressure is the internal boundary condition and can be calculated using the equation 4.26:

$$P_f = \rho_{Steel} g H \tag{4.26}$$

where: $P_f$ – the ferrostatic pressure [Pa]; $\rho_{steel}$ – the steel density [$Kg.m^{-3}$]; g – the acceleration due to gravity [$m.s^{-2}$]; H – the distance from the meniscus [m].

The external boundary condition is the support rollers that hold the as-cast and react to the force caused by the ferrostatic pressure.

# 5. Paper I - Mathematical modelling of the continuous casting of blooms and beam blanks

Daniela Fátima Gomes*, Bernardo Martins Braga, Roberto Parreiras Tavares, Maurício Covcevich Bagatini

Metallurgical and Materials Engineering Department, School of Engineering, Federal University of Minas Gerais, Av. Presidente Antônio Carlos 6627, 31270-901 Belo Horizonte, Brazil.

*Corresponding author: danielafg05@gmail.com ORCID ID's: 0000-0002-0965-3847 (Fátima Gomes D.), 0000-0003-0634-5416 (Braga Martins B.), 000-0001-9348-2181 (Parreiras Tavares R.), 0000-0002-3986-9833 (Covcevich Bagatini M.)

## 5.1 Abstract

Defects and discontinuities generated in continuous casting are directly related to heat transfer during the process and the stresses to which the material is subjected. Knowledge of these phenomena is essential for both process safety and the quality of the final product. The aim of this work is to analyze the thermo-mechanical behavior of blooms and beam blanks during continuous casting. The continuous casting machine considered in this study is used to cast both blooms and beam blanks. The secondary cooling can be divided into cooling zone z0, cooling zone z1, cooling zone z2, and cooling zone z3. For each geometry, there are specific molds, z0, z1, z2 (sprays and support rollers), which need to be replaced when there is a geometry shift. The changing of the cooling segments brings security risks for the operators and reduces the continuous casting availability. Therefore, it is desired to have a common z2 for both blooms and beam blanks to reduce operational risk exposure and increase the machine production rate. For this to be possible, it is necessary to assess the temperature and resistance of the solidified skin, the effects of thermal stresses, ferrostatic pressure, and contact stresses. This work is the first step in this study. A thermo-mechanical model was developed for both geometries. The thermal model was verified by temperature measurement and shell measurements of blackouts. Finally, the results were analyzed and compared. Keywords: continuous casting, mathematical modeling, beam blanks and blooms.

## 5.2 Introduction

The continuous casting process is the most frequently used method to obtain as-cast products in the steel industry. The high productivity and potential to obtain different shapes are some of the advantages of this technique [Bobadilla et al., 1993]; [Thomas, 2002] [Vynnycky, 2018]. During this process, liquid steel is poured from a ladle to a tundish and then flows from the tundish to a copper mold which is cooled by water running in the interior of its walls. The material starts to solidify in the mold and, as it moves forward, the semi-solid as-cast enters the secondary cooling zone. There, a set of sprays sprinkles water onto its skin, creating a forced convection flow that accelerates the cooling process. By the time the material reaches the end of the machine, the solidification is complete, and the as-cast can be cut by the oxygen cutting machine.

During this process, the steel is supported by rolls that guide its trajectory until the transportation table. The position and size of the rolls are chosen to balance the mechanical forces and avoid geometry distortions that might lead to defects later in the process.

To model this process, many aspects need to be taken into consideration [Lee et al., 2000] [Mahapatra et al., 1991] [Schmidt and Josefsson, 1974]. The heat transfer, the phase change (liquid to solid) and the mechanical deformations due to the thermal tensions, ferrostatic pressure, contact between solid layer and foot rolls, and distortions in the as-cast because of the machine radius.

The relevant process parameters for these phenomena are steel superheat, water flow and pressure around the mold and in the spray nozzles, the casting powder, the casting speed, and the machine set up. The use of inappropriate process parameter values can cause breakouts, shape defects, and the formation of cracks.

The continuous casting machine considered in this study is used to cast both blooms and beam blanks. For each geometry, there are specific mold and secondary cooling setups (sprays and support rollers) which need to be replaced when there is a geometry shift. The changing of the cooling segments brings security risks for the operators and reduces the continuous casting availability. Therefore, it is desirable to reduce the need to exchange at least one of the segments. For this to be possible, it is necessary to know the phenomena involved and verify the interferences in the quality of the as-cast products. This paper describes the development of an integrated mathematical model of the heat transfer, solidification and, thermal tensions for the continuous casting process of blooms and beam blanks. The results of the computational simulations are discussed, and the particularities of each geometry analyzed.

## 5.3 Methodology

In this section a brief description of the casting machine will be presented, along with the numerical procedure, considerations made in the development of the models, boundary conditions, physical equations, steel physical properties, and the experiments for temperature measurement of the strand. Commercial software ANSYS CFX 17.1 and ANSYS 17.1 Mechanical were used to solve the thermal and mechanical equations.

### 5.3.1 Description of the machine

The present work was developed considering a continuous casting machine of blooms and beam blanks. This machine has four strands, and it can produce blooms of 300 mm × 450 mm and 300 mm × 350 mm and beam blanks of 400 mm × 480 mm × 120 mm. The primary cooling takes place in the mold, and secondary cooling takes place in the spray chamber which has four control zones (z0 to z3). Zones z0 to z2 are different for blooms and beam blanks and are changeable. Zone z0 is part of the mold set and contains the first set of sprays and rollers, Zone z3 is a common set up. In zones z0 and z3 there are water sprays, in zones z1 and z2, there are air mist sprays. Currently, Zone z3 remains inactive. After the spray chamber, blooms or beam blanks are straightened and cut. A representation of the machine, with the length of each control zone, can be seen in 5.1.

### 5.3.2 Heat transfer and the solidification model

A two-dimensional mathematical model of heat transfer, solidification, and thermal tensions of the blooms and beam blanks was developed. The main assumptions are listed below:

- heat transfer in the casting direction was neglected due to the high Peclet number;
- the latent heat of steel solidification was converted into an equivalent specific heat capacity in the mushy zone;
- the density and emissivity of the steel was considered constant whereas the heat capacity, thermal conductivity, were considered temperature-dependent;

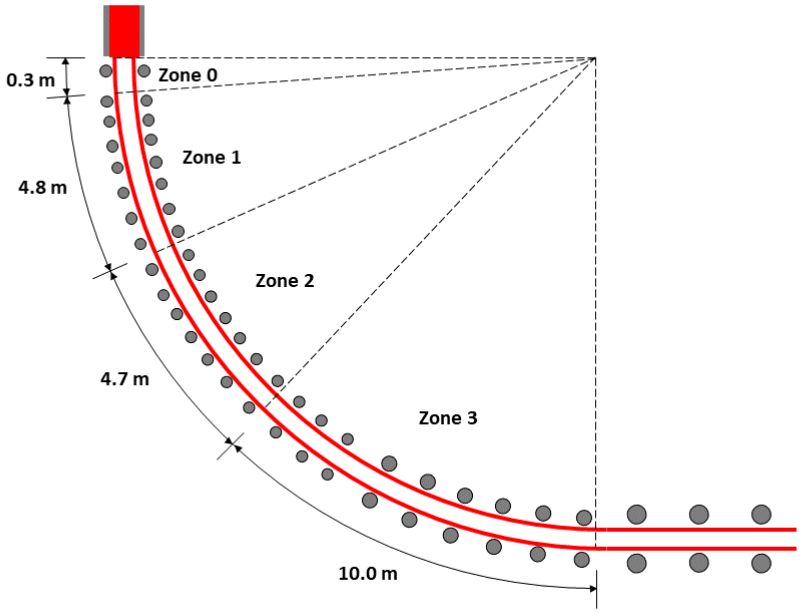


Figure 5.1: Continuous casting machine schematic

- the effects of strand shrinkage were neglected;
- the convective heat flow in the liquid pool and the mushy zone was accounted for the effective thermal conductivity [Ma et al., 2008].

The thermal model was based on the general energy equation during the unsteady state, as described 5.1:

$$\rho \frac{c_p^{eq} \partial T}{\partial t} = \frac{\partial}{\partial x}\left(k_{ef} \frac{\partial T}{\partial x}\right) + \frac{\partial}{\partial y}\left(k_{ef} \frac{\partial T}{\partial y}\right) + S \tag{5.1}$$

where: t – the time of simulation [s]; T – the temperature [$°C$]; $k_{ef}$ – the thermal conductivity [$W.m^{-1}.°C^{-1}$]; $c_p^{eq}$ – the equivalent heat capacity of steel [$J.kg^{-1}.K^{-1}$]; $\rho$ – the density of steel [$kg.m^{-3}$]; x,y – the direction of the coordinate system, along the transversal section [m].

### 5.3.3 Mechanical model

The structural mechanical model was developed in three dimensions for a one meter long as-cast piece. The simulations presented in this work were carried out for the zone z2 region, which is the zone where there is an interest in using a common segment for blooms and beam blanks. The main assumptions are listed below:

- the as-cast bloom and beam blank were considered flexible and the rollers rigid as it was interested in evaluating the deformations and stresses in those continuous casting geometries;
- unsteady state phenomena;
- friction contact between the rollers and the as-cast pieces;
- free rotation rollers.

The thermo-elastic–plastic material model, with bilinear isotropic hardening, was used to calculate the strain and stress distributions, which are important to provide information about the as-cast product quality, especially the occurrence of cracks. The total value of the deformation vector was calculated using 5.2, according to the Von Misses criteria as used by [Chen et al., 2009], [Liu et al., 2017], and [Zeng et al., 2020]. The influence of the ferrostatic pressure was also be taken into consideration.

$$\{\epsilon\} = \{\epsilon^{el}\} + \{\epsilon^{pl}\} + \{\epsilon^{th}\} \tag{5.2}$$

where: $\{\epsilon\}$ - total deformation [%]; $\{\epsilon^{el}\}$ - incremental elastic strain component [%]; $\{\epsilon^{pl}\}$ - incremental plastic strain component [%]; $\{\epsilon^{th}\}$ - incremental thermal strain component [%].

The stress is related to the elastic strain by:

$$\{\sigma\} = [D]\{\epsilon^{el}\} \tag{5.3}$$

where: $\{\sigma\}$ - the stress vector; [D] - the elasticity or elastic stiffness matrix or stress-strain matrix.

$$\{\epsilon^{el}\} = \{\epsilon\} - \{\epsilon^{pl}\} - \{\epsilon^{th}\} \tag{5.4}$$

$$\{\epsilon\} = \{\epsilon^{pl}\} + \{\epsilon^{th}\} + [D^{-1}]\{\sigma\} \tag{5.5}$$

where: $\{\epsilon\}$ - the total strain vector; $\{\epsilon^{pl}\}$ - plastic strain vector; $\{\epsilon^{th}\}$ - the thermal strain vector; $\{\epsilon^{th}\} = \Delta T[\alpha_x^{se}\alpha_y^{se}\alpha_z^{se}\ 0\ 0\ 0]^T$

$$[D]^{-1} = \begin{bmatrix} 1/E_x & -\nu_{xy}/E_x & -\nu_{xz}/E_x & 0 & 0 & 0 \\ -\nu_{yx}/E_y & 1/E_y & -\nu_{yz}/E_y & 0 & 0 & 0 \\ -\nu_{zx}/E_z & -\nu_{zy}/E_z & 1/E_z & 0 & 0 & 0 \\ 0 & 0 & 0 & 1/G_{xy} & 0 & 0 \\ 0 & 0 & 0 & 0 & 1/G_{yz} & 0 \\ 0 & 0 & 0 & 0 & 0 & 1/G_{xz} \end{bmatrix} \tag{5.6}$$

$\alpha_x^{se}$ is the secant coefficient of thermal expansion in the x direction.

$$\Delta T = T - T_{ref} \tag{5.7}$$

where: T the temperature in the point in question. $T_{ref}$ reference (strain-free) temperature (input).

### 5.3.4 Initial and boundary conditions

To obtain the solution for the differential equations, it is necessary to define the initial and boundary conditions. The temperature value in the mold was adopted as the initial condition.

$$T = T_0 \tag{5.8}$$

is the temperature of the liquid steel entering the mold. This temperature was assumed to be 1560°C. The heat flux is specified in the mold region. The heat flux in primary cooling can be calculated using 5.9, described by [Ji et al., 2016], [Lee et al., 1998], [Qin et al., 2019],

and [Assunção et al., 2014].

$$q = 268000 - 227\sqrt{\frac{L_m}{v}} \tag{5.9}$$

where: $L_m$ – effective length of mold [m]; v – casting speed $[m.min^{-1}]$; q – heat flux at the surface of the mold $[W.m^{-2}]$.

In the secondary cooling zone, heat is transferred mostly due to convection and radiation, due to the high temperature values of the strand. The heat flow in the spray region was be calculated using equations 5.10 and 5.10:

$$q = h_{spray}(T_s - T_w) \tag{5.10}$$

$$h_{spray} = aW^b \tag{5.11}$$

where: $h_{spray}$ – heat transfer coefficient in the spray cooling $[W.m^2.^{\circ-1}]$; $T_s$ – temperature in the as-cast surface $[^\circ C]$; $T_w$ – temperature of the water $[^\circ C]$; $W$ – water flow rate density $[L.m^2.min^{-1}]$; a, b – empirical constants dependent on the type of the spray nozzles. a=0.336 b=0.724 for air mist spray nozzle a=0.25 b=0.64, for the water spray nozzle. Those values were provided by the spray fabricant SMS group. Each spray was considered as an individual heat extraction source in the model developed.

The radiation heat flow zone was be calculated by 5.12:

$$q = \sigma\epsilon(T_s^4 - T_e^4) \tag{5.12}$$

where: $sigma$ – Stefan–Boltzmann constant; $\epsilon$ – emissivity; $T_e$ – temperature of the environment [°C].

The ferrostatic pressure exerted by the liquid portion inside the geometry is one of the forces that generate tension in the walls and can cause deformations. This pressure was calculated using the 5.13:

$$P_f = \rho_{steel} g H \tag{5.13}$$

where: $P_f$ – the ferrostatic pressure [Pa]; $\rho_{steel}$ – the steel density $[Kg.m^{-3}]$; g – the acceleration due to gravity $[m.s^{-2}]$; H – the distance from the meniscus [m].

To calculate this pressure, the as-cast geometry was considered as a solidified shell with a thickness equal to that calculated by the thermal model. The temperature profile was also imported from the thermal model. The interior is filled with liquid steel but to simulate the phenomenon of liquid pressure on the walls, this interior was considered as a void where the inner walls suffer a force in the axial direction. The strain free temperature is considered equal to solidus temperature.

$$T_{ref} = T_{solidus} = 1481°C \tag{5.14}$$

Both thermal and mechanical calculations are made by the Ansys software using the FEM method.

### 5.3.5 Physical properties of steel

The physical properties of the steel have a great influence on the predictions of the model and therefore must be carefully chosen to guarantee the accuracy of the solution. The properties considered in the simulations are shown in 5.1.

### 5.3.6 Experimental procedures

To verify the predictions of the models, experiments were carried out in the industrial plant to verify the surface temperature and the thickness of the solidified layer. The surface temperatures of the blocks and beam blanks were measured using a FLIR model FLIR E75 thermographic camera. The same method was used by [Ji et al., 2014] to validate a thermomechanical model for the soft reduction of a bloom. As the spray chamber is closed, measurements were taken after the straightener, where there are no sprays or water steam, and images can be taken with good resolution. The shell thickness was obtained by analyzing breakouts shells that occurred during operational problems in the casting of blooms and beam blanks. 5.2 and 5.3 show the occurrences of such incidents.

The thickness of the solidified layer was measured using a caliper. The measurements were made both down the mold narrow face and around the perimeter. The plant's supervisory system allows the collection of process parameters at the time of the occurrence of blackouts.

Table 5.1: Physical properties of the steel

| Parameter | Value |
|---|---|
| Density $[kg.m^{-3}]$ [Lee et al., 2000] | 7020 |
| Solidification latent heat $[J.kg^{-1}]$ [Lee et al., 2000] | 27200 |
| Solidus temperature [°C] | 1481 |
| Liquidus temperature [°C] | 1513 |
| Specific heat $[J.kg^{-1}]$ [Wang et al., 2005] | $481.8 + 0.19 \cdot T_{Steel}$ |
| Thermal conductivity $[W.m^{-1}.K^{-1}]$ | $15.9 + 0.11 \cdot T_{Steel}$ |
| Emissivity [Lee et al., 2000] | 0.8 |
| Young Modulus [GPa] [Kozlowski et al., 1992] | $968 - 2.33 \cdot T_{Steel} + 1.9 \cdot 10^{-3} \cdot T_{Steel}^2 - 5.18 \cdot 10^{-7} \cdot T_{Steel}^3$ |
| Poisson ratio | 0.3 |
| Friction coefficient [Qin et al., 2014] | 0.01 |
| Yield strength limit [Pa] | $6.62 \cdot 10^6$ |
| Shear modulus [Pa] | $4.6154 \cdot 10^9$ |

Figure 5.2: Solid shell of a bloom

Figure 5.3: Solid shell of a beam blank

Thus, to compare the measured data with the results of the models, the same parameters from the moment of the blackout were used. Skin breakages occur due to situations where the skin loses strength and which are not the ideal process, however the remaining skin can be used to validate heat transfer models [Meng and Thomas, 2003].

## 5.4 Results and discussion

In this chapter, the results of surface temperature, solid shell thickness, and stress due to the ferrostatic pressure, calculated by the computational model, will be presented. In the simulations shown, ASTM A572 steel (structural steel) was considered. This is the most frequently produced product and allows the collection of a considerable amount of experimental data. The casting conditions used in the simulations in this section are shown in 5.2.

### 5.4.1 Temperature profiles

5.4 and 5.5 show the locations and values of the temperatures of the bloom as a function of the distance to the meniscus. The results of the experimental measurements are also included in the figure and demonstrate the good agreement of the predictions and the experimental data. 5.6 and 5.7 depict similar results for the simulation of the casting of the beam blank.

Table 5.2: Casting conditions considered in the simulations.

| Variable | Bloom | Beam Blank |
|---|---|---|
| Casting speed $[m.min^{-1}]$ | 0.9 | 0.9 |
| Mold wide face water flow $[L.min^{-1}]$ | 1260.0 | 1620.0 |
| Mold narrow face water flow $[L.min^{-1}]$ | 720.0 | 820.0 |
| Superheat temperature $[°C]$ | 30.0 | 35.0 |
| Z0 total water flow $[L.min^{-1}]$ | 85.0 | 143.0 |
| Z1 total water flow $[L.min^{-1}]$ | 420.0 | 649.0 |
| Z2 total water flow $[L.min^{-1}]$ | 168.0 | 255.0 |

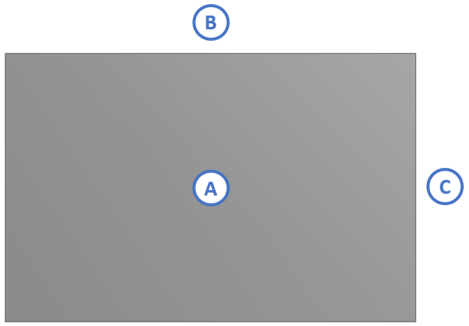


Figure 5.4: Bloom temperature profiles

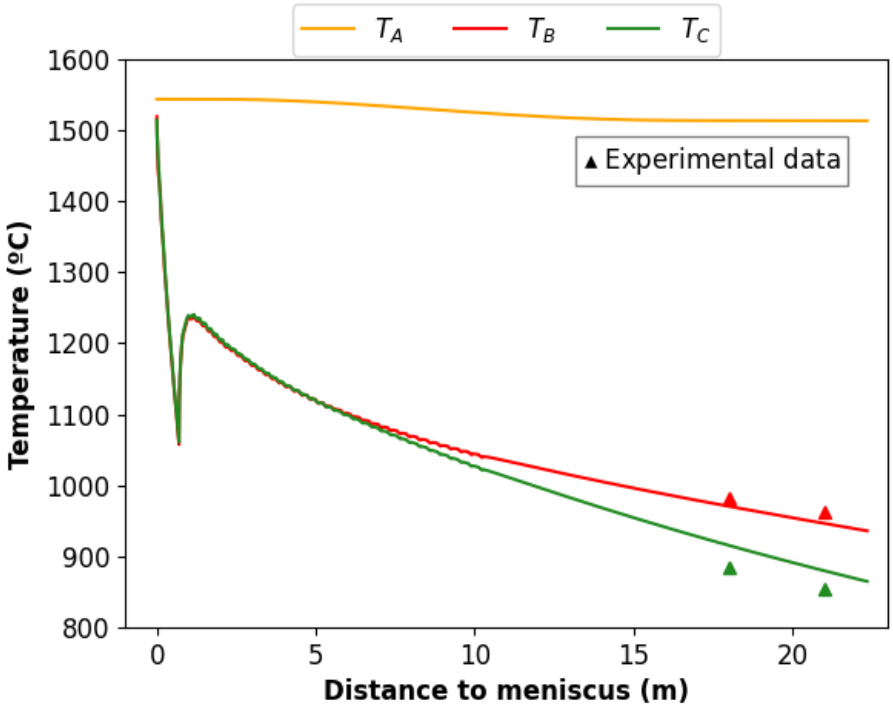


Figure 5.5: Bloom temperature profiles

The temperatures profiles are very similar to those found in the literature [Assunção et al., 2014], [Ohba et al., 2008]. The model was able to predict the temperature values in the wide face (B) and the narrow face (C), with an error of 1.5% and 3.3%, respectively. In the case of the wide face, the model predicts a lower temperature than the measurement with the thermographic camera. The measurement in this position has difficulties because it is not possible to be positioned exactly on the side of the as-cast ingot. This factor may have contributed to this difference. An improved analysis of radiation in the case of the beam blank will be implemented in the future.

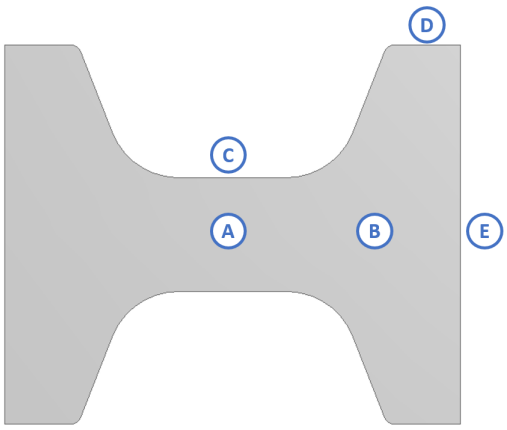


Figure 5.6: Beam blank temperature profiles

Due to the more complex geometry of the beam blank, the temperature profiles are shown

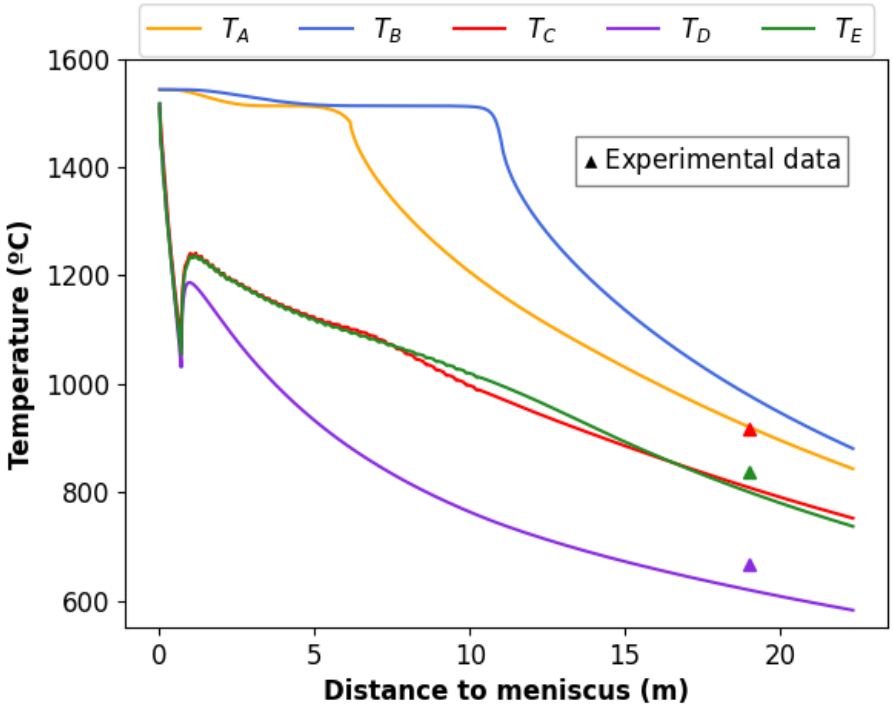


Figure 5.7: Beam blank temperature profiles

in a higher number of positions to improve the analysis. Similar to the bloom, the temperature profiles are similar results identified in the literature [Hibbeler et al., 2009] [Lee et al., 1998] [Xu et al., 2010]. The model predicted temperatures in positions C, D, and E with errors of 11.6%, 6.9%, and 4.5%, respectively. The beam blank model was less accurate than the bloom model, especially for the C point. In addition to the measurement difficulties, some considerations made in the present work regarding the casting of blooms are not entirely valid for a more complex geometry such as beam blanks, particularly the uniform distribution of water sprays and radiation between the curved region of the beam blank.

### 5.4.2 Solid shell

5.8 and 5.9 shows the solid shell thickness calculated by the computational model at the wide and narrow faces of the bloom and in the flange and web of the beam blank. The shell thickness calculated by the model was compared to the values obtained by measuring the pieces remaining from breakouts. Breakouts occurred at the beginning of the casting when conditions are different from the continuous process. However, there was a good concordance between the order of magnitude of the measured and calculated shell thickness.

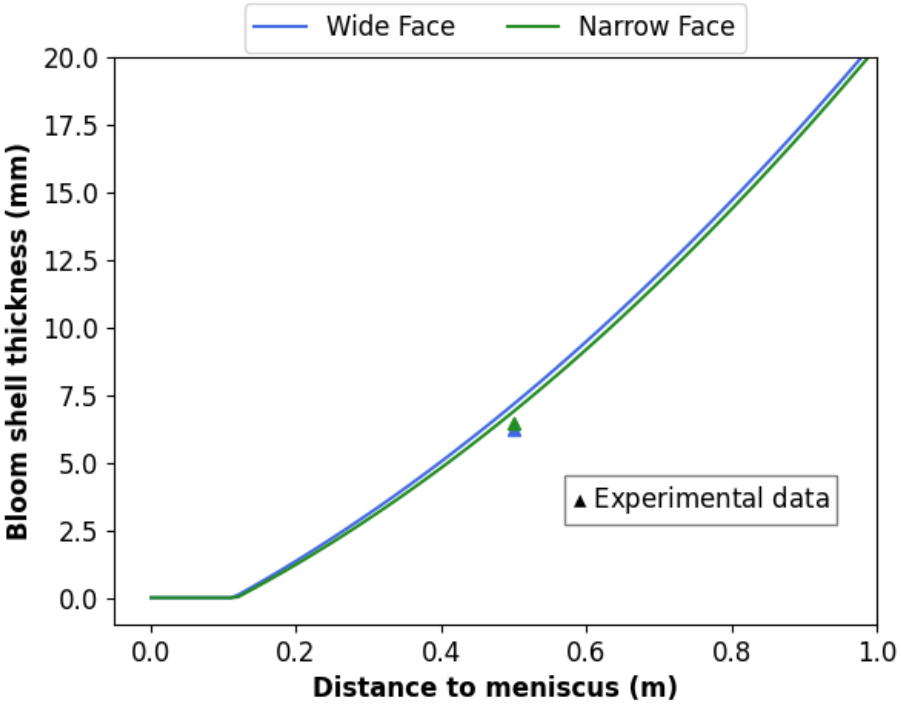


Figure 5.8: Bloom solid shell thickness

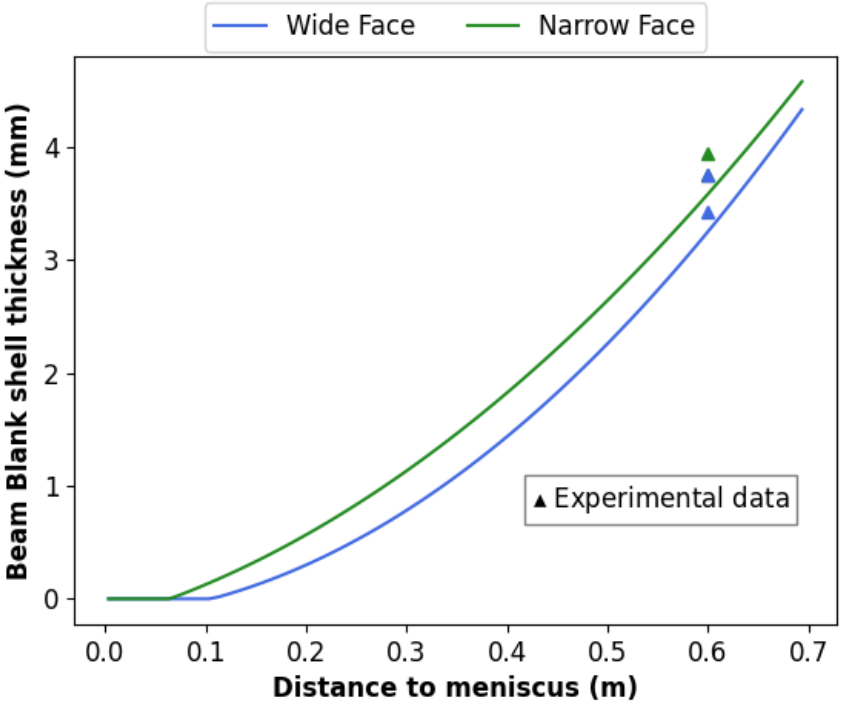


Figure 5.9: Beam Blank solid shell thickness

The model calculated the skin and obtained the following percentage errors: Bloom wide face 14.4%, Bloom narrow face 6.2%, Beam blank wide face 9.2%, Beam blank narrow face 7.0%

### 5.4.3 Stress calculations

One of the objectives of this work is to evaluate the possibility of using a common zone 2 for blooms and beam blanks. Thus, it is necessary to know the solidified shell thickness along this zone and the stresses involved considering the current assembly. Figure 6 illustrates the solidified shell of blooms and beam blanks in the current setup.

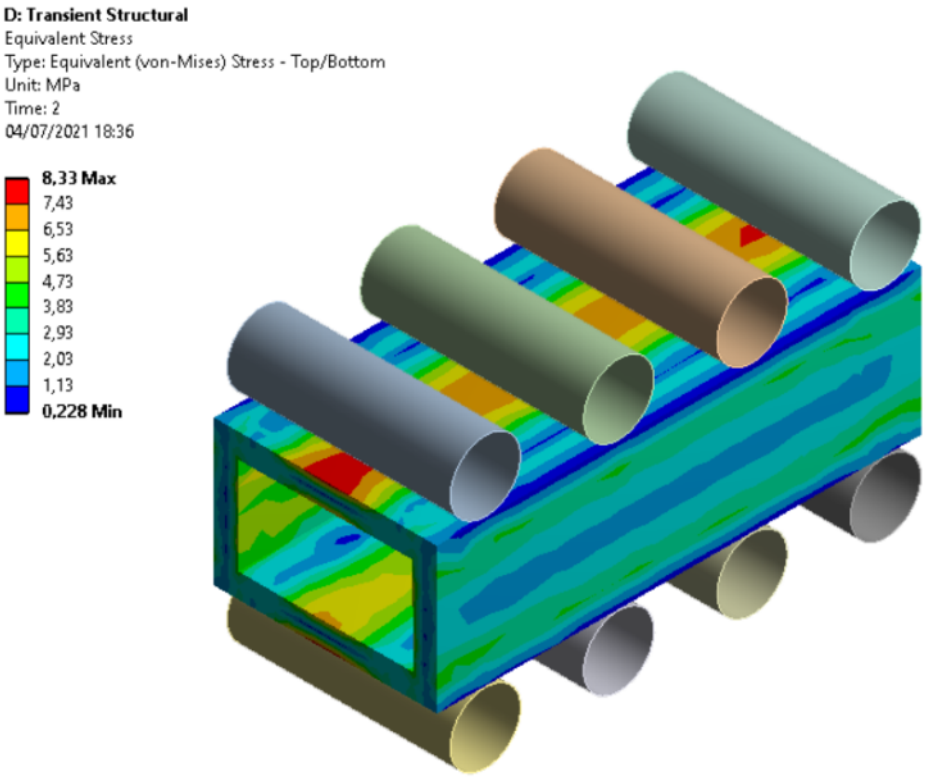


Figure 5.10: Bloomstress at the beginning of the secondary cooling zone

When observing the figures, it can be seen that the beam blank reaches higher stress values than the bloom. This is expected due to the complexity of the geometry. The highest value of stress observed in the beam blank occurs at the corner. The bloom has stress values around 4 MPa and the beam blank around 5.5MPa. Values close to the material yield stress limit even below it. Both geometries have regions where the stress was greater than the yield point. However, this is a small portion of the as-cast volume. A mechanical model was developed and

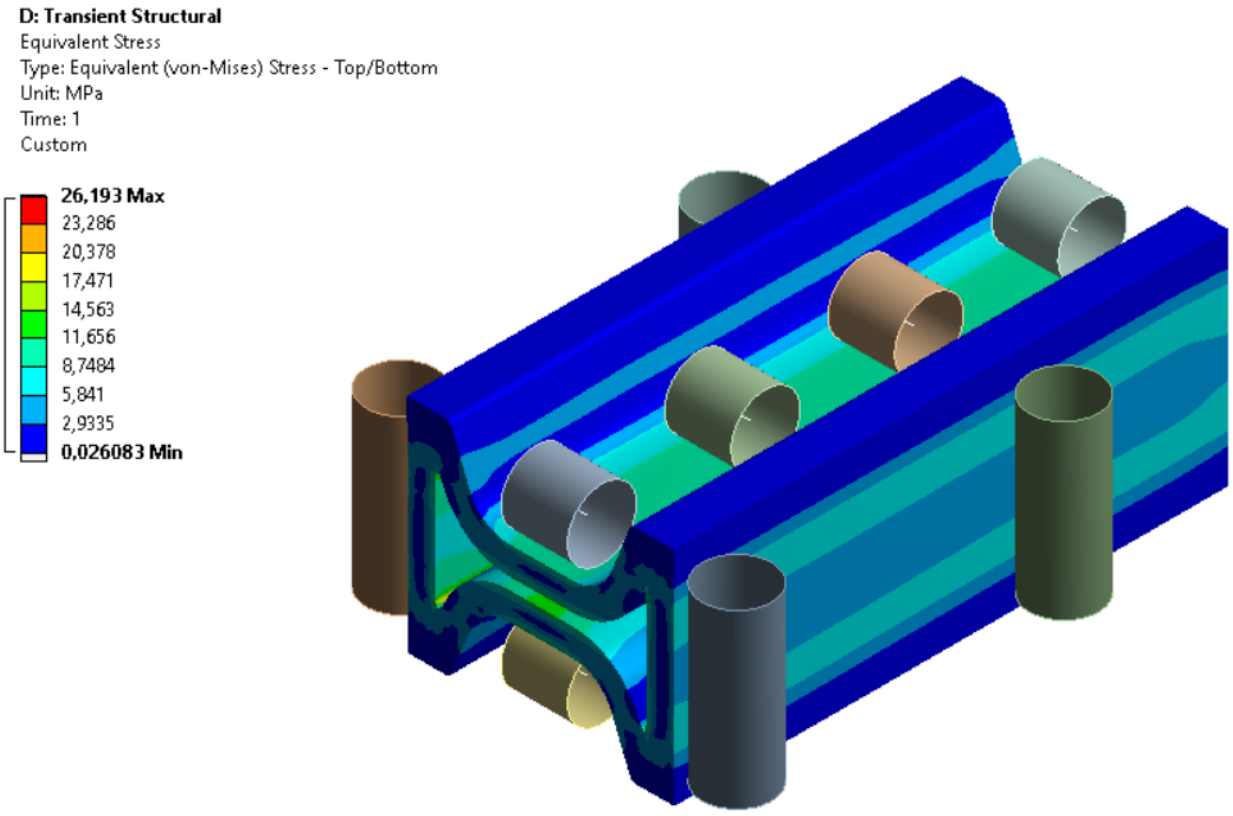


Figure 5.11: Beam blank stress at the beginning of the secondary cooling zone

permitted the analysis of the stresses involved in the casting process of blooms and beam blanks.

## 5.5 Conclusions

This paper describes the temperature profile and solid shell thickness of blooms and beam blanks. Some conclusions are:

- The model for the bloom could predict the temperature values in the wide face (B) and the narrow face (C), with an error of 1.5% and 3.3%. In the case of the wide face, the model is predicting a lower temperature than the measurement with the thermographic camera.
- The model for the beam blank predicted temperatures in positions C, D, and E with errors of 11.6%, 6.9%, and 4.5%, respectively. The beam blank model was less accurate than the bloom model, especially for the C point.
- The beam blank cools faster than the bloom for the same casting conditions.
- Some considerations made in this work do not affect a simple geometry as the bloom in the same way but can affect a more complex geometry such as beam blanks. For example, the uniform distribution of water sprays and radiation between the curved region of the beam blank.
- A mechanical model was developed and allowed to analyze the stresses involved in the casting process of blooms and beam blanks and the stress values in the cooling zone analyzed can reach the yield stress limit.

# 6. Paper II - Thermal behavior of blooms and beam-blanks during continuous casting: Development and validation of a mathematical model for heat transfer

Daniela Fátima Gomes*, Bernardo Martins Braga, Roberto Parreiras Tavares, Maurício Covcevich Bagatini, Carlos Berlini Filho, Gabriela Pereira Maciel

Metallurgical and Materials Engineering Department, School of Engineering, Federal University of Minas Gerais, Av. Presidente Antônio Carlos 6627, 31270-901 Belo Horizonte, Brazil.

*Corresponding author: danielafg05@gmail.com

ORCID ID's: 0000-0002-0965-3847 (Fátima Gomes, D.), 0000-0003-0634-5416 (Braga Martins, B.), 000-0001-9348-2181 (Parreiras Tavares, R.), 0000-0002-3986-9833 (Covcevich Bagatini, M.), 0000-0001-6640-3564 (Filho Berlini, C.), 0000-0002-3752-5148 (Maciel Pereira, G.)

## 6.1 Abstract

This work analyzes the thermal behavior of blooms and beam blanks during continuous casting. A 2D mathematical model of heat transfer was developed for both geometries and results were validated by breakout measurements, thermal imaging camera and embedded thermocouple tests. The same machine is used to cast both blooms and beam blanks. For each geometry, there are specific molds and segments (sprays and support rollers), which need to be replaced. The changing of these segments brings security risks and reduces the continuous casting availability. The model is used to simulate the influence of operational parameters on thermal and solidification profiles of the strand and was developed to study the behavior in secondary cooling, and thus be used to evaluate the possibility of producing both geometries with a common segment. It predicts the temperature profile and solidified shell thickness along the domain. Results are consistent with experimental data. The model was able to predict the solidified shell thickness within 5 mm and temperature within 70°C in the dry area. The

thermocouple experiments allowed the assessment of temperature values in the spray zone and improve the validation of the model.

Keywords: continuous casting, mathematical modeling, heat transfer, beam blank, bloom.

## 6.2 Introduction

To model heat transfer in the continuous casting process, many aspects need to be taken into account [Lee et al., 2000], [Mahapatra et al., 1991], [Schmidt and Josefsson, 1974]. In the secondary cooling zone, heat extraction occurs through three mechanisms: (1) forced convection by water and air-mist sprays, (2) conduction provided by contact with rolls, and (3) radiation due to the high temperature of the strand. The relevant process parameters for these phenomena are steel superheat, water flow rate, casting speed, and steel chemical composition. The use of inappropriate process parameter values can cause breakouts, shape defects, and the formation of cracks. Many works for continuous casting aim to optimize the operational parameters to minimize the occurrence of these defects [Chen et al., 2010], [Brezina et al., 2021], [Chen et al., 2009]. The model developed in this work can be used for this purpose, but the main goal of this research is to verify the possibility of manufacturing blooms and beam blanks with a common secondary casting configuration. No similar work has been found in the open literature. The continuous casting machine considered in the present study is used to cast both blooms and beam blanks and is described in a previous work [Gomes et al., 2021]. For each geometry, specific mold, and secondary cooling segments (sprays and support rollers) need to be replaced when there is a geometry change. The changing of the cooling segments brings security risks for the operators and reduces the continuous casting availability. Therefore, it is desired to have a common z2 for both blooms and beam blanks. The objective of the present work is to develop a mathematical model for the heat transfer in blooms and beam blanks to study the thermal behavior of both geometries in the secondary cooling zone, more specifically in z2, and finally, evaluate the possibility of casting blooms and beam blanks with this common zone. 2D thermal models were developed for both geometries to simulate them. Those models were validated with solidified shell thickness measurements from breakout shells, thermal imaging camera measurements and embedded thermocouple tests. No work was found in the open literature that aims to evaluate the possibility of having a common segment in the secondary cooling for blooms and beam blanks. Also, no results were found for model validation with an embedded thermocouple in a beam blank during secondary cooling.

## 6.3 Methodology

In this section, a brief description of the casting machine is presented, followed by a description of the mathematical model, including the numerical procedure, main physical equations, and thermo-physical properties of the steel. Next, the experiments performed to validate the heat transfer model are outlined. The commercial software ANSYS CFX 17.1 was used to solve the heat transfer equations.

### 6.3.1 Description of the machine

The present work was based on a continuous casting machine of blooms and beam blanks. This machine has four strands, a radius of 12m and it can produce blooms of 300mm × 450mm and 300mm × 350mm and beam blanks of 400mm × 480mm × 120mm. The primary cooling takes place in the mold while the secondary cooling takes place in the spray chamber which has four control zones (z0 to z3). Zones z0, z1 and z2 are different for blooms and beam blanks and are changeable. Zone z0 is part of the mold set and contains the first set of sprays and rollers, zone z3 has a common setup for both geometries. In zones z0 and z3 there are water sprays, and in zones z1 and z2, there are air mist sprays. Currently, the zone z3 sprays are inactive. But there are air sprays that are directed to the region of the internal radius, whose function is to disperse the water that may be trapped in the wide face of the bloom or the beam blank web. When the operational team observes the presence of accumulated water, these air sprays are switched on. This water accumulation tends to be more pronounced in the beam blank due to its 'H' shape. After the spray chamber, blooms or beam blanks are straightened and cut. A representation of the machine is shown in figure 6.1.

### 6.3.2 Heat transfer and solidification model

A two-dimensional transient mathematical model of heat transfer and solidification of blooms and beam blanks was developed in the previous work [Gomes et al., 2021]. Modifications were introduced to improve the accuracy of the model, including the incorporation of emissivity as a function of the temperature, the consideration of heat exchanged through

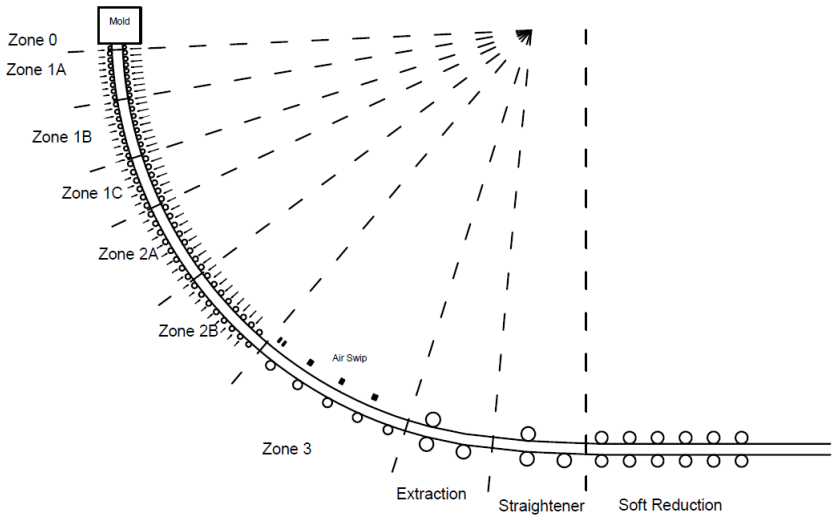


Figure 6.1: Schematic view of the continuous casting machine

radiation between the beam blank flanges, and the evaluation of the heat extraction in the region of contact with the rolls. The main assumptions are listed below: This model considers a slice of the strand geometries that moves along the machine according to the casting speed [Gomes et al., 2019], [Assunção et al., 2014], [Zhao et al., 2014]. Heat transfer by conduction in the casting direction was neglected due to the high Peclet number [Patankar, 1980], [Versteeg and Malalasekera, 2007]. The Peclet number is close to 900 for both geometries. The latent heat of steel solidification was modeled increasing the specific heat capacity in the mushy zone. The density of the steel was considered constant while the heat capacity, emissivity and thermal conductivity were considered temperature-dependent. The effects of strand shrinkage were neglected. The convective heat flow in the liquid pool and the mushy zone was accounted for through an effective thermal conductivity [Ma et al., 2008]. The thermal model was based on the general energy equation for unsteady-state heat transfer in two dimensions, as described by equation 6.1:

$$\rho \frac{c_p^{eq} \partial T}{\partial t} = \frac{\partial}{\partial x}\left(k_{ef} \frac{\partial T}{\partial x}\right) + \frac{\partial}{\partial y}\left(k_{ef} \frac{\partial T}{\partial y}\right) \tag{6.1}$$

where: t – the time of simulation [s]; T – the temperature [$^{\circ}C$]; $k_{ef}$ – the thermal conductivity [$W.m^{-1}.^{\circ}C^{-1}$]; $c_p^{eq}$ – the equivalent heat capacity of steel [$J.kg^{-1}.K^{-1}$]; $\rho$ – the density of steel [$kg.m^{-3}$]; x,y – the direction of the coordinate system, along the transversal section [m].

In the secondary cooling zone, heat is transferred mostly due to convection (area C), contact with the support rolls (area B), and radiation due to the high-temperature values of the strand (area A). Figure 6.2 shows a schema of the cooling phenomena in the spray chamber.

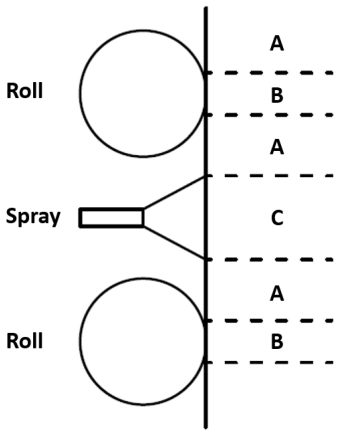


Figure 6.2: Schematic of the secondary cooling system

Equation 6.2 shows the heat flux calculation that describes the boundary conditions due to the roll contact:

$$q = h_{roll}(T - T_{roll}) \tag{6.2}$$

Where: q - the heat flux due de contact with the roll $[W.m^{-2}]$, $h_{roll}$ - the heat transfer coefficient $[W.m^{-2}.°C^{-1}]$, and $T_{roll}$ - the roll temperature $[°C]$.

The heat flow in the spray region was calculated using equations 6.3 and 6.4:

$$q = h_{spray}(T_s - T_w) \tag{6.3}$$

$$h_{spray} = aW^b \tag{6.4}$$

where: $h_{spray}$ – heat transfer coefficient in the spray cooling $[W.m^{-2}.K^{-1}]$; $T_s$ – the temperature in the strand surface $[°C]$; $T_w$ – the temperature of the water $[°C]$; $W$ – the water flow rate density $[L.min^{-1}.m^{-2}]$; a, b – empirical constants dependent on the type of spray nozzle. For the air-mist type, a=238 and b=0.65; for the water type, a=23.3 b=0.65.

Each spray was considered as an individual heat extraction source in the model developed. The radiation heat flow zone was calculated using equation 6.5:

$$q = \sigma\epsilon(T_s^4 - T_e^4) \tag{6.5}$$

where: $sigma$ – Stefan–Boltzmann constant $[W.m^{-2}.K^{-4}]$; $\epsilon$ – emissivity; $T_e$ – temper-

ature of the environment [°C].

Radiation between the flanges of the beam blank was modeled using the Mont Carlo method and the surfaces involved were treated as gray bodies. Figures 6.3 and 6.4 show a scheme of the radiation in bloom and beam blank, where is possible to visualize the radiation between beam blank flanges.

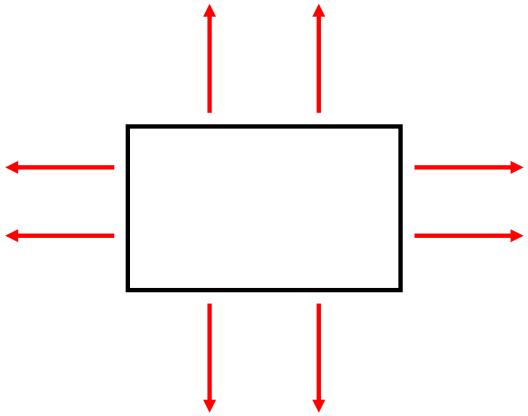

Figure 6.3: Schematic view of the radiation heat transfer in blooms

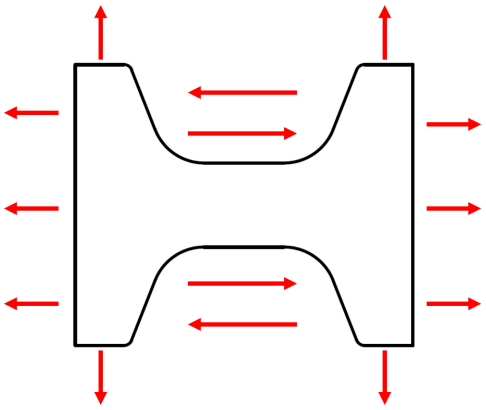

Figure 6.4: Schematic view of the radiation heat transfer in beam blanks

A grid independence study was performed to ensure consistent results and reasonable simulation times. The bloom's mesh contains 50566 nodes and 24960 elements, and the beam blank's mesh has 122534 nodes and 60768 elements. The physical properties of steel, cooling water, and contact rollers considered in the simulations are shown in table 6.1.

Table 6.1: Physical properties of the steel

| Parameter | Value |
|---|---|
| Density $[kg.m^{-3}]$ [Lee et al., 2000] | 7020 |
| Solidification latent heat $[J.kg^{-1}]$ [Lee et al., 2000] | 272000 |
| Solidus temperature [K] | 1754.15 |
| Liquidus temperature [K] | 1786.15 |
| Specific heat Liquid steel $[J.kg^{-1}]$ [Bergman et al., 2011] | 824.6157 |
| Specific heat $[J.kg^{-1}]$ [Wang et al., 2005] | $481.8 + 0.19 \cdot T_{Steel}$ |
| Thermal conductivity $(T >= T_{Peritetic})$ $[W.m^{-1}.K^{-1}]$ [Mills et al., 2016] | $20.4 + 0.009\dot{T}_{Steel}$ |
| Thermal conductivity $(T < T_{Peritetic})$ $[W.m^{-1}.K^{-1}]$[Mills et al., 2016] | $21.6 + 0.008 \cdot T_{Steel}$ |
| Thermal conductivity Liquid steel $[W.m^{-1}.K^{-1}]$ [Bergman et al., 2011] | 39.0 |
| Emissivity [Wang et al., 2012] | $T_{Steel}/1000 \cdot (0.25 \cdot T_{Steel} - 0.38) + 1.1$ |
| Specific heat of the water $[J.kg^{-1}.K^{-1}]$[Bergman et al., 2011] | 4184 |
| Water temperature [K] | 298.15 |
| Heat transfer coefficient at the roll surface $[W.m^{-2}.K^{-1}]$ [AISE Steel Foundation, 2003] | 1500 |

### 6.3.3 Mathematical model validation

To validate the predictions of the models, experiments were carried out in the industrial plant to measure the surface temperature of the strand. As described in [Gomes et al., 2021], the following steps were followed:

- Thermal imaging camera FLIR model FLIR E75 was used to measure the temperature in the dry region of the machine, at the exit of the straightener, 18 m from the meniscus, and at the entry of the soft reduction, 21 m from the meniscus.
- The solid shell thickness was measured by analyzing breakout shells that occurred during operational problems in the casting of blooms and beam blanks.

In addition, the embedded thermocouple method was used to obtain temperature values in the secondary cooling. As the thermal imaging camera experiments and the breakout analysis were already detailed before, only the thermocouple tests will be described.

### 6.3.4 Embedded thermocouple experiments

The measurements of the strand surface temperatures using thermocouples were particularly challenging. The region of interest was the secondary cooling zone, in which not only the temperature is remarkably high (approximately 1400°C), but also there are water droplets, and a large amount of water vapor is formed. Such an environment is not well suited for regular instrumentation systems, hence it required the usage of a customized technique. In it, the tip of a long and thin thermocouple was embedded in the strand using an adhesion pad. The thermocouple was pulled by the moving strand, measuring the temperature of a small area along the length of the strand. The setup used a type K thermocouple (1.5 mm diameter) silver soldered to an adhesion pad, the same setup used by [B. Barber, B. Patrick, P. Watson, R. York, F. Kitching, H. Sha and Spitzer, 1996]. The temperature values were registered with a sample rate of 1Hz, using the data acquisition system assembled specifically for this project and the software FieldChart, a data acquisition system developed by the Brazilian company NOVUS. A metal tube was positioned through an inspection window to the strand. The thermocouple was introduced through the tube until it reached the moving strand. The guide tube was inserted in the middle of Zone 1, between rolls 16 and 17. This procedure allowed the measurement of the temperature along all the secondary cooling.

Table 6.2: Chemical composition of the steel.

| Steel Grade | %C | %Mn | %P | %S | %Si | %Cu | %Ni | %Cr |
|---|---|---|---|---|---|---|---|---|
| ASTM A572 | 0.18 | 0.85 | 0.04 | 0.03 | 0.18 | 0.00 | 0.00 | 0.00 |

Table 6.3: Casting conditions considered in the simulations.

| Variable | Bloom | Beam Blank |
|---|---|---|
| Casting speed $[m.min^{-1}]$ | 0.9 | 0.9 |
| Mold wide face water flow $[L.min^{-1}]$ | 1260.0 | 1620.0 |
| Mold narrow face water flow $[L.min^{-1}]$ | 720.0 | 820.0 |
| Superheat temperature $[°C]$ | 30.0 | 35.0 |
| Z0 total water flow $[L.min^{-1}]$ | 85.0 | 143.0 |
| Z1 total water flow $[L.min^{-1}]$ | 420.0 | 649.0 |
| Z2 total water flow $[L.min^{-1}]$ | 168.0 | 255.0 |

## 6.4 Results and Discussion

In this section, the calculated temperature values, calculated solid shell thickness, and the results of the embedded thermocouple experiment are presented and discussed. ASTM A572 steel (structural steel) was considered in the simulations. The chemical composition of this steel is presented in table 6.2:

The casting conditions used in the simulations are shown in table 6.3.

### 6.4.1 Temperature and solidified shell thickness profiles

In the first 0.7 m, it is possible to see the largest temperature drop that occurs due to solidification in the mold as well as the skin formed in this region. At that moment, the

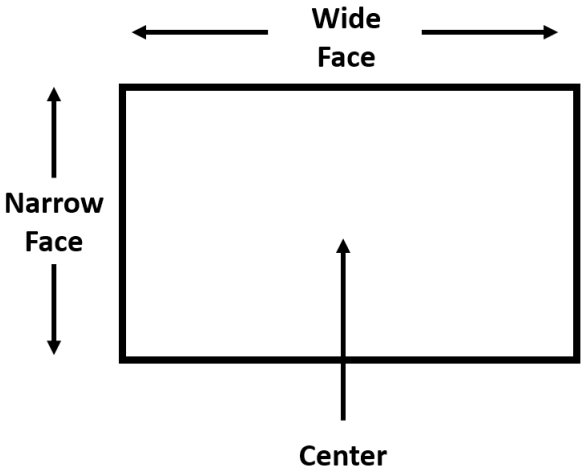


Figure 6.5: Bloom faces naming convention

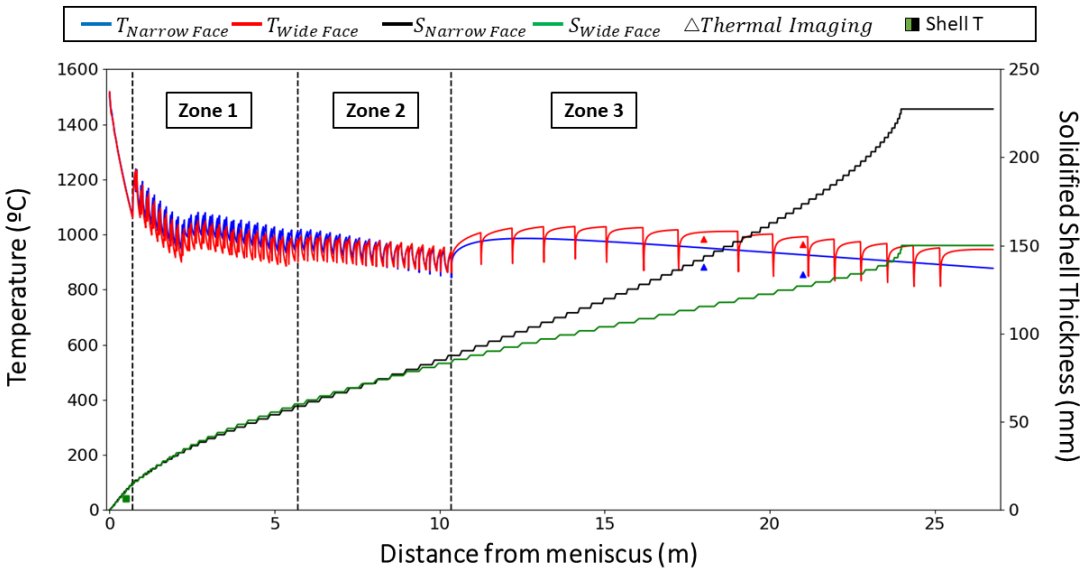


Figure 6.6: Calculated temperature and solidified shell thickness in the wide and narrow faces of the bloom. It is also shown the experimental data of thermal imaging camera, and blackout shell measurements

temperature values on the faces are very close. The results of the skin breakout measurements allowed validation of the skin calculated in this region. On the wide face, the difference between the calculated and measured skin was 4.8 mm and on the narrow face 4.2 mm. The temperature curve shows peaks and valleys characteristic of contact with rolls and sprays. At zone 1, the reheating is of the order of 100 °C/m and at zone 2 of the order of 70 °C/m. Zone 1 has a greater number of rolls (23) than Zone 2 (15). At zone 2, there is a discontinuity of the side rolls. It is important to note that the highest water flow rate is used in the first spray zone, which causes an intense cooling in Zone 1. On the wide face, the difference between the calculated and measured temperature was close to 20°C, and on the narrow face, 70°C. It is believed that this difference was greater on the narrow face due to the difficulty of positioning the camera in this region. In the tests performed, the measurements were manual, and the narrow face was in a field of view where it was necessary to obtain the images with the camera inclined.

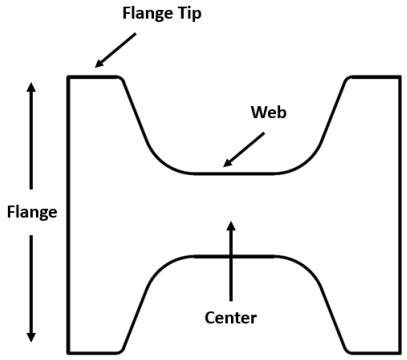


Figure 6.7: Beam-blank faces naming convention

The skin measurements allowed validation of the skin calculated in the mold exit at 0.7m from the meniscus. On the web, the difference between the calculated and measured skin was 4.84mm and on the flange 4.24mm. In the sprays chamber region, the temperature presents the characteristic dips due to rolls and sprays. In Zone 1, the reheating is of the order of 100°C and in Zone 2 of the order of 60°C. The measurements with a thermal imaging camera were carried out in the dry area of the machine at the exit of the straightener, 18 m from the meniscus. On the flange, the difference between the calculated and measured temperature was close to 20°C. This value was 70°C on the web face, and 25°C on the flange tip.

### 6.4.2 Embedded thermocouple results

Figures 6.9 and 6.10 show the results of the embedded thermocouples that were anchored in the wide face of the bloom and the web of the beam blank, respectively.

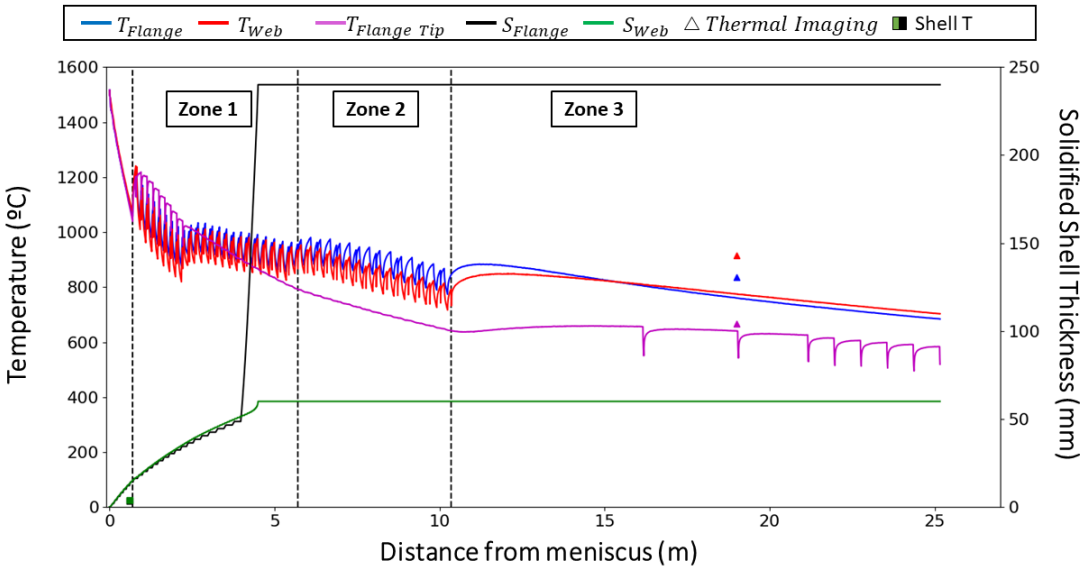


Figure 6.8: Calculated temperature and solidified shell thickness values in the center, flange, web and flange tip faces of the beam blank. It is also shown the experimental data from a thermal imaging camera, and breakout shell measurements.

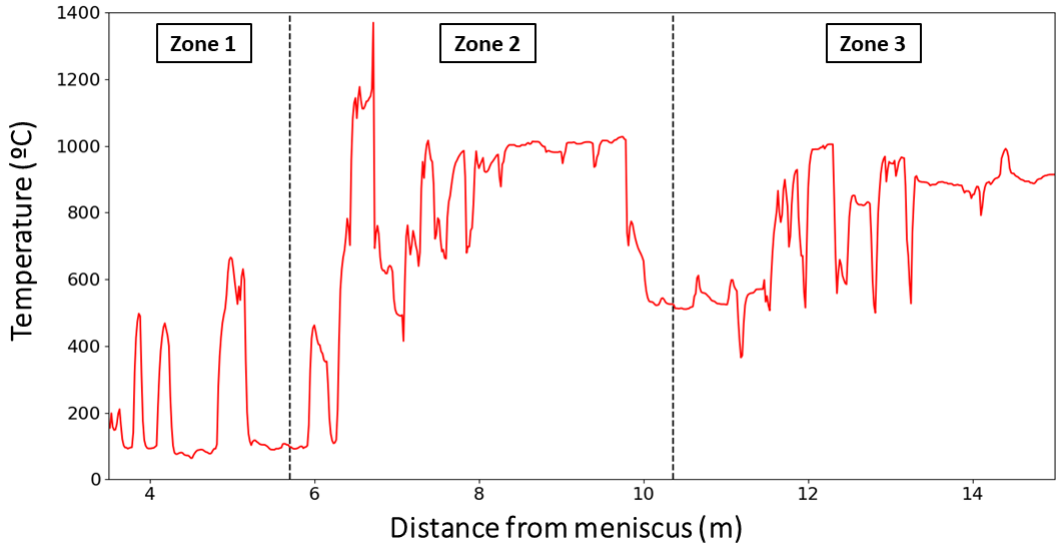


Figure 6.9: Temperature measured at the bloom wide face using the embedded thermocouple technique.

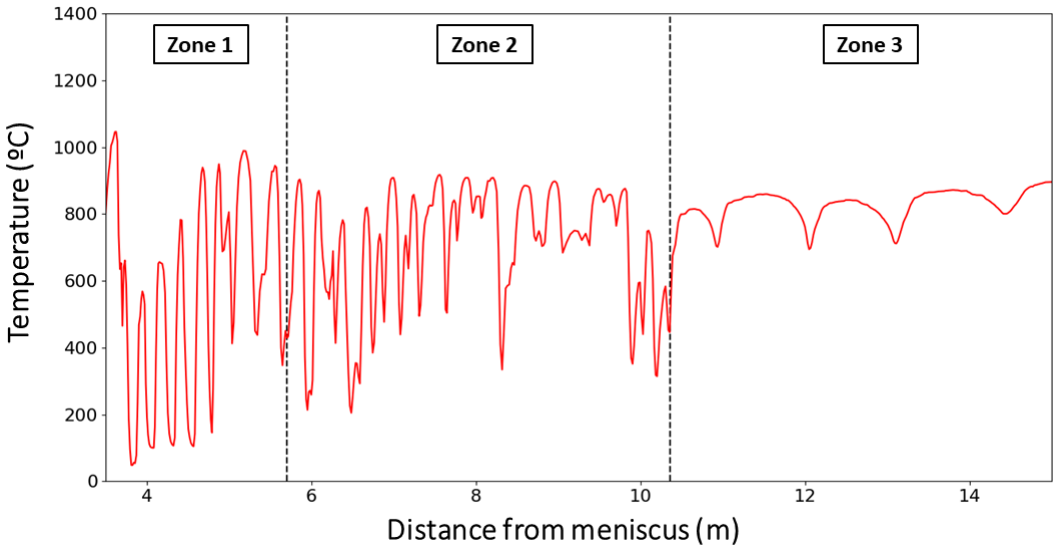


Figure 6.10: Temperature measured at the beam-blank web using the embedded thermocouple technique.

The measurements presented in figures 6.9 and 6.10 show peaks and valleys of the temperature values. In the case of the studied machine, the sprays and the rolls are close together, which means that the thermocouple passes between the sprays and the rolls in a short time, 10 minutes which causes instability in the measuring instrument. This factor, added to the measurement frequency of 1Hz and the slow thermocouple response time, leads to a delay in the measurements. However, the top temperatures within the spray area of this machine are very consistent with the measurements of [B. Barber, B. Patrick, P. Watson, R. York, F. Kitching, H. Sha and Spitzer, 1996] and the dry zone temperatures are similar to those obtained with a thermal imaging camera, which were between 800°C and 900°C. For both geometries, exceptionally low temperatures, in the range of 100ºC to 200ºC, were measured, especially in Zone 1. These results are most likely related to the boiling effect of the water that could be trapped between the rolls. In Zone 3, it is possible to see four temperature deeps that reach a temperature close to 700°C, the position of those deeps matches the air sprays employed to disperse residual water. This confirms the reliability of the measurements.

### 6.4.3 Comparison of the model results with embedded thermocouple measurements

The measured temperatures and the values predicted by the model are in close agreement in the region which corresponds to the reheating of the material. However, the model does not predict such high dips and the shape presented by the model curve is more regular than the one

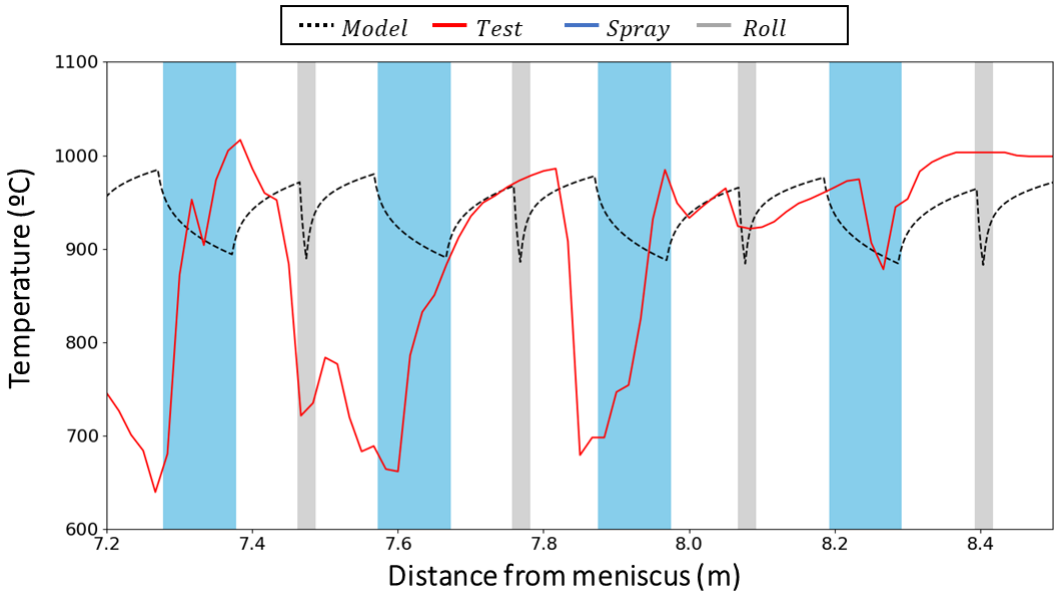


Figure 6.11: Temperature calculated using the bloom model and the embedded thermocouple measurements in the wide face.

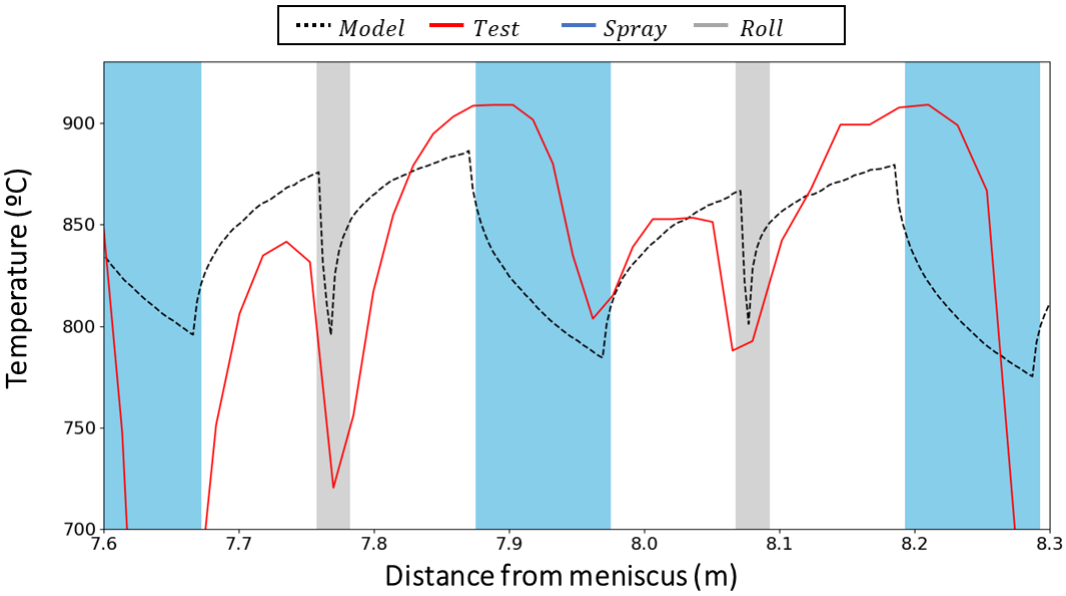


Figure 6.12: Temperature calculated using the beam blank model and the embedded thermocouple measurements in the wide face.

obtained by the embedded thermocouple. Among the factors that contribute to these differences are the low frequency of the experimental data recording and the thermocouple limitations of response time, maximum temperature limit, and instrument error. It is important to remember that the model does not incorporate the effect of trapped water that is frequently observed in the beam blank web. The thermocouple experiments allowed the verification of the temperature in the spray region, which corresponds to the region of interest of this work. The temperatures predicted in the model and those measured by the thermocouple were around 1000°C for the bloom in Zone 2 and 900°C in the same zone for the beam blank.

## 6.5 Conclusions

This work developed a mathematical model that can be used to study the thermal behavior of blooms and beam blanks along the entire length of the casting machine. From the results obtained, it is possible to conclude that the model developed was successfully validated for both bloom and beam blank. The model can predict the temperature and solidified shell thickness with reasonable accuracy, as confirmed by the experiments done using breakout shells (difference less than 5 mm), measurements from a thermal imaging camera in the dry area of the casting machine (difference from 20°C to 70°C depending on the position) and tests with an embedded thermocouple (agreement of the temperature ranges and very close measurements at the temperature peaks). Moreover, this work shows tests with an embedded thermocouple on beam blanks, which were not found in the literature. The thermocouple experiments proved to be challenging because of the limitations of the technique and the low frequency of the data acquisition system employed. However, it allowed the assessment of the temperature values in the spray chamber and further validation of the model. The temperatures predicted by the model and measured by the thermocouple were around 1000°C for the bloom in Zone 2 and 900°C for the blank beam.

## 6.6 Acknowledgements

The authors are grateful to the (PPGEM) at UFMG, to the CAPES-PROEX, CAPES FAPEMIG.

# 7. Paper III - Mechanical behavior on blooms and beam blanks' continuous casting: Development of a mathematical model for stress and distortion

Daniela Fátima Gomes*, Bernardo Martins Braga, Roberto Parreiras Tavares, Maurício Covcevich Bagatini, Carlos Berlini Filho, Gabriela Pereira Maciel

Metallurgical and Materials Engineering Department, School of Engineering, Federal University of Minas Gerais, Av. Presidente Antônio Carlos 6627, 31270-901 Belo Horizonte, Brazil.

*Corresponding author: danielafg05@gmail.com

ORCID ID's: 0000-0002-0965-3847 (Fátima Gomes D.), 0000-0003-0634-5416 (Braga Martins B.), 000-0001-9348-2181 (Parreiras Tavares R.), 0000-0002-3986-9833 (Covcevich Bagatini M.), 0000-0001-6640-3564 (Filho Berlini C), 0000-0002-3752-5148 (Maciel Pereira G)

## 7.1 Abstract

Defects and discontinuities generated in continuous casting are directly related to heat transfer and the stresses to which the material is subjected during the process. Knowledge of these phenomena is essential for both process safety and the quality of the final product. This work aims to analyze the mechanical behavior of blooms and beam blanks during continuous casting. The continuous casting machine considered in this study is used to cast both blooms and beam blanks. The secondary cooling can be divided into cooling zone z0, cooling zone z1, cooling zone z2, and cooling zone z3. For each geometry, there are specific molds, z0, z1 and z2 (sprays and support rollers), which need to be replaced when there is a geometry shift. The changing of the cooling segments brings security risks for the operators and reduces the continuous casting availability. Therefore, it is desired to have a common z2 for both blooms and beam blanks to reduce operational risk exposure and increase the machine production rate. For this to be possible, it is necessary to assess the effects of thermal stresses, ferrostatic pressure, and contact stresses. Two mechanical models were developed for each geometry to analyze the stress and distortions of both geometries during the solidification.

Keywords: continuous casting, mechanical modeling, beam blanks and blooms.

## 7.2 Introduction

Continuous casting is the most used process to produce billets, blooms, slabs, and beam blanks in steel melting shop. With the growing demand for quality and high-performance materials, knowledge of the phenomena involved is increasingly important. Although Physical experiments in this process are difficult both on a laboratory scale and even more so in the industrial process. In this context, mathematical simulation is a helpful tool to analyze continuous casting processes. Thermal models have been developed for the solidification but then alone are not able to provide a complete understanding of the product quality [Thomas and Bellet, 2018]. To understand the deformations suffered by the solidified skin and the mechanisms of crack formation, an analysis of stresses and distortions is crucial. Some publications study the mechanical interactions in continuous casting (1) Mold Shrinkage phenomena (2) the Straightening process, where the formation of cracks may occur depending on the temperature, applied force value, and additional stresses due to roller misalignment [Fernandes Reis, 2012], [Fernandes, 2005]. (3) soft reduction, which is used to improve the internal quality of the ingot material by the application of compression force, (4) Bulging phenomena, which is defined as the maximum deformation of the slab between the two casting rolls [Qin and Yang, 2017].

The continuous casting machine considered in this study is used to cast both blooms and beam blanks. For each geometry, there are specific mold and secondary cooling setups (sprays and support rollers) which need to be replaced when there is a geometry shift. The changing of the cooling segments brings security risks for the operators and reduces the continuous casting availability. Therefore, it is desirable to reduce the need to exchange at least one of the segments. For this to be possible, it is necessary to know the phenomena involved and verify the interference in the quality of the as-cast products. This paper describes the development of mathematical models for stress and distortion caused by thermal gradients and roll contact in the casting process of blooms and beam blanks. The results of the computational simulations are discussed, and the particularities of each geometry are analyzed.

## 7.3 Methodology

In this section, a brief description of the casting machine will be presented, along with the numerical procedure, considerations made in the development of the models, boundary conditions, physical equations, steel physical properties, and the experiments for the hot ductility test. Separate models were developed to calculate the mechanical stresses due to the thermal gradient and to calculate the mechanical stresses due to contact with the rolls. Commercial software ANSYS CFX 17.1 and ANSYS 17.1 Mechanical were used to solve the thermal and mechanical equations.

### 7.3.1 Description of the machine

The present work was developed considering a continuous casting machine of blooms and beam blanks. This machine has four strands, and it can produce blooms of 300mm × 450mm and 300mm × 350mm and beam blanks of 400mm × 480mm × 120mm. The primary cooling takes place in the mold, and secondary cooling takes place in the spray chamber which has four control zones (z0 to z3). Zones z0, z1 and z2 are different for blooms and beam blanks and are changeable. Zone z0 is part of the mold set and contains the first set of sprays and rollers, Zone z3 is a common setup. In zones z0 and z3 there are water sprays, in zones z1 and z2, there are air mist sprays. Currently, Zone z3 remains inactive. After the spray chamber, blooms or beam blanks are straightened and cut. A representation of the machine, with the length of each control zone, can be seen in figure 7.1.

### 7.3.2 Mathematical Model

To study the mechanical deformations due to temperature differences, a transient, three-dimensional thermal model was built with a 1.2m long as-cast piece. It was considered a piece with an empty interior, with a constant solidified skin. It was considered that between the entrance of zone 2 the surface has reached thermal equilibrium. From there, the as-cast cooled according to the secondary cooling boundary conditions. In parallel with the solution of the thermal problem, the thermal stress model solves the stress and distortion model equations.

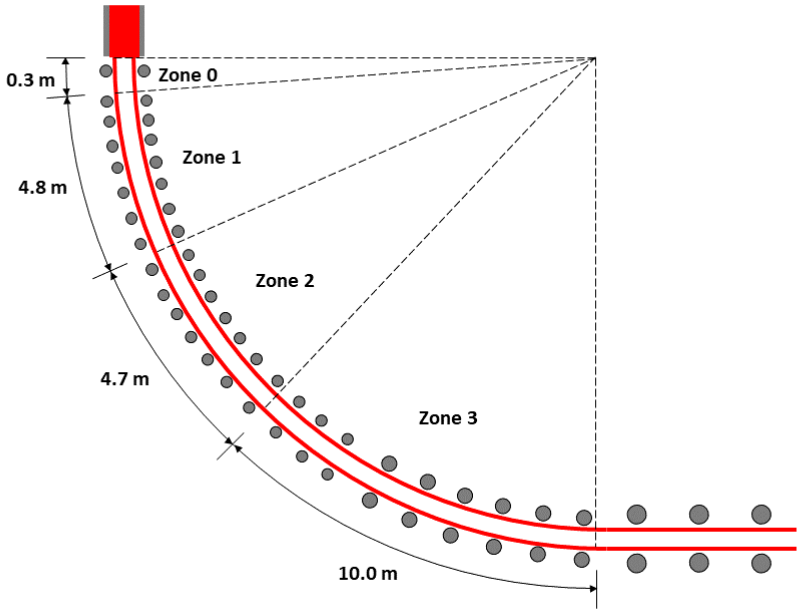


Figure 7.1: Schematic view of the continuous casting machine

To study the contact deformation, a stationary three-dimensional thermal model was used, an as-cast photo during secondary cooling. In parallel with the solution of the thermal problem, the thermal stress model solves the stress and distortion equations due to the contact with the rolls. The stress and distortion due to the thermal gradient and roll contact were modeled separately to focus on each phenomenon and obtain a better performance of time simulation. Figure 7.2 shows a schema of the mathematical model.

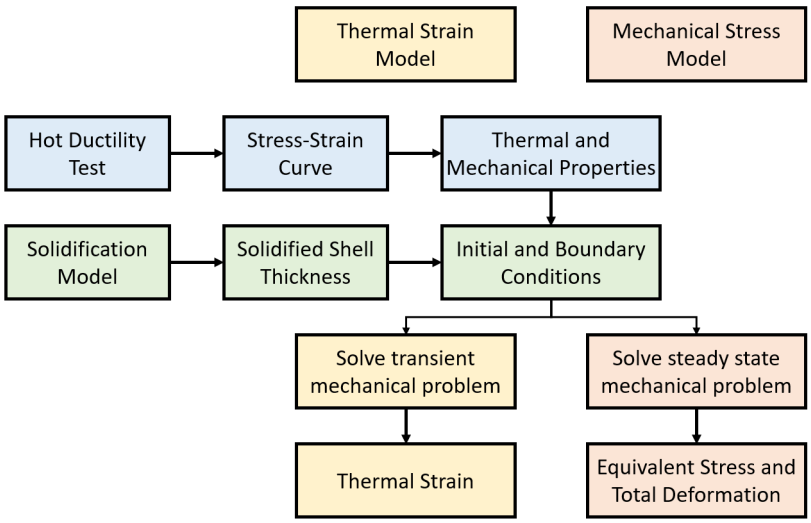


Figure 7.2: Schematic of the mathematical models

### 7.3.3 Heat transfer models

Three-dimensional mathematical models of heat transfer, solidification of the blooms and beam blanks were developed. The main assumptions are (1) The latent heat of steel solidification was modeled increasing the specific heat capacity in the mushy zone. (2) The density of the steel was considered constant while the heat capacity, emissivity and thermal conductivity were considered temperature-dependent. (3) The effects of strand shrinkage were neglected. (4) The convective heat flow in the liquid pool and the mushy zone was accounted for through an effective thermal conductivity [Ma et al., 2008].

The 3D transient heat transfer model was based on the general energy equation during the transient state, as described in equation 7.1:

$$\rho \frac{c_p^{eq} \partial T}{\partial t} = \frac{\partial}{\partial x}\left(k_{ef}\frac{\partial T}{\partial x}\right) + \frac{\partial}{\partial y}\left(k_{ef}\frac{\partial T}{\partial y}\right) + \frac{\partial}{\partial z}\left(k_{ef}\frac{\partial T}{\partial z}\right) + S \tag{7.1}$$

where: t – the time of simulation [s]; T – the temperature [$^{\circ}C$]; $k_{ef}$ – the thermal conductivity [$W.m^{-1}.^{\circ}C^{-1}$]; $c_p^{eq}$ – the equivalent heat capacity of steel [$J.kg^{-1}.K^{-1}$]; $\rho$ – the density of steel [$kg.m^{-3}$]; x, y, z – the direction of the coordinate system, along the transversal section [m].

The 3D steady state heat transfer model was based on the general energy equation during the unsteady state, as described in equation 7.2:

$$\frac{\partial}{\partial x}\left(k_{ef}\frac{\partial T}{\partial x}\right) + \frac{\partial}{\partial y}\left(k_{ef}\frac{\partial T}{\partial y}\right) + \frac{\partial}{\partial z}\left(k_{ef}\frac{\partial T}{\partial z}\right) + S = 0 \tag{7.2}$$

### 7.3.4 Mechanical model

The structural mechanical model was developed in three dimensions for a one-meter-long as-cast piece. The simulations presented in this work were carried out for the zone z2 region, which is the zone where there is an interest in using a common segment for blooms and beam blanks. The main assumptions are (1) The as-cast bloom and beam blank were considered flexible and the rollers rigid as it was interested in evaluating the deformations and stresses in those continuous casting geometries (2) Transient state phenomena (3) friction contact between the rollers and the as-cast pieces (4) free rotation rollers. The thermo-elastic–plastic

material model, with multi-linear isotropic hardening, was used to calculate the strain and stress distributions. The total value of the deformation vector was calculated using equation 7.3, according to the Von Misses criteria as used by [Chen et al., 2009], [Liu et al., 2017], and [Zeng et al., 2020]. The influence of the ferrostatic pressure was also taken into consideration.

$$\{\epsilon\} = \{\epsilon^{el}\} + \{\epsilon^{pl}\} + \{\epsilon^{th}\} \tag{7.3}$$

where: $\{\epsilon\}$ total deformation [%]; $\{\epsilon^{el}\}$ incremental elastic strain component [%]; $\{\epsilon^{pl}\}$ incremental plastic strain component [%]; $\{\epsilon^{th}\}$ incremental thermal strain component [%].

The stress is related to the elastic strain by:

$$\{\sigma\} = [D]\{\epsilon^{el}\} \tag{7.4}$$

where: $\{\sigma\}$ - the stress vector; [D] - the elasticity or elastic stiffness matrix or stress-strain matrix.

$$\{\epsilon^{el}\} = \{\epsilon\} - \{\epsilon^{pl}\} - \{\epsilon^{th}\} \tag{7.5}$$

$$\{\epsilon\} = \{\epsilon^{pl}\} + \{\epsilon^{th}\} + [D^{-1}]\{\sigma\} \tag{7.6}$$

where: $\{\epsilon\}$ - the total strain vector; $\{\epsilon^{pl}\}$ - plastic strain vector; $\{\epsilon^{th}\}$ - the thermal strain vector; $\{\epsilon^{th}\} = \Delta T[\alpha_x^{se}\alpha_y^{se}\alpha_z^{se}\ 0\ 0\ 0]^T$

$$[D]^{-1} = \begin{bmatrix} 1/E_x & -\nu_{xy}/E_x & -\nu_{xz}/E_x & 0 & 0 & 0 \\ -\nu_{yx}/E_y & 1/E_y & -\nu_{yz}/E_y & 0 & 0 & 0 \\ -\nu_{zx}/E_z & -\nu_{zy}/E_z & 1/E_z & 0 & 0 & 0 \\ 0 & 0 & 0 & 1/G_{xy} & 0 & 0 \\ 0 & 0 & 0 & 0 & 1/G_{yz} & 0 \\ 0 & 0 & 0 & 0 & 0 & 1/G_{xz} \end{bmatrix} \tag{7.7}$$

$\alpha_x^{se}$ is the secant coefficient of thermal expansion in the x direction.

$$\Delta T = T - T_{ref} \tag{7.8}$$

where: T the temperature in the point in question. $T_{ref}$ reference (strain-free) temperature (input).

The plastic behavior of the material was considered by a multilinear isotropic hardening that uses the von Mises yield criterion with the associated flow rule and isotropic (work) hardening.

### 7.3.5 Initial and boundary conditions

To obtain the solution for the differential equations, it is necessary to define the initial and boundary conditions. The external temperature value in Zone 2 was adopted as the initial condition in the external surface of bloom and beam blank and the internal temperature was considered equal to the solidus temperature.

$$T = T_0 \tag{7.9}$$

$T_0$ in the external surface of the as-cast is the temperature calculated in the entry of Zone 2 by a thermal model developed in the previous work [Gomes et al., 2021] and equal 1000°C. The internal temperature is equal to the solidus temperature, 1485°C. In the secondary cooling zone, heat is transferred mostly due to convection and radiation, due to the high-temperature values of the strand. The heat flow in the transient heat transfer model in the spray region was calculated using equations 7.10 and 7.11:

$$q = h_{Spray}(T_S - T_W) \tag{7.10}$$

$$h_{Spray} = aW^b \tag{7.11}$$

where: $h_{spray}$ – heat transfer coefficient in the spray cooling $[W.m^2.°C^{-1}]$; $T_s$ – the temperature in the as-cast surface $[°C]$; $T_w$ – the temperature of the water $[°C]$; $W$ – water flow rate density $[L.m^2.min^{-1}]$; a, b – empirical constants dependent on the type of spray nozzles. For the air mist type, a=0.336, b=0.724. For the water type, a=0.25, b=0.64. Each spray was considered as an individual heat extraction source in the model developed.

The radiation heat flow in the transient heat transfer model was calculated by equation 7.12:

$$q = \sigma\epsilon(T_s^4 - T_e^4) \tag{7.12}$$

where: $sigma$ – Stefan–Boltzmann constant; $\epsilon$ – emissivity; $T_e$ – temperature of the environment [°C].

In the case of the steady-state model, the boundary conditions are equal to the initial conditions. In this approach, the problem is analyzed in an instant of time, as a picture of the process at a specific moment. The ferrostatic pressure exerted by the liquid portion inside the geometry is one of the forces that generate tension in the walls and can cause deformations. This pressure was calculated using the equation 7.13:

$$P_f = \rho_{steel} g H \tag{7.13}$$

where: $P_f$ – the ferrostatic pressure [Pa]; $\rho_{steel}$ – the steel density [$Kg.m^{-3}$]; g – the acceleration due to gravity [$m.s^{-2}$]; H – the distance from the meniscus [m].

In the case of the problem studied, the ferrostatic pressure is of the order of 0.34MPa. To calculate this pressure, the as-cast geometry was considered as a solidified shell with a thickness equal to that calculated by the transient model. The interior is filled with liquid steel but to simulate the phenomenon of liquid pressure on the walls, this interior was considered as a void where the inner walls suffer a force in the axial direction.

Figure 7.3 shows a force diagram.

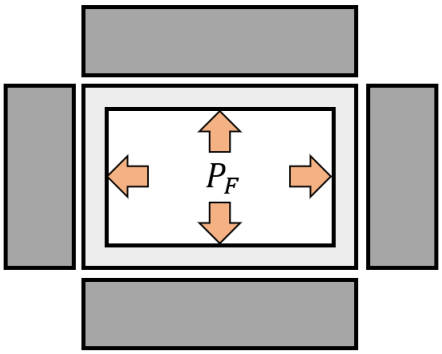


Figure 7.3: Schematic diagrams of forces

The strain-free temperature is considered equal to the solidus temperature of the steel simulated, 1485°C, obtained by ThermoCalc. Both thermal and mechanical calculations are made by the Ansys software using the FEM method.

### 7.3.6 Physical properties of steel

The physical properties of the steel have a great influence on the predictions of the model and therefore must be carefully chosen to guarantee the accuracy of the solution. The properties considered in the simulations are shown in table 7.1.

*Liquidus and solidus temperatures were calculated using the commercial software ThermoCalc.

### 7.3.7 Experimental procedures

A hot ductility test with partial melting of the sample was performed in a Gleeble machine to obtain the strain-stress curve. Gleeble 3500 is a thermo-mechanical simulator in which the samples are heated by electrical resistance. Sample cooling can be achieved by simple cooling, anvil/grips, or by any combination of air/inert gas/water quenching as described by [Moon and Dippenaar, 2004]. Testing can be done in either ambient or inert atmosphere or under a vacuum. It is possible to deform under uni-axial tensile, uni-axial compression or plane strain compression conditions at the desired temperature. In this work, uni-axial tensile tests were performed. The specimen was obtained from ASTM A572 steel. To prepare the samples for the hot ductility test, parts of the cast material were removed in the region between the center and the surface, to avoid regions where the chemical composition is affected by segregation. Cylindrical test samples were machined from the as-cast with 120 mm of length and 10 mm of diameter. The specimens were heated until they reached the liquidus temperature with partial fusion of the sample, then cooled at a rate of 20°C/min (0.33°C/s) to the test temperature (1150°C). After holding for 1 minute at the test temperature, the specimens were pulled to fracture at a low strain rate of $110^{-4}s^{-1}$. This cycle is presented in figure 7.4.

Table 7.1: Physical properties of the steel

| Parameter | Value |
|---|---|
| Density $[kg.m^{-3}]$ [Lee et al., 2000] | 7020 |
| Solidification latent heat $[J.kg^{-1}]$ [Lee et al., 2000] | 272000 |
| Solidus temperature [K] | 1754.15 |
| Liquidus temperature [K] | 1786.15 |
| Specific heat Liquid steel $[J.kg^{-1}]$ [Bergman et al., 2011] | 824.6157 |
| Specific heat $[J.kg^{-1}]$ [Wang et al., 2005] | $481.8 + 0.19 \cdot T_{Steel}$ |
| Thermal conductivity $(T >= T_{Peritetic})$ $[W.m^{-1}.K^{-1}]$ [Mills et al., 2016] | $20.4 + 0.009\dot{T}_{Steel}$ |
| Thermal conductivity $(T < T_{Peritetic})$ $[W.m^{-1}.K^{-1}]$[Mills et al., 2016] | $21.6 + 0.008 \cdot T_{Steel}$ |
| Thermal conductivity Liquid steel $[W.m^{-1}.K^{-1}]$ [Bergman et al., 2011] | 39.0 |
| Emissivity [Wang et al., 2012] | $T_{Steel}/1000 \cdot (0.25 \cdot T_{Steel} - 0.38) + 1.1$ |
| Specific heat of the water $[J.kg^{-1}.K^{-1}]$[Bergman et al., 2011] | 4184 |
| Water temperature [K] | 298.15 |
| Heat transfer coefficient at the roll surface $[W.m^{-2}.K^{-1}]$ [AISE Steel Foundation, 2003] | 1500 |
| Thermal expansion Coefficient $[C^{-1}]$ [Hada la et al., 2011] | $27 \cdot 10^{-6}$ |
| Poisson ratio [Ha et al., 2001] | 0.33 |
| Friction coefficient [Qin et al., 2014] | 0.01 |

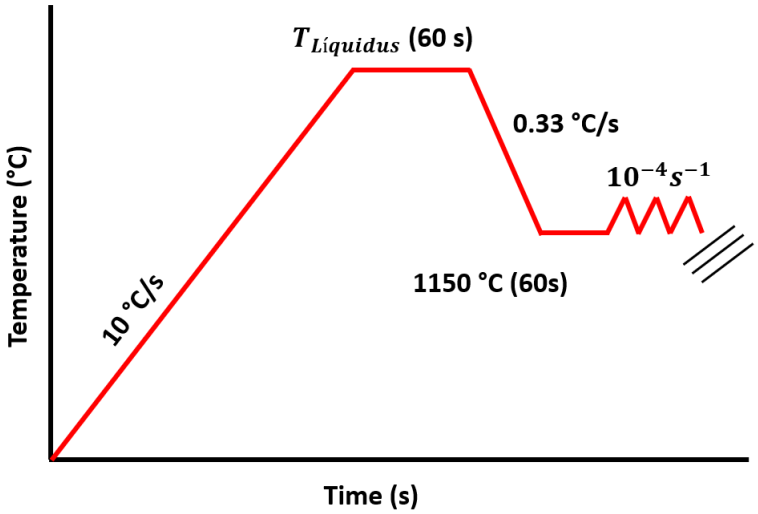


Figure 7.4: Schematic diagram of thermo-mechanical cycles for hot ductility tests under the conditions of continuous casting

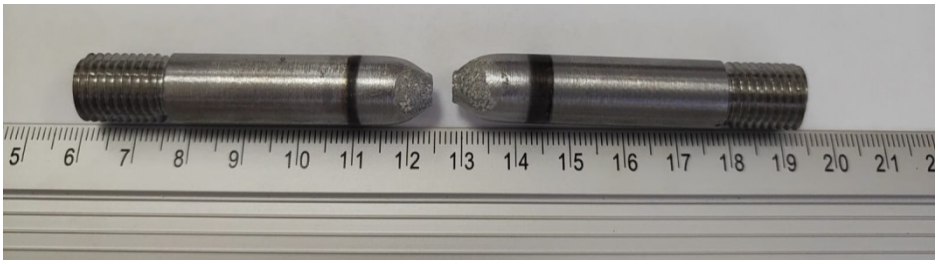

Figure 7.5: GLEEBLE specimen after hot ductility test

## 7.4 Results and Discussion

In this chapter, the results of the hot ductility test and stress and distortion, calculated by the computational model, will be presented. The hot ductility test allowed the derivation of the stress-strain curve of the material chosen in this study, ASTM A572 steel (structural steel), the same steel was considered to perform the simulations. This is the most frequently produced product. The chemical composition of this steel is presented in table 7.2:

The casting conditions used in the simulations are shown in the table 7.3.

In the following results, the ANSYS auto-scale mode was used to facilitate the visualization of distortions.

### 7.4.1 Hot Ductility Test

As described in the methodology, the test temperature for hot traction was 1150°C. Since Gleeble provides the force results, the stress is calculated by dividing it by the initial area of the specimen [Callister, 2007]. The deformation is obtained from the information on displacement of the grip that indirectly represents that of the specimen. Ansys use the true stress-strain curve, so it calculated both the true and the engineering stress curve. Figure 7.6 shows the True Strain Stress Curve.

With the data provided by the hot ductility test, Young's modulus (3273 MPa), Yield strength limit (15MPa) and Tensile strength limit (24MPa) of the material were calculated.

Table 7.2: Chemical composition of the steel.

| Steel Grade | %C | %Mn | %P | %S | %Si | %Cu | %Ni | %Cr |
|---|---|---|---|---|---|---|---|---|
| ASTM A572 | 0.18 | 0.85 | 0.04 | 0.03 | 0.18 | 0.00 | 0.00 | 0.00 |

Table 7.3: Casting conditions considered in the simulations.

| Variable | Bloom | Beam Blank |
|---|---|---|
| Casting speed $[m.min^{-1}]$ | 0.9 | 0.9 |
| Mold wide face water flow $[L.min^{-1}]$ | 1260.0 | 1620.0 |
| Mold narrow face water flow $[L.min^{-1}]$ | 720.0 | 820.0 |
| Superheat temperature $[°C]$ | 30.0 | 35.0 |
| Z0 total water flow $[L.min^{-1}]$ | 85.0 | 143.0 |
| Z1 total water flow $[L.min^{-1}]$ | 420.0 | 649.0 |
| Z2 total water flow $[L.min^{-1}]$ | 168.0 | 255.0 |

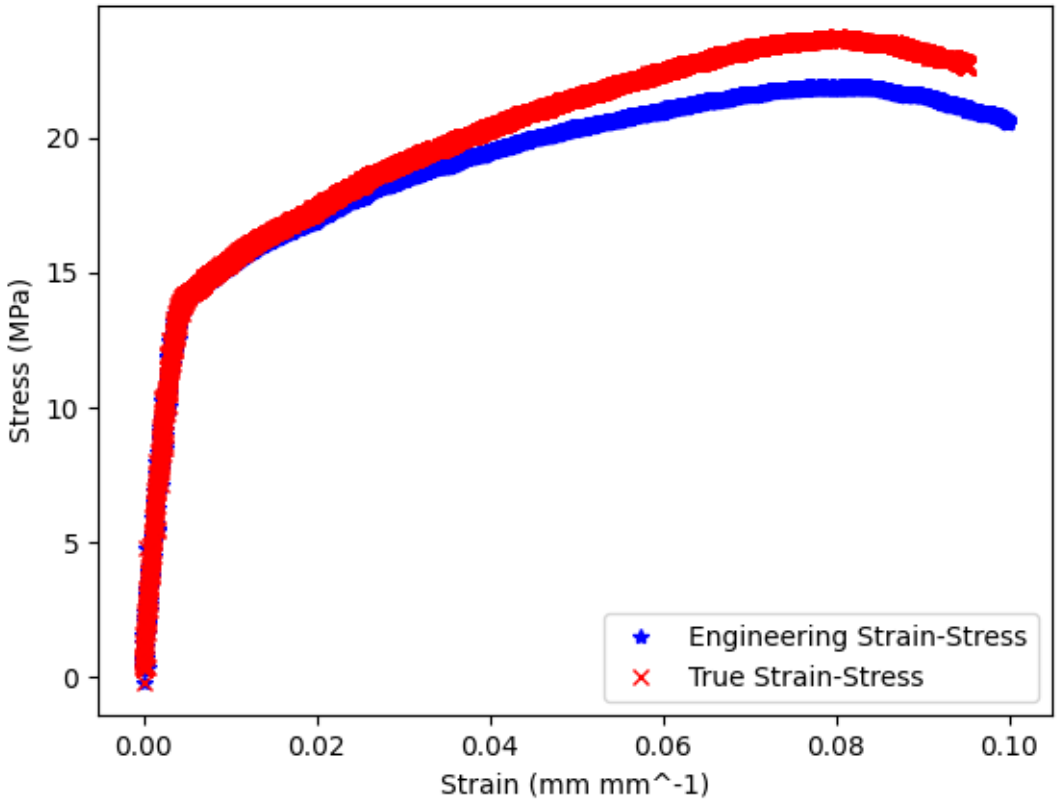


Figure 7.6: True Strain-Stress Curve

### 7.4.2 Thermal Von Misses Stress and distortion

The mechanical stresses and strains generated due to temperature differences were very low, in the order of $10^{-15}$ Pa and $10^{-8}$ m respectively.

### 7.4.3 Contact Von Misses Stress and Distortion

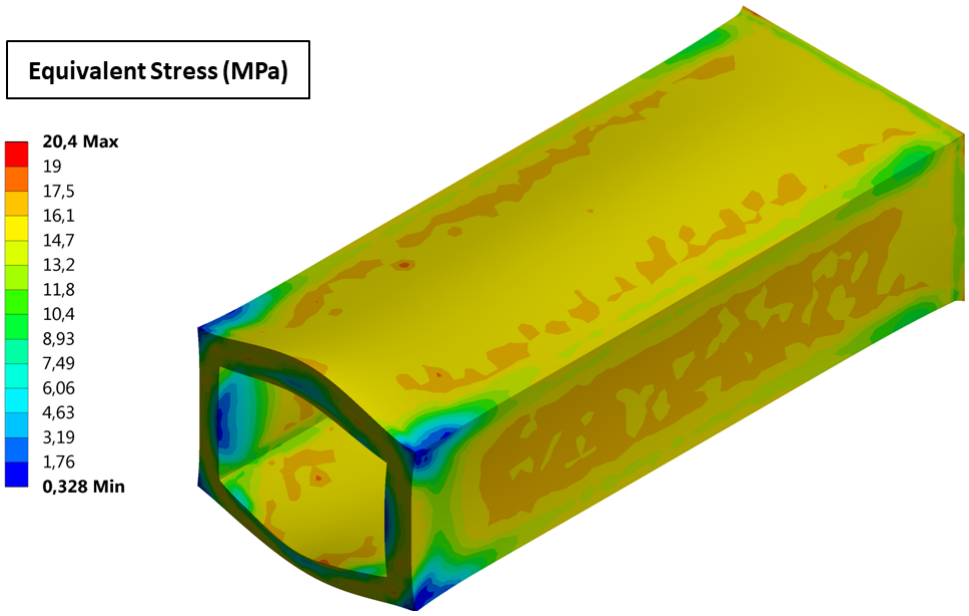


Figure 7.7: Bloom Stress

The simulation shows that the bloom suffers stress with values between 13MPa and 16MPa, and distortion that can reach 4mm. It is necessary to consider that these higher values are in a region that suffers a corner effect and does not represent the other regions of the geometry but, in most parts, it does not reach 2mm.

The simulation shows that the bloom suffers stress between 14MPa to 17MPa and distortion that can reach 1.67mm, in a region that suffers a corner effect and es not represent the other regions of the geometry. But, in most parts, but, in most parts, it does not reach 1mm.

As expected, these stress and distortion values in both geometries bloom and beam blanks are lower than the values found for the material's straightening region [Moon and Dippenaar, 2004] and bulging formation [Ha et al., 2001]. The order of magnitude of the results is similar to those found in the example described by [Thomas and Bellet, 2018] that analyze stresses and strains

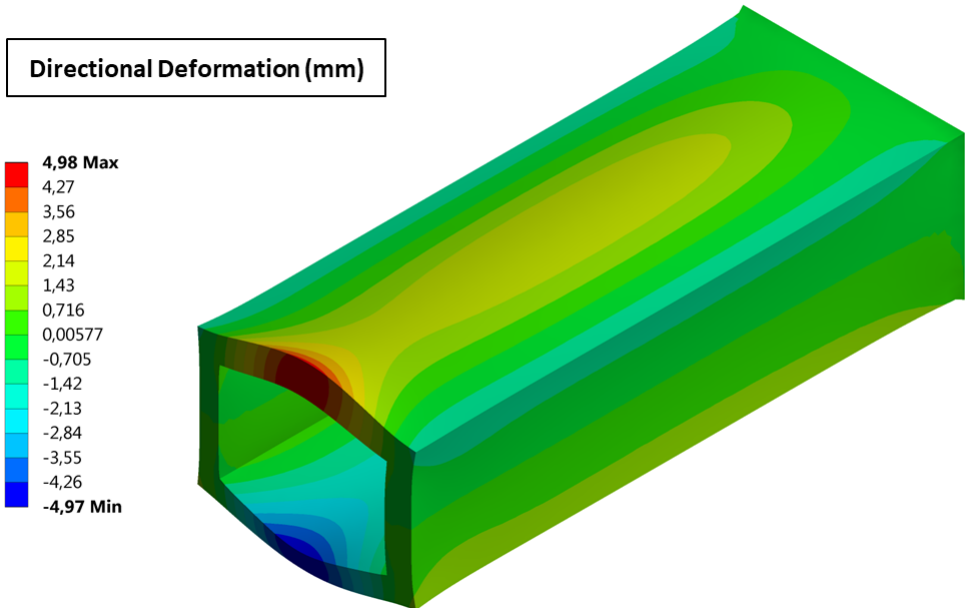


Figure 7.8: Bloom Deformation

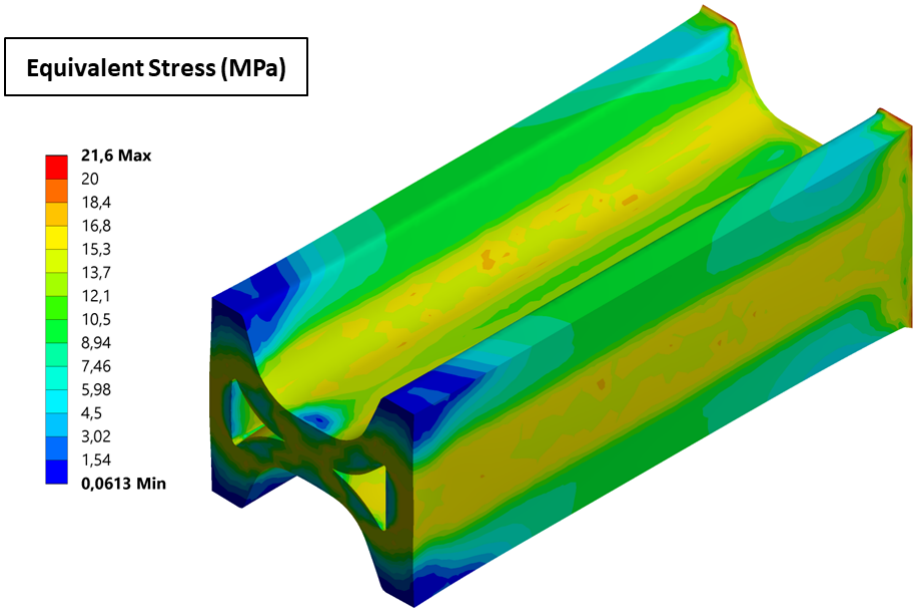


Figure 7.9: Beam Blank Stress

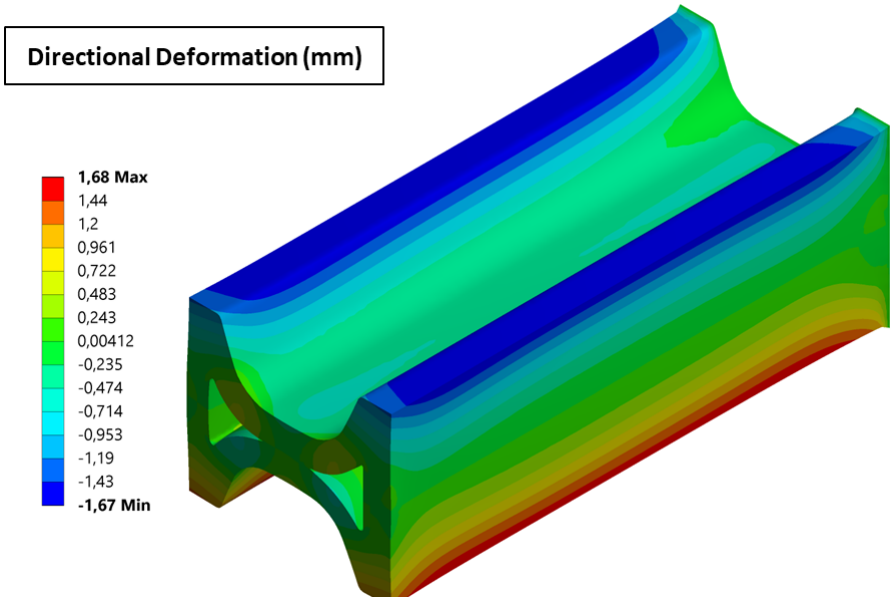


Figure 7.10: Beam Blank Deformation

both in the mold and in the secondary cooling zone below in a slab cast process. Stress values may be close to the yield point in some regions but do not exceed the strength limit. Thus, we can conclude that the material presents some irreversible deformation but does not form cracks. In fact, in the process of the simulated material (A572) under normal conditions, the formation of cracks is not observed.

## 7.5 Conclusions

Mathematical models were developed to calculate the stress and strain caused by thermal gradients and contact with the rollers. The mechanical properties were obtained by hot ductility testing in a GLEEBLE simulator. The thermomechanical stresses and strains proved to be of little significance when compared to the contact stresses and strains in the order of $10^{-15}$ Pa and $10^{-8}$ m respectively. The models showed that the contact stresses generated in the casting of blooms are of the order of 13 MPa to 16MPa generated in the casting of beam blanks are of the order of 14 MPa to 17MPa. The blooms present distortion that reaches medium values of 2mm and the beam blank presents distortion that reaches medium values of 1mm. The as-cast material, stress exceeds the yield strength limit, but does not reach the tensile strength limit, so it is not probable to occurs crack formation during the as-cast conditions simulated. In fact, in the process of the simulated material (A572) under normal conditions, the formation of cracks is not observed

## 7.6 Acknowledgements

The authors are grateful to the (PPGEM) at UFMG, to the CAPES-PROEX, CAPES FAPEMIG.

# 8. Paper IV - Thermal and Mechanical Behavior of blooms and beam-blanks continuous casting: Analysis of secondary cooling to cast both geometries with the same roll configuration

Daniela Fátima Gomes*, Bernardo Martins Braga, Roberto Parreiras Tavares, Maurício Covcevich Bagatini, Carlos Berlini Filho, Gabriela Pereira Maciel

Metallurgical and Materials Engineering Department, School of Engineering, Federal University of Minas Gerais, Av. Presidente Antônio Carlos 6627, 31270-901 Belo Horizonte, Brazil.

*Corresponding author: danielafg05@gmail.com

ORCID ID's: 0000-0002-0965-3847 (Fátima Gomes, D.), 0000-0003-0634-5416 (Braga Martins, B.), 000-0001-9348-2181 (Parreiras Tavares, R.), 0000-0002-3986-9833 (Covcevich Bagatini, M.), 0000-0001-6640-3564 (Filho Berlini, C.), 0000-0002-3752-5148 (Maciel Pereira, G.)

## 8.1 Abstract

A single continuous casting machine can be used to produce different products. However, it is necessary to switch molds and segments (sprays and support rollers) whenever there is a geometry change. The machine considered in this work produces blooms and beam blanks. Its secondary cooling zone can be subdivided into cooling zones z0 to z3. A geometry change requires a replacement of zones z0 to z2. This process raises security risks and reduces availability. If both geometries were cast with a common z2, one segment switch would be avoided, the operational risk mitigated, and availability increased. The current work aims to simulate the effect of a common z2 setup in the cooling of blooms and beam blanks. No similar study has been found in the open literature. To evaluate this possibility, it is necessary to fully understand the heat transfer and the mechanical behavior of both products. Two common roll setups were proposed, simulated, and compared. The results obtained suggest that is possible to cast blooms and beam blanks with the same setup.

Keywords: continuous casting, common setup, heat transfer, stress, distortion beam blanks, and blooms.

## 8.2 Introduction

Continuous casting is a widely used technique to produce steel billets, blooms, and slabs. More recently, the production of beam blanks also began to be done using this method. Mathematical modeling of the solidification is a powerful tool to access the product quality, optimize operational parameters and control the process online. [Jin et al., 2009] developed a 2D mathematical model for heat transfer and a 2D thermal-elastic-plastic stress model to analyze the temperature distribution and stress-strain of thin slabs in the continuous casting. The simulation results provided a theoretical guide for the optimization of continuous casting process parameters and the improvement of the quality of thin slabs. [Chen et al., 2009] developed a transient thermo-mechanical model to compute the temperature and stress profile in beam blank continuous casting. An online verifying model of this optimization model has been put into practice, and according to the author, proved that it is very useful to control production. To investigate the formation of internal cracks in GCr15 bearing steels during the soft reduction process in rectangular bloom continuous casting, fully coupled thermomechanical finite element models were developed using the commercial software MSC. MARC by [Li et al., 2012], this analysis resulted in better control of the applied reductions and minimized the formation of cracks. Simulations are also used to understand undesired conditions in the process that can cause defects, such as the effect of roll misalignment and bulging, [Ha et al., 2001], [Fernandes Reis, 2012].

In the secondary cooling zone of the continuous, which is the focus of this work, heat extraction occurs mainly through three different phenomena [AISE Steel Foundation, 2003]: (1) forced convection from water and air sprayed by the cooling system, (2) conduction due to contact with the support rollers, and (3) radiation because of the high-temperature values.

The relevant process parameters for the secondary cooling are the casting speed, the spray's water flow rate and wet area, the temperature of the strand, the diameter of the rolls, and the area of contact of these rolls with the strand, [Zhao et al., 2014], [Costes et al., 2003]. The continuous casting machine considered in this study is used to cast both blooms and beam blanks and is described in the previous work [Gomes et al., 2021]. For each geometry, specific mold, and secondary cooling setups (sprays and support rollers) need to be replaced when there is a geometry shift. The changing of the cooling segments brings security risks for the operators and reduces the continuous casting availability. The objective of this work is to simulate the effect of a common z2 setup in the cooling of the blooms and beam blanks. Two common setup

rolls were proposed and analyzed. Thermal and mechanical models were developed for both geometries to simulate the possibilities. To evaluate the common setup proposals, a comparison was made between the results of the thermal and stress simulations of the current condition and the proposed conditions. It is worth mentioning that the current conditions were considered adequate since it is not observed the formation of shape defects or cracks.

## 8.3 Methodology

This section will present a brief description of the casting machine, the numerical procedure, the main physical equations, steel physical properties, and two proposed setups for a common z2. Commercial software ANSYS CFX 17.1 was used to solve the thermal equations.

### 8.3.1 Description of the machine

The present work was developed considering a continuous casting machine of blooms and beam blanks. This machine has four strands, and it can produce blooms of 300 mm × 450 mm and 300 mm × 350 mm and beam blanks of 400 mm × 480 mm × 120 mm. The primary cooling takes place in the mold, and secondary cooling takes place in the spray chamber which has four control zones (z0 to z3). Zones z0, z1 and z2 are different for blooms and beam blanks and are changeable. Zone z0 is part of the mold set and contains the first set of sprays and rollers, Zone z3 is a common setup. In zones z0 and z3 there are water sprays, in zones z1 and z2, there are air mist sprays. Currently, Zone z3 water sprays remain inactive. In Zone 3 there are air sprays that are fixed in the region of the internal radius, whose function is to break up the water that may be trapped in the wide face of the bloom or the beam blank flange. This accumulation is more pronounced in the beam blank due to the H shape. After the spray chamber, blooms or beam blanks are straightened and cut. A representation of the machine can be seen in figure 8.1.

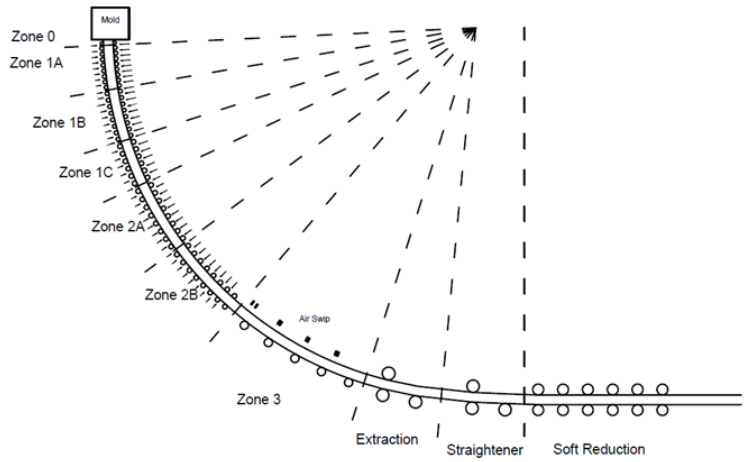


Figure 8.1: Schematic view of the continuous casting machine

### 8.3.2 Heat transfer and the solidification model

A two-dimensional transient mathematical model of heat transfer and solidification of blooms and beam blanks was developed. Figure 8.2 shows a representation of bloom and figure 8.3 of a beam blank.

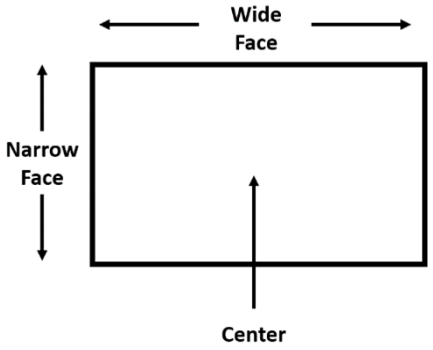


Figure 8.2: Representation of a bloom

The heat transfer model used for the simulations was described in the previous work, [Gomes et al., 2021]. This model was improved, and tests were carried out with a traveling thermocouple to make the validation more robust in the spray region. The initial condition and the boundary condition in the mold were detailed in the previous work. 3D mechanical models were developed in the work of the same author, ”Mechanical behavior on blooms and beam blanks’ continuous casting: Development of a mathematical model for stress and distortion”. So, the mechanical approach also will not be detailed in this paper. To validate the predictions of the models, experiments were carried out in the industrial plant to verify the surface temperature. Thermal imaging camera FLIR model FLIR E75 and the embedded thermocouple method. The shell

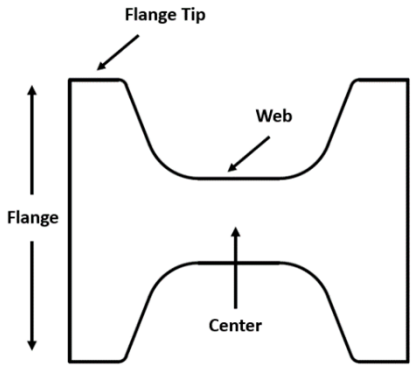


Figure 8.3: Representation of a beam blank

thickness verification was made by analyzing breakouts shells that occurred during operational problems in the casting of blooms and beam blanks. Embedded thermocouple tests were also performed to access the model validation in the secondary cooling. This technique is explained elsewhere [B. Barber, B. Patrick, P. Watson, R. York, F. Kitching, H. Sha and Spitzer, 1996]. In this work, the same setup was used, the temperature values were registered with a sample rate of 1Hz, using the data acquisition system assembled specifically for this project and the FieldChart supervisory and data acquisition software, developed by the Brazilian company NOVUS

To evaluate the common z2 setup, a comparison was made between the results of the thermal and mechanical simulations of the current condition and the proposed conditions. The current conditions were considered satisfactory since it is not observed the formation of shape defects or cracks

### 8.3.3 Proposition for a common Zone 2 for blooms and beam blanks

As the bloom has a smaller section, two setups were proposed:

- Proposition I: Cast the bloom with the original beam blank setup. For this, the side and web rolls need to fit the bloom. Thus, the web rolls must move 90mm away from the initial position to adjust to the bloom and the beam blank lateral rolls must approach 10mm each other, as shown in figures 8.4 and 8.5.
- Proposition II:Adjust the bloom rolls set up to fit the beam blank. In this case, the side rolls need to approach 10mm each other, and the inner and outer radius rolls need to move 50mm to fit the beam blank, as shown in figures 8.6 and 8.7.

In the second setup, the beam blank has no web support during the Z2.

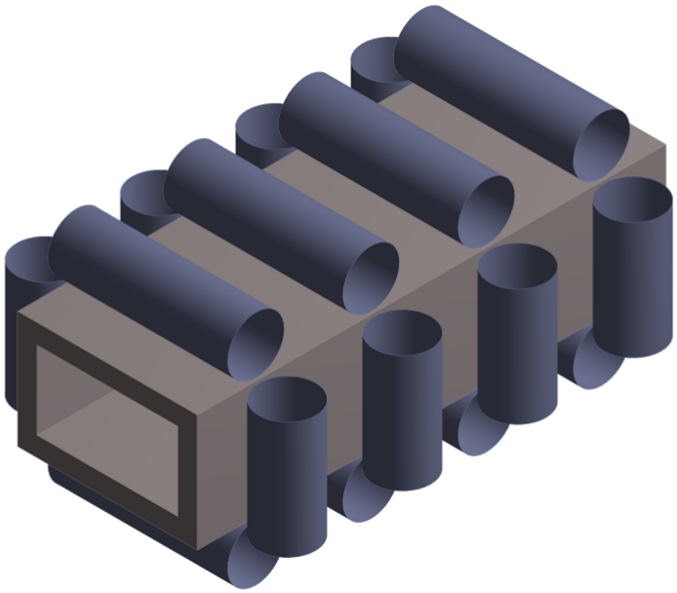

Figure 8.4: Schematic of the current position of the rolls in the bloom

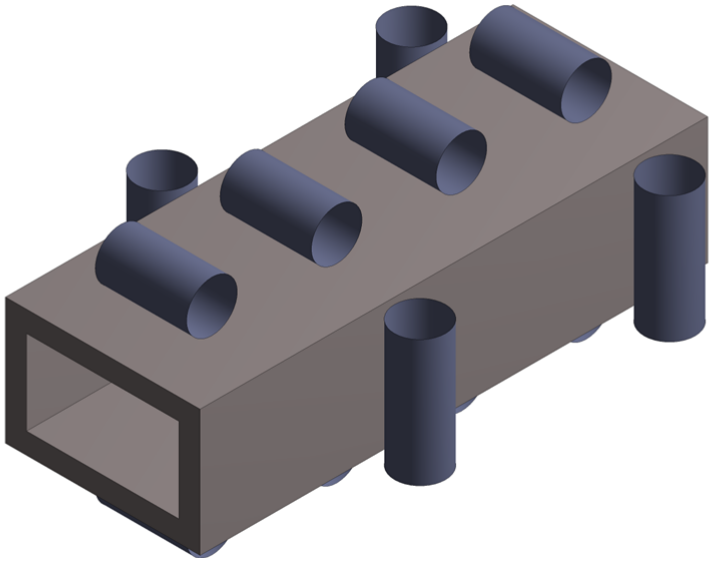

Figure 8.5: Schematic of the first proposal for a common setup

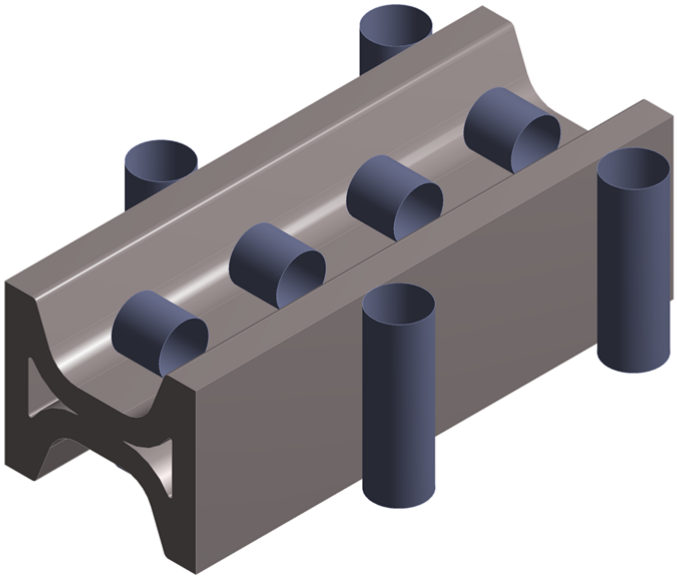

Figure 8.6: Schematic of the current position of the rolls in the beam blank

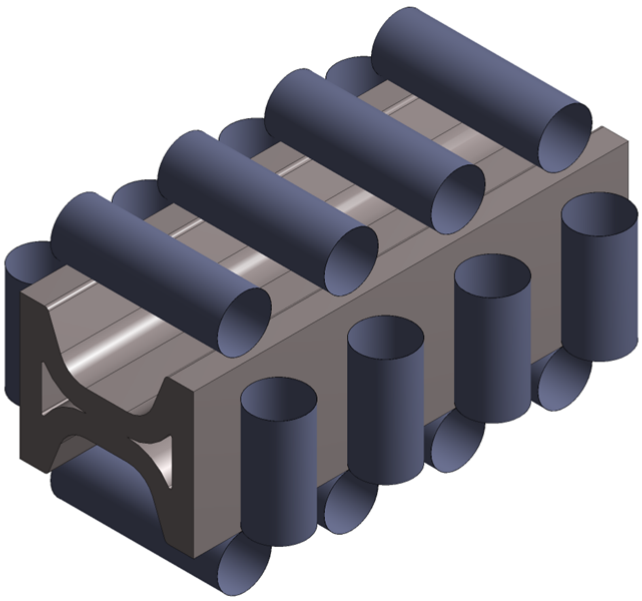

Figure 8.7: Schematic of the second proposal for a common setup

## 8.4 Results and Discussion

This chapter shows the heat flux, surface temperatures, stress and distortion for bloom and beam blank with the current setup and the two proposed setups.

### 8.4.1 Casting blooms with beam blank setup

#### Total heat Flux

The total heat flux in the bloom surface is shown in figure 8.8; The wide and low peaks correspond to the heat flux due to the sprays and the high and thin peaks correspond to the heat flux due to the rolls.

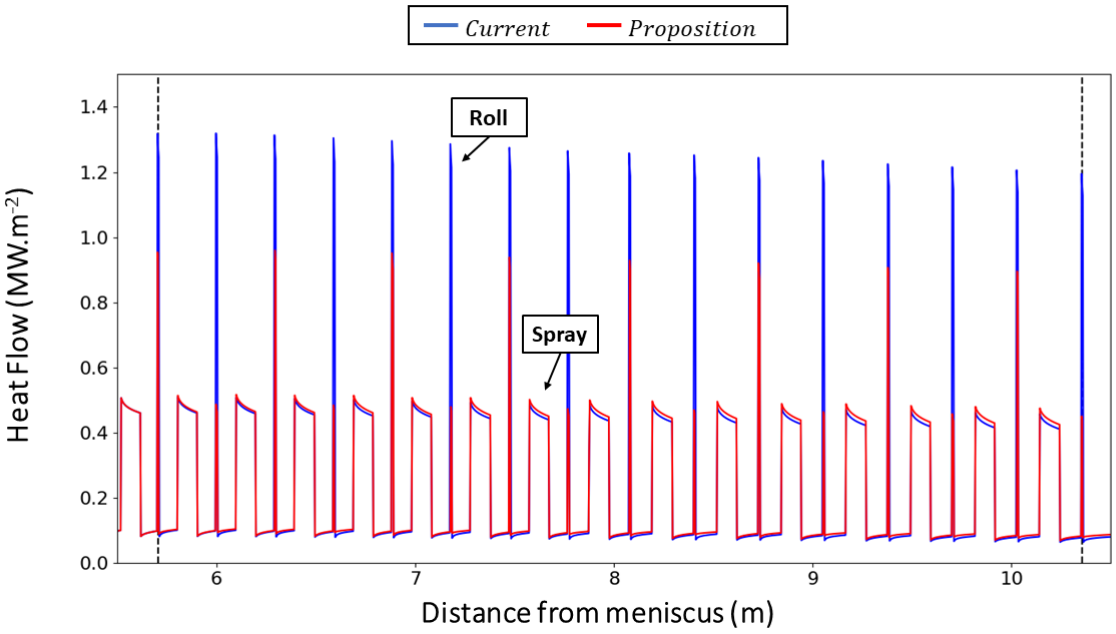


Figure 8.8: Global average heat flux in the bloom surface: current and first proposed setups

When changing the bloom rolls to the first common setup, the wide-face rolls are replaced by rolls with a smaller length and diameter. The side rolls are replaced by lengthier rolls but the total number of rolls on the narrow face is reduced. Hence, the total heat flux becomes smaller by 0.48% with the new setup.

**Temperature Measurements**

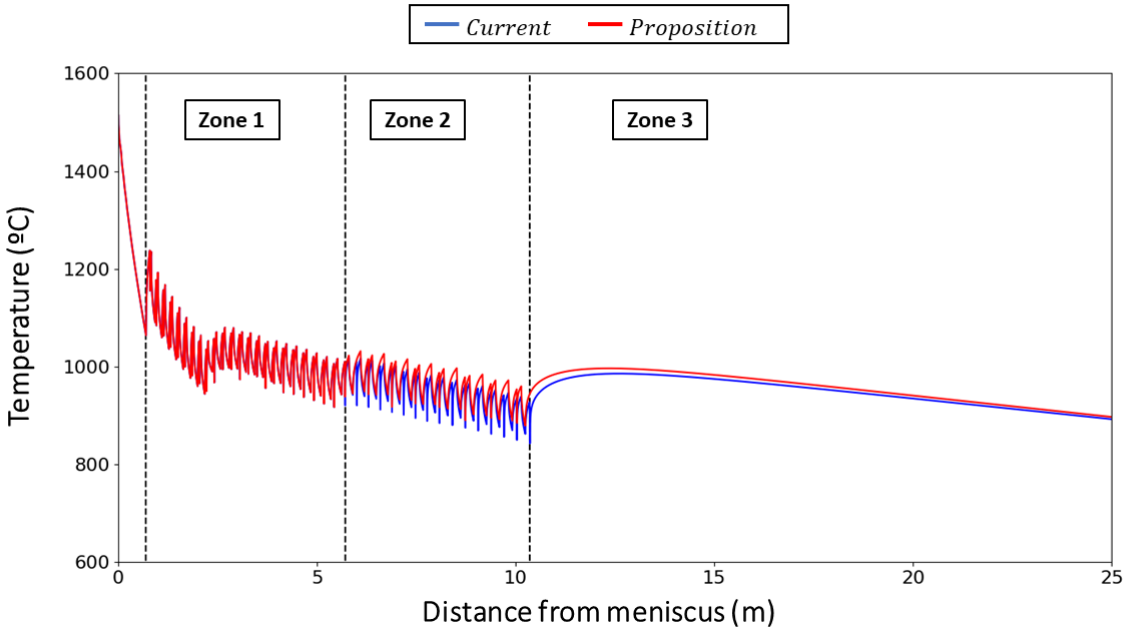


Figure 8.9: Temperature profile in the narrow face of the bloom: current setup and in the first setup option

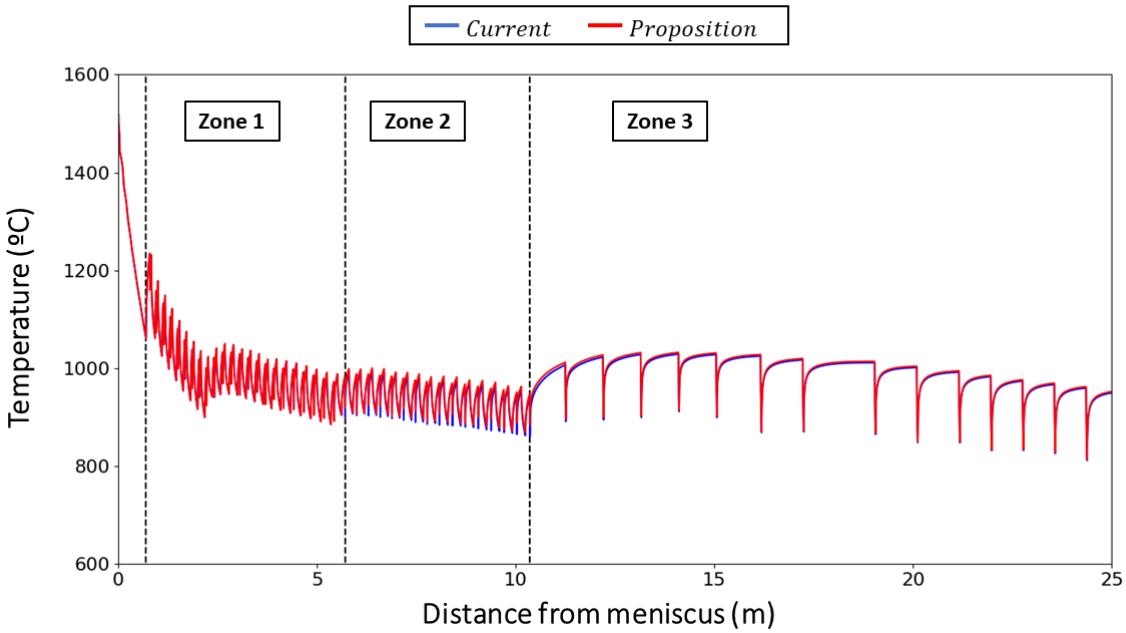


Figure 8.10: Temperature profile in the wide face of the bloom: current setup and in the first setup option

As shown in figures 8.9 and 8.10, the temperature results along the center for the wide

and narrow faces confirm the lower heat flux with the new setup. The temperature difference reaches 100°C in certain positions of the wide and narrow face within zone 2. However, the temperature difference gets close to 10°C at the entry of the soft reduction. The variation of the average temperature and the magnitude of the reheats remain in the same order of magnitude, which removes the risk of crack formation by alteration in the roll arrangement.

**Solidified Shell**

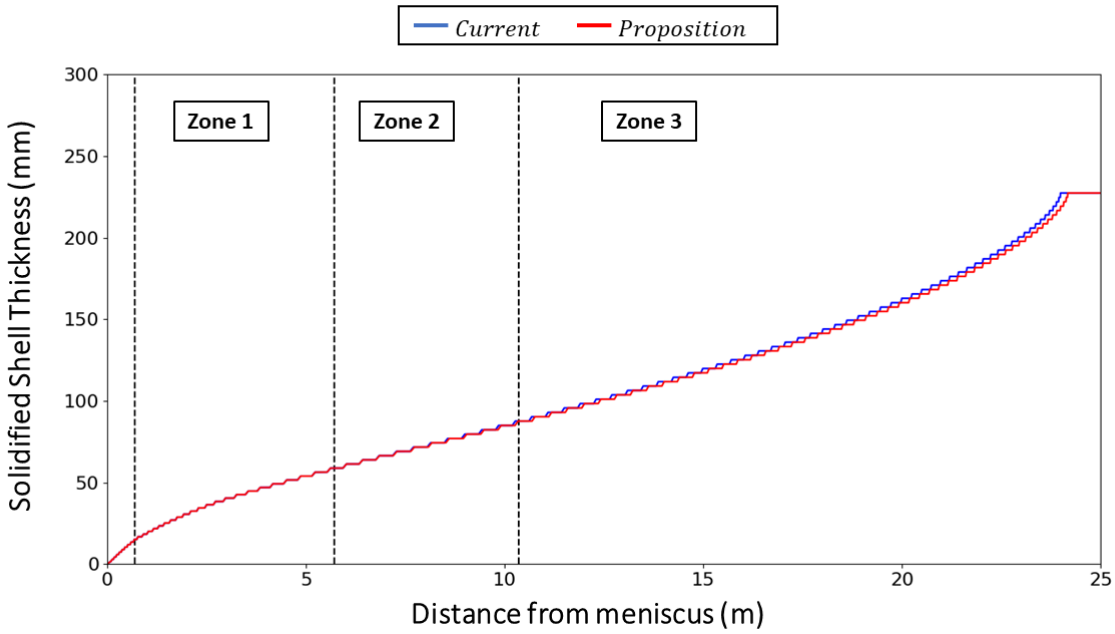


Figure 8.11: Shell thickness in the bloom: current setup and in the first setup option

As shown in figure 8.11 in the current setup, the final solidification of the bloom occurs around 24m from the meniscus, while in the proposed setup, the final solidification occurs at 0.2m further. In this position, the bloom is inside the soft reduction and more than 5m away from the cutting machine. So, the new setup offers no risk of liquid steel leakage during the cutting. It is worth mentioning that the metallurgical length of the project is 36 m from the meniscus.

**Stress and Distortion**

Von Misses stress values and the distortions suffered by the bloom along the wide face direction are shown in table 8.1

We can see that the difference in stress and strain, between the current and the proposed setup, is less than 0.5MPa and 0.5mm.

Table 8.1: Minimum, average and maximum values of stress and strain calculated for the current setup, proposed setup (Proposal I) and difference between them

| | Min Von Misses Stress (MPa) | Average Von Misses Stress (MPa) | Max Von Misses Stress (MPa) | Min Distortion (mm) | Average Distortion (mm) | Max Distortion (mm) |
|---|---|---|---|---|---|---|
| Bloom (current setup) | 0.32 | 11.47 | 20.40 | 0.5 | 2.5 | 5.0 |
| Bloom (Proposition I) | 0.30 | 11.79 | 20.40 | 0.5 | 2.5 | 5.0 |
| Difference | 0.02 | 0.32 | 0 | 0 | 0 | 0 |

### 8.4.2 Casting beam blanks with bloom setup

**Total heat Flux**

The total heat flux in the beam blank is shown in Figure 9 In this figure, the wide and low peaks correspond to the heat flux by the sprays and the high and thin peaks correspond to the heat flux by the rolls.

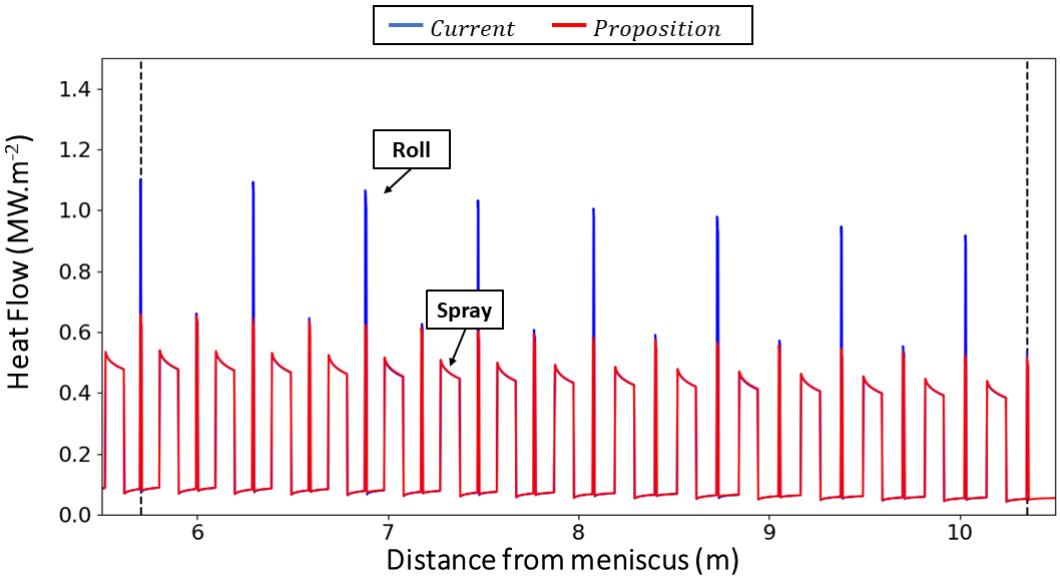


Figure 8.12: Global average heat flux in the beam blank surface: current setup and in the second proposed setup

When casting beam blanks using the common setup option 2, the web rolls are substituted

by rolls that touch only the flange tip. The side rolls are replaced by lengthier rolls and the total number of rolls on the narrow face is increased. The total heat flux reduces by 0.13% with the new setup. Although the number of rollers has increased, the rollers touch a smaller area on the flange tip.

**Temperature Measurements**

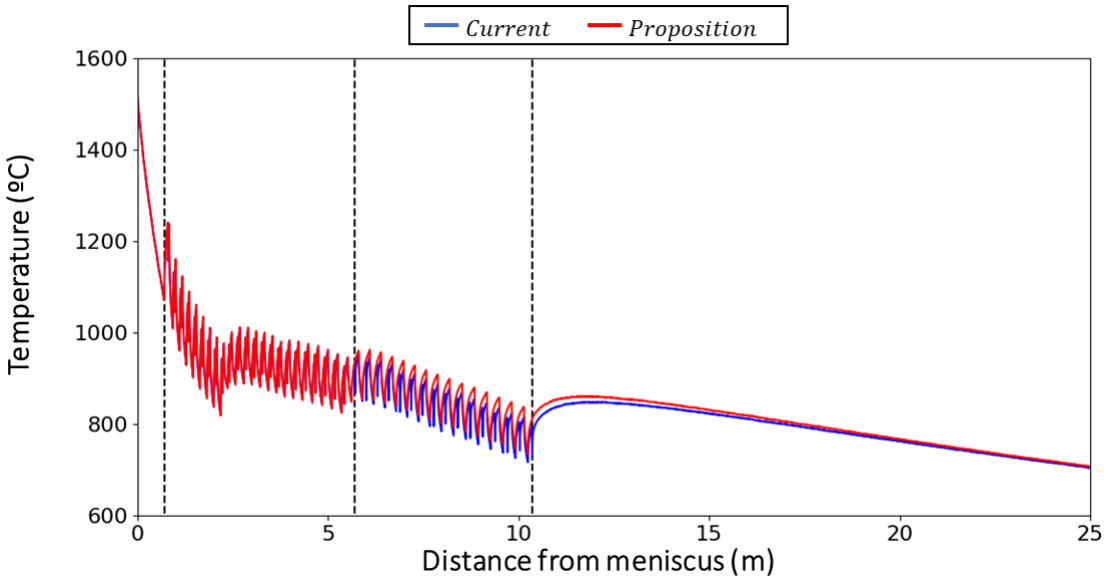


Figure 8.13: Temperature profile in the web of the beam blank: current setup and in the second setup option

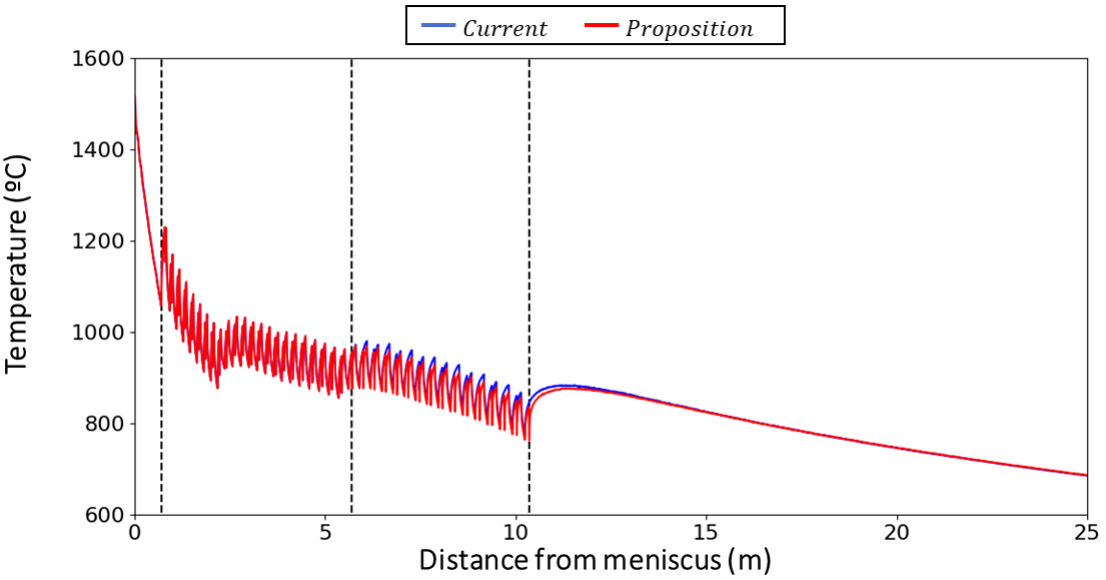


Figure 8.14: Temperature profile in the flange of the beam blank: current setup and in the second setup option

In the temperature results along the center for the web and flange faces, figures 8.13 and 8.14. The difference reaches 20°C in certain positions of the wide and narrow face within zone

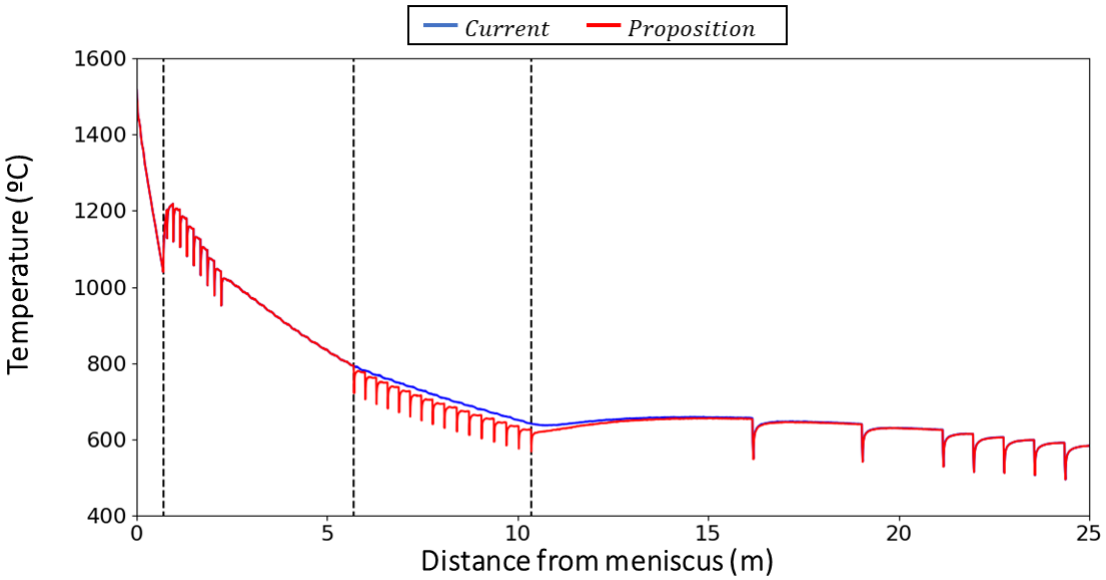


Figure 8.15: Temperature profile in the flange tip of the beam blank: current setup and in the second setup option

2, it decreases reaching close to 6°C at the entry of the soft reduction. The variation of the average temperature and the magnitude of the reheats remain in the same order of magnitude in the web and flange. However, the temperature profile of the flange tip, figure 8.15, starts to have temperature gradients that did not exist before, in the order of 50°C/m. This can affect the surface quality of the beam blank in this region.

**Solidified Shell**

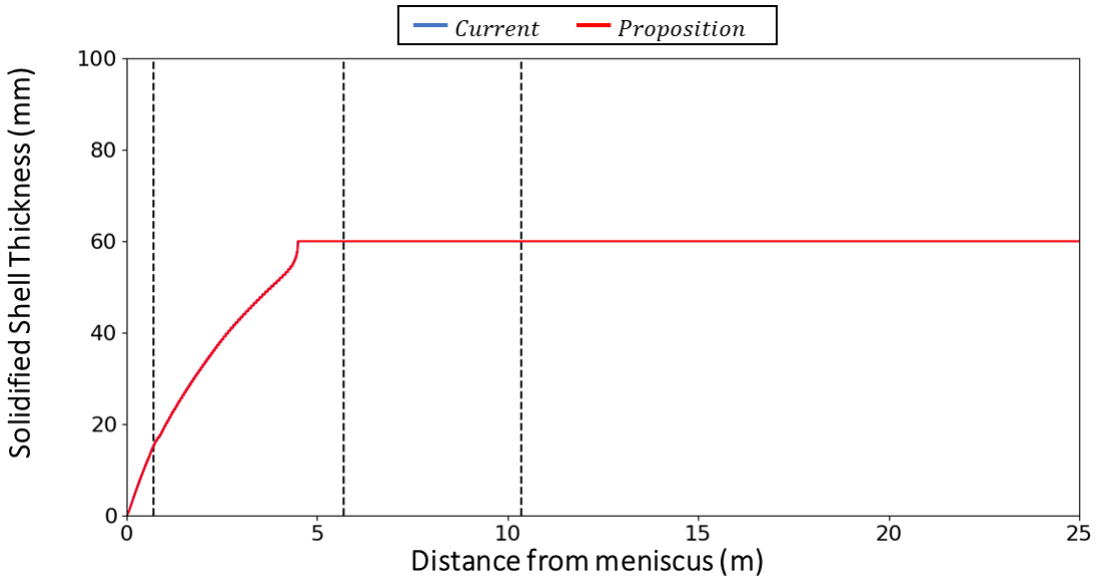


Figure 8.16: Shell thickness in the beam blank: current setup and in the second setup option

Figure 8.16 shows the solidified shell in the beam-blank web. The minor heat flux in

proposal 2 did not impact the solidified skin of the beam blank the position where the total solidification of the beam blank takes place is not altered, thus does not offer a risk of leakage when cutting the as-cast. It is worth mentioning that the metallurgical length of the project is 36m from the meniscus.

**Stress and Distortion**

Von Misses stress values and the distortion suffered by the beam blank along the flange direction are shown in table 8.2.

Table 8.2: Minimum, average and maximum values of stress and strain calculated for the current setup, proposed setup (Proposal II) and the difference between them.

| | Min Von Misses Stress (MPa) | Average Von Misses Stress (MPa) | Max Von Misses Stress (MPa) | Min Distortion (mm) | Average Distortion (mm) | Max Distortion (mm) |
|---|---|---|---|---|---|---|
| Beam Blank (current setup) | 0.1 | 11.0 | 21.7 | 0.18 | 0.8 | 1.7 |
| Beam Blank (Proposition II) | 0.1 | 10.8 | 21.4 | 0.15 | 0.6 | 1.7 |
| Difference | 0 | 0.2 | 0.3 | 0.03 | 0.2 | 0 |

We can see that the difference between the stresses and strains between the current and the proposed setup are less than 0.5MPa or 0.5mm

## 8.5 Conclusions

In this work, simulations of two different configurations were simulated (Proposition I and II) for the Zone 2 rolls of the studied machine. Proposition I: Cast the bloom with the original beam blank setup and maintain the beam blank setup. Proposition II:Adjust the bloom rolls set up to fit the beam blank and maintain the bloom setup. These simulations aimed to study the possibility of producing the two geometries with the same Zone 2. In ”Proposition I”, the bloom heat extraction becomes 0.48% smaller with the new setup. The temperature differences reach 100°C in certain positions of the wide and narrow face within zone 2 it decreases, reaching close to 10°C at the entry of the soft reduction. In the current setup, the final solidification of

the bloom occurs at 24m from the meniscus, while in the proposed setup, the final solidification occurs at 24.2m from the meniscus. The difference in stress and strain, between the bloom current and the proposed setup, is less than 0.5MPa or 0.5mm

When changing the beam blank rolls to the common setup ”Proposition II”, the heat extracted becomes 0.13% smaller with the new setup. The temperature differences reach 20°C in certain positions of the web and flange within zone 2, but it decreases to about 6°C at the entry of the soft reduction. The minor heat extraction in ”Proposition II” did not impact on solidified skin of the beam blank. The variation of the average temperature and the magnitude of the reheats remain in the same order of magnitude in ”Proposition I”, and offer no risk of crack formation by alteration in the roll arrangement. However, in ”Proposition II”, the temperature profile of the flange tip starts to have temperature gradients that did not exist before, in the order of 50°C/m. This can affect the surface quality of the beam blank in this region. The difference in stress and strains, between the beam blank in the current and the proposed setup, is smaller than 0.5MPa or 0.5m

Thermal and Mechanical analysis suggests that it is possible to have a common Setup for blooms and beam blanks in Zone 2. Proposition I is preferred as it is less disruptive to the current standard.

## 8.6 Acknowledgments

The authors are grateful to the (PPGEM) at UFMG, the CAPES-PROEX, and CAPES FAPEMIG.

# 9. Conclusions, Original Contributions and Suggestions for Future Works

In this chapter, the conclusions of this work, the original contributions and suggestions for future work are presented.

## 9.1 Conclusions

This work developed a mathematical model that can be used to study the thermal behavior of blooms and beam blanks along the entire length of the casting machine. From the results obtained, it is possible to conclude that the heat transfer model developed was successfully validated for both bloom and beam blank.

The model can predict the temperature and solidified shell thickness with reasonable accuracy, as confirmed by the experiments done using breakout shells (difference less than 5mm), measurements from a thermal imaging camera in the dry area of the casting machine (difference from 20°C to 70°C depending on the position) and tests with an embedded thermocouple (agreement of the temperature ranges and very close measurements at the temperature peaks). Moreover, this work shows tests with an embedded thermocouple on beam blanks, which were not found in the literature. The thermocouple experiments proved to be challenging because of the limitations of the technique and the low frequency of the data acquisition system employed. However, it allowed the assessment of the temperature values in the spray chamber and further validation of the model. The temperatures predicted by the model and measured by the thermocouple were around 1000°C for the bloom in Zone 2 and 900°C for the beam blank.

Mathematical models were developed to calculate the stress and strain caused by thermal gradients and contact with the rollers. The mechanical properties were obtained by hot ductility testing in a GLEEBLE simulator.

The thermomechanical stresses and strains proved to be of little significance when compared to the contact stresses and strains in the order of $10^{-15}$Pa and $10^{-8}$m respectively. The models showed that the contact stress generated in the casting of blooms is of the order of 13MPa to 16MPa, and generated in the casting of beam blanks are of the order of 14 MPa to 17MPa. The blooms present average distortion values of 2mm and beam blanks of 1mm. The

as-cast material stress exceeds the yield strength limit but does not reach the tensile strength limit, so it is not probable to occurs crack formation during the as-cast conditions simulated. In fact, in the process of the simulated material (A572) under normal conditions, the formation of cracks is not observed.

In this work, simulations of two different configurations were made (Proposition I and II) for the Zone 2 rolls of the studied machine. (I) Cast the bloom with beam blank rolls (II) Cast the beam blank with blooms rolls. These simulations aimed to study the possibility of producing the two geometries with the same Zone 2.

In ”Proposition I”, the bloom heat extraction becomes 0.48% smaller with the new setup. The temperature differences reach 100°C in certain positions of the wide and narrow face within zone 2 it decreases, reaching close to 10°C at the entry of the soft reduction. In the current setup, the final solidification of the bloom occurs at 24m from the meniscus, while in the proposed setup, the final solidification occurs at 24.2m from the meniscus.

The difference in stress and strain, between the bloom current and the proposed setup, is less than 0.5MPa or 0.5mm When changing the beam blank rolls to the common setup ”Proposition II”, the heat extracted becomes 0.13% smaller with the new setup. The temperature differences reach 20°C in certain positions of the web and flange within zone 2, but it decreases to about 6°C at the entry of the soft reduction.

The minor heat extraction in ”Proposition II” did not impact on solidified skin of the beam blank. The variation of the average temperature and the magnitude of the reheats remain in the same order of magnitude in ”Proposition I”, and offer no risk of crack formation by alteration in the roll arrangement. However, in ”Proposition II”, the temperature profile of the flange tip starts to have temperature gradients that did not exist before, in the order of 50°C/m. This can affect the surface quality of the beam blank in this region.

The difference in stress and strains, between the beam blank in the current and the proposed setup, is smaller than 0.5MPa or 0.5m. Thermal and Mechanical analysis suggests that it is possible to have a common Setup for blooms and beam blanks in Zone 2. However, in ”Proposition II”, the temperature profile of the flange tip starts to have temperature gradients 50°C/m. This can affect the surface quality of the beam blank in this region.

So ”Proposition I” is preferred to support both geometries.

## 9.2 Original Contributions

The original contributions of this work are:

- Study of thermal and mechanical behavior where two geometries were analyzed aiming at the production with part of the common secondary cooling.
- Development of mechanical models for blooms and beam blanks whose region of interest is the secondary cooling zone.
- Hot ductility test data for the studied steel, ASTM A572.
- Results of tests with the traveling thermocouple technique in the beam blank as-cast geometry.

## 9.3 Suggestions for future works

These are suggestions for future work:

- Perform hot tests with a common Zone 2.
- Improve the experimental technique of the traveling thermocouple using a data acquisition system with a higher sampling frequency (¿= 2Hz)
- To analyze the microstructural transformations undergone by the blooms and beam blanks during the casting process.
- Expand models developed for the straightening region of blooms and beam blanks.
- Expand models to analyze the bloom soft reduction process.

# 10. Conclusões, Contribuições Originais e Sugestões para Trabalhos Futuros

Nesse capítulo, as conclusões desse trabalho, as contribuições originais a literatura e sugestões para trabalhos futuros são apresentadas.

## 10.1 Conclusões

Esse trabalho desenvoleu um modelo matemático que pode ser utilizada para analisar o comportamento térmico de blocos e beam blanks durante todo o comprimento da maquina de lingotamento. Com base nos resultados obtidos, é possível de se concluir que o modelo de transferência de calor foi validado com sucesso para as duas geometrias.

O modelo pode prever a temperatura e a espessura da pele solidificada com acurácia razoavel, como confirmado pelos experimentos utilizando cascas de breakout (diferença menor do que 5mm), medidas com câmera termográfica na área seca da máquia de lingotamento (diferenças de 20 a 70 ºC dependendo da posição) e testes com termopar acoplado (faixas de valores de temperatura em acordo e medidas de pico de temperatura bem próximas).

Além disso, esse trabalho mostra testes com termopar acoplado com beam blanks, o que não foi encontrado em trabalhos publicados. Os ensaios com termopar se provaram desafiadores devido as limitações da ténica e a baixa frequência de amostra do sistema de aquisição de dados utilizado (1Hz). Entretando, eles permitiram a avaliação da temperatura na câmata de sprays e maior confiabilidade nas previsões do modelo. As temperaturas calculadas pelo modelo e medidas pelo termopar são aproximadamente 1000°C para blocos na Zona 2 e 900°C para o beam blank.

Modelos matemáticos foram desenvolvidos para calular a tensão e deformação causada por gradiente térmico e contato com rolos. As propriedades mecânicas foram obtidas por testes de tração a quente em um simulador de processos GLEEBLE.

As tensões e deformações termomecânicas calculadas estão na ordem de $10^{-15}$Pa e $10^{-8}$m, respectivamente, e podem ser desprezadas em comparação com a tensão causada pela pressão ferrostatica de açõ líquido no iterior da pele solidificada que está em contato com os rolos de apoio .

Os modelos mostram que a tensão gerada no lingotamento de blocos está na ordem de 13 a 16MPa, e no lingotamento de beam blanks está na ordem de 14 a 17MPa. O bloco apresenta deformação média de 2mm e beam blanks de 1mm. O valor de tensão calculado excede o limite de escoamento mas não ultrapassa o limite de resistência, então não é provável que ocorram trincas. De fato, no processo do material simulado (A572) sob condições normais, não são observadas formação de trincas.

Nesse trabalho, simulações de duas configurações são realizadas (Proposta I e II) para os rolos da zona 2 da máquina estudada. (I) Lingotametno de blocos com os rolos de beam blank, (II) Lingotamento de beam blank com rolos de bloco. Esses simulações tem como objetivo um estudo de viabilidade da produção de ambas geometrias com a mesma configuração de rolos na zona 2.

Na ”Prosposta I”, o calor extraído do bloco diminui em 0.48% com a nova configuração. A diferença de temperatura alcança 100ºC em certas posições das faces larga e estreita na zona 2, mas vai para próximo de 10ºC na entrada da soft reduction. Na configuração atual, a solidificação total do bloco acontece à 24m do menisco, enquanto no nova proposta, acontece 0.2 metros depois. A diferença de tensão e deformação no bloco entre a configuração atual e a ”Proposta I” é de menos de 0.5MPa e 0.5mm.

Na ”Proposta II”, o calor estraído do beam blank diminui em 0.13% com a nova configuração A diferença de temperatura alcança 20ºC em certas posições da alma e flange na zona 2, mas cai para próximo de 6ºC na entrada da soft reduction. A pequeça alteração na extração de calor na ”Proposta II” não alterou o perfil da espessura da pele solidificada no beam blank. A diferença de tensão e deformação no beam blank entre a configuração atual e a ”Proposta II” é de menos de 0.5MPa e 0.5mm.

A variação da temperatura média e a ordem de grandeza dos picos de temperatura continua o mesmo na ”Proposta I” e não indica aumento na possibildiade da formação de trincas devido a alteração nos rolos. Porém, na ”Proposta II”, o perfil de temperatura da ponta dos flanges do beam blank passam a ter um gradiente de temperatura que não existe na configuração atual, na ordem de 50ºC/m. Isso pode afetar a qualidade superficial do beam blank nessa reguão.

Análises térmicas e mecânicas sugerem que é possível utilizar uma configuração única de rolos no resfriamento secundário para o lingotamento de blocos e beam blanks. Devido a inserção de novos gradientes de temperatura na ”Proposta II”, a ”Proposta I” é a mais recomendada.

## 10.2 Contribuições originais

As contribuições originais para a literatura desse trabalho são:

- Estudo do comportamento teérmico e mecânico de duas geometrias onde o objetivo é a produçao com uma configuração comum do resfriamento secundário.
- Desenvolvimento de modelos trmomecânicos para blocos e beam blanks em que a região de interesse é a zona de resfriamento secundário.
- Testes de ensaio de tração a quente para o aço estudado, ASTM A572.
- Resultados dos testes com termopar em acoplado ao produto lingotado para a geometria de beam blank.

## 10.3 Sugestões para trabalhos futuros

Essas são as sugestões para trabalhos futuros:

- Realizar testes a quente com a configuração comum na zona 2.
- Melhorar a técnica do experimento com o termopar para utilizar um sistema de aquisição de dados com frequência de amostragem maior (¿= 2Hz).
- Analisar as transformações microestruturais que ocorrem durante o lingotamento contínuo de blocos e beam blanks.
- Expandir os modelos desenvolvidos para cobrir a região de desempenadeira de blocos e beam blanks.
- Expandir os modelos desenvolvidos para cobrir a região de soft reduction de blocos e beam blanks.

# References

[AISE Steel Foundation, 2003] AISE Steel Foundation (2003). *Making, Shaping and Treating of Steel: Casting Volume*, volume Casting. Assn for Iron & Steel Technology, 11th edition.

[Assunção et al., 2014] Assunção, C., Parreiras, R., and Oliveira, G. (2014). Water Distribution Assessment Applied to Mathematical Model of Continuous Casting of Steel. pages 2895–2906.

[B. Barber, B. Patrick, P. Watson, R. York, F. Kitching, H. Sha and Spitzer, 1996] B. Barber, B. Patrick, P. Watson, R. York, F. Kitching, H. Sha, K. K. and Spitzer, K.-H. (1996). Determination of strand surface temperature and heat transfer during continuous casting. *La Revue de Metallurgie*, pages 1403–1412.

[Bergman et al., 2011] Bergman, T. L., Lavine, A. S., Incropera, F. P., and Dewitt, D. P. (2011). *Fundamentals of Heat and Mass Transfer*. John Wiley & Sons, seventh edition.

[Bobadilla et al., 1993] Bobadilla, M., Jolivet, J. M., Lamant, J. Y., and Larrecq, M. (1993). Continuous casting of steel: a close connection between solidification studies and industrial process development. *Materials Science and Engineering A*, 173(1-2):275–285.

[Brezina et al., 2021] Brezina, M., Mauder, T., Klimes, L., and Stetina, J. (2021). Comparison of optimization-regulation algorithms for secondary cooling in continuous steel casting. *Metals*, 11(2):1–19.

[Brimacombe and Sorimachi, 1977a] Brimacombe, J. K. and Sorimachi, K. (1977a). Crack formation in the continuos casting of Steel. *Metallurgical transactions B*, 8B:489–505.

[Brimacombe and Sorimachi, 1977b] Brimacombe, J. K. and Sorimachi, K. (1977b). Crack formation in the continuous casting of steel. *Metallurgical Transactions B*, 8(2):489–505.

[Callister, 2007] Callister, W. D. (2007). *Materials Science and Engineering*. John Wiley & Sons, Danvers,USA, seventh edition.

[Chen et al., 2010] Chen, W., Zhang, Y. Z., and Wang, B. X. (2010). Optimisation of continuous casting process parameters based on coupled heat and stress model. *Ironmaking and Steelmaking*, 37(2):147–154.

[Chen et al., 2009] Chen, W., Zhang, Y. Z., Zhang, C. J., Zhu, L. G., Lu, W. G., Wang, B. X., and Ma, J. H. (2009). Thermo-mechanical simulation and parameters optimization for beam blank continuous casting. *Materials Science and Engineering A*, 499(1-2):58–63.

[Costes et al., 2003] Costes, F., Heinrich, A., and Bellet, M. (2003). 3D thermomechanical simulation of the secondary cooling zone of steel continuous casting. *Modeling of Casting, Welding and Advanced Solidification Processes*, pages 393–400.

[Fernandes, 2005] Fernandes, P. C. (2005). *Otimização dos parâmetros de lingotamento contínuo para minimizar a ocorrência de trincas superficiais no aço DIN-20MnCr5 Mod*. PhD thesis.

[Fernandes Reis, 2012] Fernandes Reis, R. (2012). *Análise Termoestrutural Do Desencurvamento De Placas No Lingotamento Contínuo*. PhD thesis, Universidade Federal de Minas Gerais.

[Gomes et al., 2021] Gomes, D. F., Braga, B. M., Tavares, R. P., and Bagatini, M. C. (2021). Mathematical modelling of the continuous casting of blooms and beam blanks. *Computer Methods in Material Science*, 21(3):1–8.

[Gomes et al., 2019] Gomes, D. F., Tavares, R. P., and Braga, B. M. (2019). Mathematical model for the temperature profiles of steel pipes quenched by water cooling rings. *Journal of Materials Research and Technology*, 8(1):1197–1202.

[Ha et al., 2001] Ha, J. S., Cho, J. R., Lee, B. Y., and Ha, M. Y. (2001). Numerical analysis of secondary cooling and bulging in the continuous casting of slabs. *Journal of Materials Processing Technology*, 113(1-3):257–261.

[Hada la et al., 2011] Hada la, B., Cebo-Rudnicka, A., Malinowski, Z., and Go ldasz, A. (2011). The influence of thermal stresses and strand bending on surface defects formation in continuously cast strands. *Archives of Metallurgy and Materials*, 56(2):367–378.

[Hardin et al., 2003] Hardin, R. A., Liu, K., Beckermann, C., and Kapoor, A. (2003). A transient simulation and dynamic spray cooling control model for continuous steel casting. *Metallurgical and Materials Transactions B*, 34B(June):297–306.

[Hibbeler et al., 2009] Hibbeler, L. C., Xu, K., Thomas, B. G., Koric, S., and Spangler, C. (2009). Thermomechanical Modeling of Beam Blank Casting. *Iron and Steel Technology*, 6(7):60–73.

[Huespe et al., 2000] Huespe, A. E., Cardona, A., and Fachinotti, V. (2000). Thermomechanical model of a continuous casting process. *Computer Methods in Applied Mechanics and Engineering*, 182(3-4):439–455.

[Ji et al., 2016] Ji, C., hui Wu, C., and yong Zhu, M. (2016). Thermo-Mechanical Behavior of the Continuous Casting Bloom in the Heavy Reduction Process. *Jom*, 68(12):3107–3115.

[Ji et al., 2014] Ji, C., Luo, S., and Zhu, M. (2014). Analysis and application of soft reduction amount for bloom continuous casting process. *ISIJ International*, 54(3):504–510.

[Jin et al., 2009] Jin, X., Chen, D., Zhao, Y., and Long, M. (2009). Study on mathematical model of temperature and stress for thin slab in continuous casting. *Proceedings - 2009 International Conference on Computational Intelligence and Software Engineering, CiSE 2009*, (1):2–6.

[Kim et al., 1991] Kim, Y., Farouk, B., and Keverian, J. (1991). A mathematical model for thermal analysis of thin strip casting of low carbon steel. *Journal of Manufacturing Science and Engineering, Transactions of the ASME*, 113(1):53–58.

[Kozlowski et al., 1992] Kozlowski, P. F., Thomas, B. G., Azzi, J. A., and Wang, H. (1992). Simple constitutive equations for steel at high temperature. *Metallurgical Transactions A*, 23(3):903–918.

[Kromhout, 2013] Kromhout, J. A. (2013). Mould powder development for continuous casting of steel. *Transactions of the Indian Institute of Metals*, 66(5-6):587–596.

[Lait et al., 1974] Lait, J. E., Brimacombe, J. K., and Weinberg, F. (1974). Mathematical Modelling of Heat Flow in Continuous Casting of Steel. *Ironmaking & Steelmaking*, 2:90–97.

[Lee et al., 2000] Lee, J.-E., Yeo, T.-J., OH, K. H., Yoon, J.-K., and Yoon, U.-S. (2000). Prediction of cracks in continuously cast steel beam blank through fully coupled analysis of fluid flow, heat transfer, and deformation behavior of a solidifying shell. *Metallurgical and Materials Transactions A: Physical Metallurgy and Materials Science*, 31(1):225–237.

[Lee et al., 1998] Lee, J.-E., Yoon, J.-K., and Han, H. N. (1998). 3-Dimensional Mathematical Model for the Analysis of Continuous Beam Blank Casting Using Body Fitted Coordinate System. *ISIJ International*, 38(2):132–141.

[Li et al., 2012] Li, X. B., Ding, H., Tang, Z. Y., and He, J. C. (2012). Formation of internal cracks during soft reduction in rectangular bloom continuous casting. *International Journal of Minerals, Metallurgy and Materials*, 19(1):21–29.

[Liu et al., 2017] Liu, K., Wang, C., Liu, G. L., Ding, N., Sun, Q. S., and Tian, Z. H. (2017). Research on soft reduction amount distribution to eliminate typical inter-dendritic crack in continuous casting slab of x70 pipeline steel by numerical model. *High Temperature Materials and Processes*, 36(4):359–372.

[Liu et al., 2008] Liu, Q., Wang, L., Zhang, L., Cao, L., Ding, X., Liang, M., and Qi, Y. (2008). Mathematical model of heat transfer for bloom continuous casting. *Journal of University of Science and Technology Beijing: Mineral Metallurgy Materials (Eng Ed)*, 15(1):17–23.

[Luo et al., 2012] Luo, W., Yan, B., Xiong, Y. X., Wen, G. H., and Xu, H. L. (2012). Improvement to secondary cooling scheme for beam blank continuous casting. *Ironmaking and Steelmaking*, 39(2):125–132.

[Ma et al., 2008] Ma, J., Xie, Z., and Jia, G. (2008). Applying of Real-time Heat Transfer and Solidification Model on the Dynamic Control System of Billet Continuous Casting. *ISIJ International*, 48(12):1722–1727.

[Mahapatra et al., 1991] Mahapatra, R. B., Brimacombe, J. K., and Samarasekera, I. V. (1991). Mold behavior and its influence on quality in the continuous casting of steel slabs: Part II. Mold heat transfer, mold flux behavior, formation of oscillation marks, longitudinal off-corner depressions, and subsurface cracks. *Metallurgical Transactions B*, 22(6):875–888.

[Meng and Thomas, 2003] Meng, Y. A. and Thomas, B. G. (2003). Heat-transfer and solidification model of continuous slab casting: CON1D. *Metallurgical and Materials Transactions B*, 34B(October):685–705.

[Mills et al., 2016] Mills, K. C., Karagadde, S., Lee, P. D., Yuan, L., and Shahbazian, F. (2016). Calculation of physical properties for use in models of continuous casting process-Part 1: Mould slags. *ISIJ International*, 56(2):264–273.

[Mizikar, 1970] Mizikar, E. (1970). Spray Cooling Investigation For Continuous Casting Billets and Blooms. *Iron Steel Engineer*, 47:53–60.

[Moon and Dippenaar, 2004] Moon, S. C. and Dippenaar, R. (2004). The effect of austenite grain size on hot ductility of steels. *Materials Science and Technology*, 1:675–684.

[Ohba et al., 2008] Ohba, Y., Kitade, S. I., and Takasu, I. (2008). Austenite grain refining of as-cast bloom surface by reduction of oscillation mark depth. *TMS Annual Meeting*, 3(3):3–8.

[Patankar, 1980] Patankar, S. V. (1980). *Numerical heat transfer and fluid flow*.

[Prabhakar, 1980] Prabhakar, B. (1980). *An investigation of heat transfer in spray cooling*. PhD thesis.

[Qin et al., 2019] Qin, Q., Li, M., and Huang, J. (2019). Analysis of the influence of segmented rollers on slab bulge deformation. *Metals*, 9(2).

[Qin et al., 2014] Qin, Q., Shang, S., Wu, D., and Zang, Y. (2014). Comparative analysis of bulge deformation between 2D and 3D finite element models. *Advances in Mechanical Engineering*, 6.

[Qin and Yang, 2017] Qin, Q. and Yang, Z. (2017). Finite element simulation of bulge deformation for slab continuous casting. *International Journal of Advanced Manufacturing Technology*, 93(9-12):4357–4370.

[Schmidt and Josefsson, 1974] Schmidt, L. and Josefsson, A. (1974). on the Formation and Avoidance of Transverse Cracks in Continuously Cast Slabs From Curved Mould Machines.

[Sengupta et al., 2005a] Sengupta, J., Cockcroft, S. L., Maijer, D. M., and Larouche, A. (2005a). Quantification of temperature, stress, and strain fields during the start-up phase of direct chill casting process by using a 3D fully coupled thermal and stress model for AA5182 ingots. *Materials Science and Engineering A*, 397(1-2):157–177.

[Sengupta et al., 2004] Sengupta, J., Thomas, B. G., and Wells, M. a. (2004). Understanding the role water-cooling plays during continuous casting of steel and aluminum alloys. In *MS&T 2004 Conference proceedings*, pages 179–193.

[Sengupta et al., 2005b] Sengupta, J., Thomas, B. G., and Wells, M. A. (2005b). The Use of Water Cooling during the Continuous Casting of Steel and Aluminum Alloys. *Metallurgical and Materials Transactions A*, 36 A(202):187–204.

[Suzuki et al., 1982] Suzuki, H. G., Nishimura, S., and Yamaguchi, S. (1982). Characteristics of Hot Ductility in Steels Subjected To the Melting and Solidification. *Transactions of the Iron and Steel Institute of Japan*, 22(1):48–56.

[Szekeres, 2015] Szekeres, E. S. (2015). Basics of Mold Oscillation. pages 1–27.

[Thomas, 2002] Thomas, B. G. (2002). Modeling of the continuous casting of steel - Past, present, and future. *Metallurgical and Materials Transactions B: Process Metallurgy and Materials Processing Science*, 33(6):795–812.

[Thomas, 2003] Thomas, B. G. (2003). Fluid Flow in the Mold. *Casting Volume*, pages 1–41.

[Thomas and Bellet, 2018] Thomas, B. G. and Bellet, M. (2018). Modeling of Stress, Distortion, and Hot Tearing. *Casting*, 15:449–461.

[Versteeg and Malalasekera, 2007] Versteeg, H. K. and Malalasekera, W. (2007). *An Introduction to Computational FLuid Dynamics*.

[Vynnycky, 2018] Vynnycky, M. (2018). Applied mathematical modelling of continuous casting processes: A review. *Metals*, 8(11).

[Wang et al., 2005] Wang, H., Li, G., Lei, Y., Zhao, Y., Dai, Q., and Wang, J. (2005). Mathematical Heat Transfer Model Research for the Improvement of Continuous Casting Slab Temperature. *ISIJ International*, 45(9):1291–1296.

[Wang et al., 2012] Wang, H., Yu, W., and Cai, Q. (2012). Experimental study of heat transfer coefficient on hot steel plate during water jet impingement cooling. *Journal of Materials Processing Technology*, 212(9):1825–1831.

[Won and Thomas, 2001] Won, Y. M. and Thomas, B. G. (2001). Simple model of microsegregation during solidification of steels. *Metallurgical and Materials Transactions A: Physical Metallurgy and Materials Science*, 32(7):1755–1767.

[Won et al., 2000] Won, Y. M., Yeo, T. J., Seol, D. J., and Kyu Hwan, O. H. (2000). A new criterion for internal crack formation in continuously cast steels. *Metallurgical and Materials Transactions B: Process Metallurgy and Materials Processing Science*, 31(4):779–794.

[Xu et al., 2010] Xu, H. L., Wen, G. H., Sun, W., Wang, K. Z., and Yan, B. (2010). Analysis of Thermal Behavior for Beam Blank Continuous Casting Mold. *Journal of Iron and Steel Research International*, 17(12):17–22.

[Xu and Zhu, 2015] Xu, M. and Zhu, M. (2015). Transport phenomena in a beam-blank continuous casting mold and a new design of submerged entry nozzle. *Proceedings of the 6th International Congress on the Science and Technology of Steelmaking, ICS 2015*, 55(4):645–648.

[Yang et al., 2018a] Yang, G., Zhu, L., Chen, W., Yu, X., and He, B. (2018a). Initiation of surface cracks on beam blank in the mold during continuous casting. *Metals*, 8(9).

[Yang et al., 2018b] Yang, J., Meng, X., and Zhu, M. (2018b). Transient thermo-fluid and solidification behaviors in continuous casting mold: Oscillation behaviors. *ISIJ International*, 58(11):2071–2078.

[Zeng et al., 2020] Zeng, J., Gan, M., Yan, X., Wang, Q., and He, S. (2020). Mathematical Modeling of Heat Transfer and Deformation of Bloom Tube Mold in Continuous Casting Process. *Metallurgical and Materials Transactions B: Process Metallurgy and Materials Processing Science*, 51(1):213–221.

[Zhao et al., 2014] Zhao, Y., Chen, D. F., Long, M. J., Shen, J. L., and Qin, R. S. (2014). Two-dimensional heat transfer model for secondary cooling of continuously cast beam blanks. *Ironmaking and Steelmaking*, 41(5):377–386.